DOE/NASA/3163-1
NASA CR-167845

NASA-CR-167845
19830005088

Losses in Chopper-Controlled DC Series Motors

Howard B Hamilton
University of Pittsburgh

April 1982

NF02680

NOTICE

Losses in Chopper-Controlled
DC Series Motors

Howard B. Hamilton
University of Pittsburgh
Pittsburgh, Pennsylvania 15261

April 1982

N83-13359

TABLE OF CONTENTS

SUMMARY

Motors for Electric Vehicle (EV) applications must have different features than direct current (dc) motors designed for industrial applications. The motor application is characterized by the following requirements:

1. The need for highest possible efficiency from light load to over load for maximum EV range.
2. Large short time overload capability. The ratio of peak/average power varies from 5/1 in heavy city traffic to 3/1 in suburban driving situations.
3. Operation from power supply voltage levels of 84-144 volts (probably 120 volts maximum).

To meet Requirement No. 1, the mechanisms that produce losses have been identified and the influence of chopper characteristics on motor efficiency has been evaluated.

Requirement No. 2 necessitates a design approach based on commutation limits, as distinct from design based on thermal constraints (as is the usual limitation in the design of motors for conventional industrial applications).

Requirement No. 3 poses something of a dilemma in that it involves voltage levels for which a clear-cut choice of parallel or series type (lap or wave) windings cannot be made.

The objective of the research program* was the design and fabrication of a test facility suitable for conducting tests on EV motors, to develop test procedures, to obtain data which can be used to isolate losses, to visualize where motor design changes can and should be made, to indicate problems arising from chopper control, and to make recommendations with respect to test procedures, instrumentation and chopper operating modes.

A test facility utilizing a dc generator as a substitute for a battery pack was designed and utilized. Criteria for the design of such a facility is presented.

Two motors commercially available for EV use were tested. One was a solid-frame, wave-wound, self-ventilated motor; the other was a laminated-frame, non-symmetrical pole, lap-wound motor requiring external ventilation.

Major conclusions from the investigation are:

1. A dc generator can successfully power a chopper-controlled motor if parallel capacitors are used as energy-absorbing devices when the chopper is turned off.

2. Care must be taken to choose instrumentation with sufficient bandwidth. For example, if less than 1% error in power measurement is desired, theoretically, the wattmeter must respond to the tenth harmonic of the chopper repetition frequency.

3. Exact prediction of the magnitude of motor losses is a very difficult task. It is even more complex and difficult if the motor is chopper controlled. The following observations were made:

---

a. Efficiency of a motor is sharply reduced when it is chopper controlled. The higher the chopper frequency, the less the reduction in efficiency. The decrease in efficiency is more pronounced at lower values of average current.

b. Chopper control introduces additional losses not accounted for from consideration of harmonic currents and apparent resistance as measured.

4. IEEE #113, "Standard Test Code For Direct Current Machines," is not adequate as a test code for chopper controlled motors.

5. The lumped impedance, conventional motor model cannot accurately predict motor performance and efficiency. These must be obtained by test, and a standardized test procedure must be established.

6. Ability of the EV motor to commutate short-time overloads has a significant impact on motor size (weight) and range of the EV.

7. Many of the major losses in the motor can be significantly reduced by design techniques and attention. Losses identified are as follows:

a. Eddy current losses in the armature due to tooth saturation and the main flux can be significant. For example, for the wave-wound motor, at 2000 rpm this loss was calcualted as 52% of the rated copper joule loss value. This loss can be mitigated by reducing conductor height, using deeper slots, and using more iron (less flux density) in the motor.

b. Eddy current losses in the armature due to cross-slot leakage flux may be significant. This loss is one of the major components of "stray load" loss. Current harmonics due to chopper control increased this loss about 25% over the loss that exists without the harmonic currents. This loss can be mitigated and greatly reduced if fine-stranded conductors are used, since the loss is proportional to the square of the height of the conductor. Also, increasing the chopper frequency decreases this loss, since harmonic current magnitudes decrease with increasing frequency.

c. Losses in the pole-face iron due to slot effect are negligible if the poles are laminated, but a major loss if the poles are solid iron.

d. Nonconducting banding (such as Kevlar) should be used to secure the armature winding end turns, to eliminate banding losses due to harmonic fluxes.

e. Equalizer connection losses are non-existent in a wave-wound machine and are minimized in a lap winding if the proper combination of commutator bars, slots and parallel paths is utilized.

f. Losses in the coils undergoing commutation can be substantial if the brushes are located very far (10-15 degrees) off magnetic neutral and they increase with chopper frequency. The loss can be reduced by decreasing the number of turns shorted during the commutating process, using a wave winding or by using longer, less wide brushes (increasing commutator length). Interpoles will eliminate the need for brush shift and are strongly recommended. They also increase the ability of the motor to commutate heavy overloads.

g. Brush loss can be minimized by utilizing metal graphite brushes with silver if good commutation exists. Again, interpoles are strongly recommended. Attempts to secure low brush voltage drop by large brush pressure should be evaluated against increasing brush friction loss.

h. With a free wheeling diode having 0.86 volt drop, 75 watts diode loss was measured at full load current. It is important to select a low voltage drop diode for this application.

i. Losses from shaft, bearing, and housing currents due to shaft-induced emf are negligible.

j. Hysteresis losses in the magnetic structure due to chopper harmonics are negligible with laminated magnetic circuits. It is recommended that a laminated frame also be utilized.

k. For an internally fan-ventilated motor of the size for EV's, the fan loss is on the order of 0.33% of the output power rating. This type of ventilation is recommended to avoid duct losses. For an externally ventilated motor, the ducting and manifold should be carefully designed to minimize losses. Consideration of the usage of ram air for cooling should also be given in lieu of blower-produced ventilation.

The above losses are discussed in detail in this report, as are waveforms and their harmonic content, the measurement of resistance and inductance, EV motor/ chopper application criteria and motor design considerations.

CHAPTER 1

INTRODUCTION

This report details the results of an investigation* into the behavior of series dc motors, suitable for electric vehicle (EV) applications, powered from a chopper** controlled energy source, commonly referred to as a "chopper drive".

Project Objective

To design and fabricate a test facility suitable for conducting various tests; to develop test procedures and obtain data which can be analyzed to isolate losses; to visualize where motor design changes can, or should, be made; to provide a basis for analytical prediction of motor performance under chopper standard test procedures and pulse repetition rate/pulse widths used to minimize motor losses.

Background

A conventional model of dc motors has been used in theoretical analysis and prediction of efficiency and performance for many years. The model used has yielded acceptable, but not exact, results with larger departures from true values for smaller, low-voltage motors. Generally, when performance met minimum requirements, even though efficiencies calculated were quite erroneous, the analysis and design were acceptable since the vast majority of the applications were not dependent upon the power supply being propelled along with the motor, or involved motors of such a size that things like cost were deemed more important than efficiency. Further, performance was verified by test from a source of pure dc, or low-ripple rectified ac. Test standards (ref. 1) were adopted which enabled the user to evaluate specific test results based on those standards. In many instances, brush losses and so called "stray load" losses were assumed to be fixed values or fixed percentage of the output (1%).

The inherent shortcomings in the existing standards and procedures have been known for years and accepted for the reasons detailed above. However, the advent of rectified ac for supply (rather than from a dc generator) did cause concern as to the effect of the harmonics on losses and performance. This concern has been expressed mostly (on rectifier drives) as the need to standardize the measuring techniques and test procedures (ref. 2).

DC series motors have perceived advantages insofar as traction or vehicle propulsion systems are concerned; i.e. they can develop maximum torque at standstill, etc. They have been used for these purposes for many years. However, it should be noted that many EV applications will utilize shunt connected motors

---

* This work was performed under a grant funded by the Department of Energy and managed by the Lewis Research Center.

** Chopper drive implies the use of a thyristor (or other form of switch) interposed between the source and the motor and alternately applying and removing the source voltage. The applied voltage can be at either constant or variable repetition rate and for either constant or variable duration. The ratio of pulse on time, T_o, to the period of the cycle, T, is referred to as the "duty cycle." Chopper frequency is 1/T.

which have the capability of being easily connected for regeneration, i.e., pumping energy from the machine back into the supply system during braking or slowing operation.

The advent of the thyristor introduced a new era into the dc controlled motor drive arena. Basically, the use of chopper drives, with power thyristors, increased the efficiency of the overall drive system but most probably reduced the efficiency of the motor itself, due to the resulting current wave forms. Refer to Figure 1 for a simplified schematic of a chopper drive.
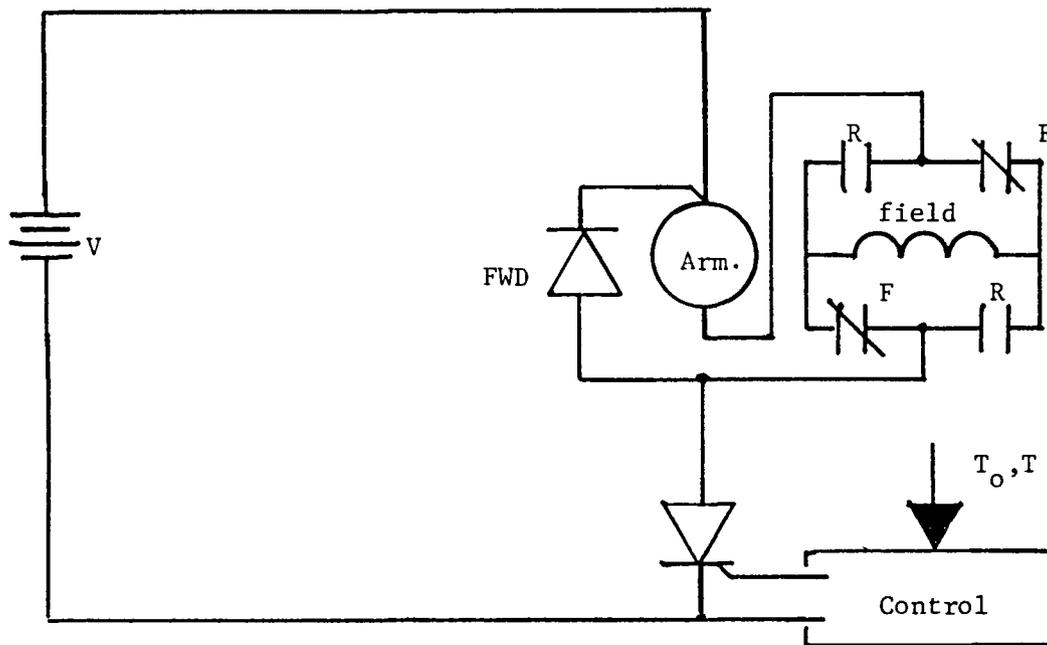
Figure 1   Schematic of Basic Chopper Drive
for Reversible DC Series Motor

Attempts to design an electric drive system for battery powered electric vehicles have increased the awareness for the need to develop reliable test and measuring techniques as well as a new model for the dc motor. This is necessary in order to:

1. minimize the losses, i.e., higher efficiency drives;
2. identify the important motor design parameters for a motor to be operated in conjunction with a battery/chopper supply;
3. improve motor performance for a specific weight/size configuration;
4. have a reliable motor model which permits reliable performance predictions;
5. have a standardized recognized test procedure so that all concerned agree on the meaning of test results.

With respect to efficiency and weight, a commonly accepted 'rule of thumb' indicates that with present motor designs and battery technology, 1% change in efficiency changes the available EV range 1.5 km., and 22.5 kg of weight change has the same effect.

Conventionally designed dc motors are usually not designed for high performance at non "design" voltages or for high harmonic content pulsed chopper supplies. In connection with the use of choppers, it should be noted that the vast majority of chopper applications have dealt with shunt wound motors (usually from alternating current supplies) and that there is a scarcity of literature on series motor applications; yet the series motor appears to be an attractive type for EV and traction applications.

There is very little information available on how to match motors and controllers (choppers). Guidelines need to be established for each, so that off-the-shelf items can be applied. The chopper designer insists on some minimum inductance, resistance and inductance/resistance ratios in the motor. The motor designer must be cognizant of the additional iron losses due to pulsating fluxes; the skin/proximity effects and additional joule losses and the performance degradation due to factors discussed above and the lessened ability of the motor to properly commutate. (Measurements reported in this report indicate a 3.5/1 change in inductance and a 6/1 change in apparent resistance over a frequency range of 30-360 Hz. as measured on a dc series motor.)

The problem areas discussed above point up the need for a better understanding of the behavior of the dc motor powered ·from a chopper supply and the need for a more exact model than that presently used, as well as the need for motor/chopper "interface" guidelines.

There are many facets of motor design that warrant investigation. Some of these stem from the fact that the motor power size, for electric vehicles, is normally designed for a higher supply voltage. For example, many of the motors are rated around 12-23 kw. A low voltage machine of this size, or larger, would normally have a parallel (lap) type winding. A regular industrial machine would normally be wound series (wave) for 250 volts, dc, or higher. The power supply for electric vehicles will most probably be in the range of 84-144 volts, which is between low and high voltages. Of the two motors examined in this investigation, one was wave, the other lap wound. How the motor is wound and the duty cycle it is designed for will have a large impact on the joule losses in the armature circuit. Another problem area for design compromise is in brush material and brush spring tension selection. Electrographic or metallic/graphitic brushes plus high spring tension can be utilized to reduce the voltage drop across the brushes - very important in low voltage motors. Yet, this approach often yields increased brush friction (rotating losses). Should the motors be "copper poor" (lower weight), an internal blower or an external source of cooling air would be required. Heavy conductors, eliminating the need for cooling, face a skin effect/ proximity effect when subjected to the harmonics associated with a chopper supply.

A series motor can be partially compensated for the effects of armature reaction upon commutation by a fixed brush shift position. This brush shift can also actually aid commutation (always a problem with a power source containing harmonics). In conventional applications, brush shift (fixed) in a series motor is a self-compensating effect, i.e., one position is suitable for all loads for

rotation always in the same direction. However, brush shift degrades performance, because of loss of some active inductors. If the brushes are not on the proper location, "rotating core losses", or losses due to joule heating in the coils undergoing commutations, can be excessive. This is an especially cogent consideration during reverse motor operation. The alternative is the use of interpoles, and possibly compensating windings. Yet these additions increase cost, weight and introduce additional joule losses in the motor.

Other aspects of motor design, for electric vehicle applications, that may be different from those in conventional applications are as follows:

1. working flux densities - how much saturation should be tolerated in the interest of light weight but at a sacrifice of performance?
2. the electrical loading - should fan cooling be required?
3. are conventional length/diameter ratios optimum?
4. air gap size and the weight/cost/design life relationships based on field maintenance and expected life realities;
5. are commutator bar-bar voltages consistent with the harmonics involved in armature current?
6. use of solid vs. laminated yokes;
7. insulation levels required - is it possible to reduce weight and cost if not overinsulated?
8. need for maximum efficiency over a wide range of output;
9. need for relatively high values of circuit inductance;
10. the design objective must be based on commutation limit as opposed to thermal constraint.

These questions can only be addressed after an examination of the various loss mechanisms.

Scope of the Investigation

Two motors (one lap, the other wave wound) were tested. Details on the test facility, the instrumentation used, the tests conducted and observed results are presented in CHAPTER 2. This chapter also discusses the complex wave forms associated with chopper control and the instrumentation required for making measurements. Theoretical performance, using the conventional motor model is compared with observed performance when the motor is powered from "ripple free" dc and when controlled by a chopper. Chopper contol does introduce complexities in the analysis of motor performance, especially in accounting for losses. The effects of chopper frequency and duty cycle, brush shift, etc. were determined by test and are presented.

IEEE #113 (ref. 1) does not address determination of the resistance and inductance variations with frequency and saturation level and thus it was necessary to make these determinations as an early part of this investigation. A technique suggested by Saunders (ref. 4) was utilized for these measurements. However, instrumentation techniques had to be developed to accomplish this.

CHAPTER 3 deals with the various loss mechanisms, both analytically and experimentally (where possible) and makes recommendations with respect to motor design. CHAPTER 4 presents the overall conclusions and summary of results. APPENDIX B presents notes on EV motor/chopper application criteria and motor considerations.

CHAPTER 2

THE TEST FACILITY

Tests detailed in this report were conducted using generator and battery sources, dynamometers for loading the test motors and necessary instrumentation for obtaining desired parameters and results.

Figure 2 is a schematic of the test circuit used. Figure 3 depicts the modification to the chopper control circuit.

The test circuit provides for powering the motor under test from either a 625 amp, 0-125 volt generator or from an 84 volt battery pack or from paralleled generator and batteries and with the chopper used for control or with the chopper bypassed. The generator has 69000 μF of capacitance across its terminals for surge voltage suppression. Two battery packs were utilized. They were 14 each, 6 volt EV 106 'golf cart' batteries and 7 each, 12 volt Exide RC-27 Heavy Duty batteries.

A complete series of tests were run on the generator and batteries in order to evaluate their characteristics and to explore the feasibility of using the generator only as a power source when the test motor is under chopper control. These test results were submitted, under GRANT NSG 3163 in a report entitled, "AN INVESTIGATION OF POSSIBLE DC POWER SOURCES FOR TESTING ELECTRIC VEHICLE MOTORS," (ref. 3) and presented in a technical paper entitled, "A DC POWER SOURCE FOR TESTING BATTERY POWERED ELECTRIC VEHICLE MOTORS" (ref. 4). The documents present waveforms to be expected and procedures for calculating the surge capacitor requirements.

The dynamometer used for load tests was a General Electric TLC-2332, Model 26G236, S/N 2483254, with cradled bearings. Maximum torque capability is 114 Nm up to 2500 rpm falling to 71 Nm at 4000 rpm. (29.8 kW) with maximum speed rating of 6000 rpm. Torque was measured using a BLH Load Cell Model T3P2B, S/N 38025, rated 446 newtons, which, with the 0.4 m arm resulted in a maximum torque measuring capability of 178 Nm. Calibration tests indicated linearity down to 8 Nm, minimum. Speed was measured using a digital strobotachometer.

In order to obtain data such as friction, rotating core losses, etc. a 3.75 kW dc shunt motor driving through an Ametek C#-30-100, 00072-2 torque transducer was utilized. This unit was found to be linear over the range from 0.5 up to 12 Nm.

The chopper used was a Cableform Model 4013-2, S/N 76073918 rated 600 amperes. The on-off time of the chopper was controlled by inserting a 5 volt square wave pulse into the chopper control module as shown in Figure 3. The thyristor in the chopper unit conducts only during the time the 5 volt square pulse is present. Minimum on-time is 0.8 milliseconds (time necessary to charge the commutating capacitors which force the thyristor shut off). A cathode ray oscilloscope was used to monitor and measure the square wave repetition frequency and pulse width.

Current measurements were made using T&M Research Products, Inc. Model K5000-10, 0.001 ohms, 6.5 MHz bandwidth, 275 amperes non-inductive shunts (NIS) with the voltage drop measured using a digital voltmeter. Voltage measurements were made using digital voltmeters.

Power measurements were made using a Clark-Hess Model 255 electronic wattmeter, which was modified to accept the output from the NIS rather than utilizing the 5 ampere internal shunt. The internal shunt yielded 100 mv for 5 ampere input.
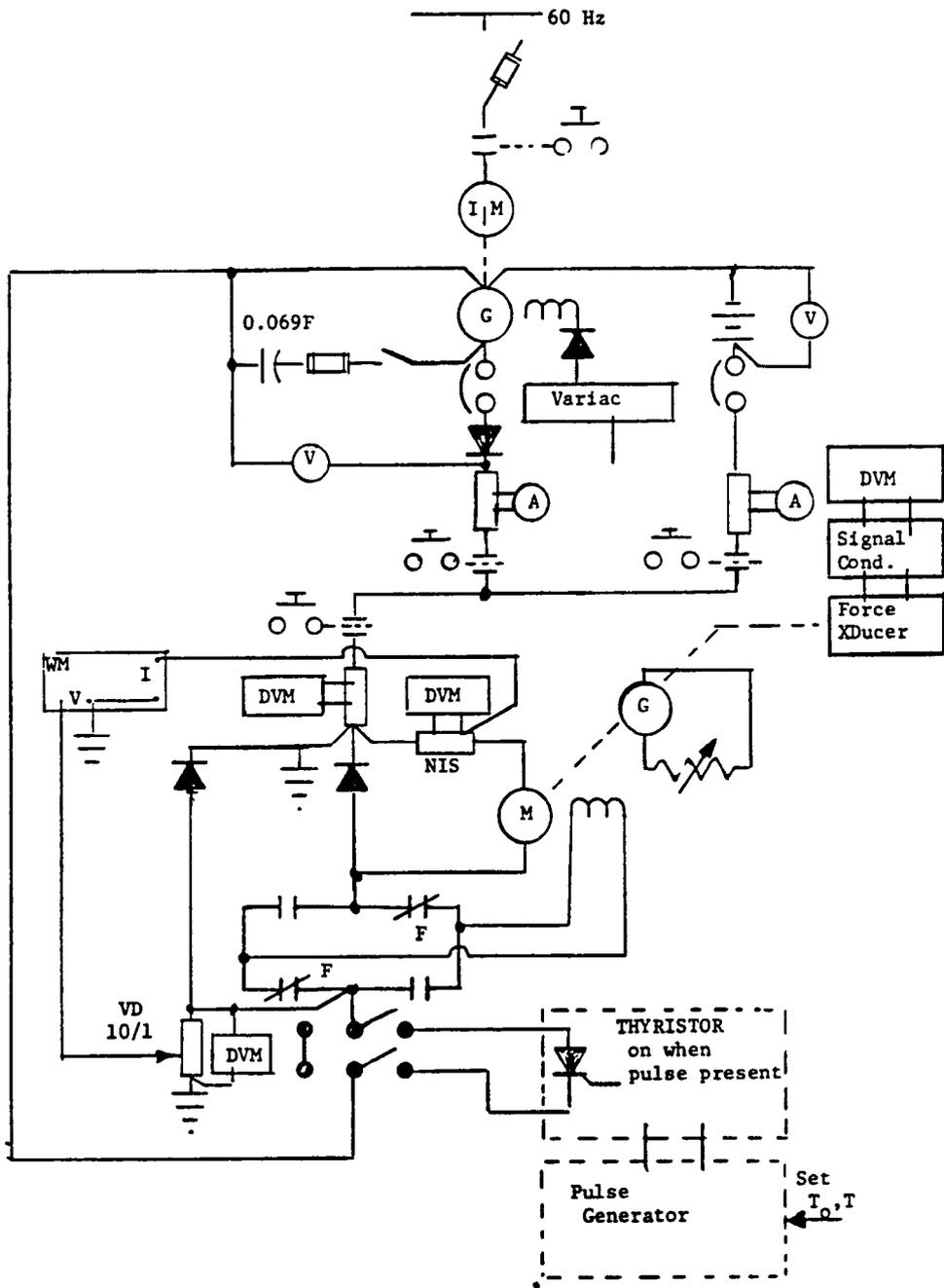
Figure 2   Test Circuit Schematic
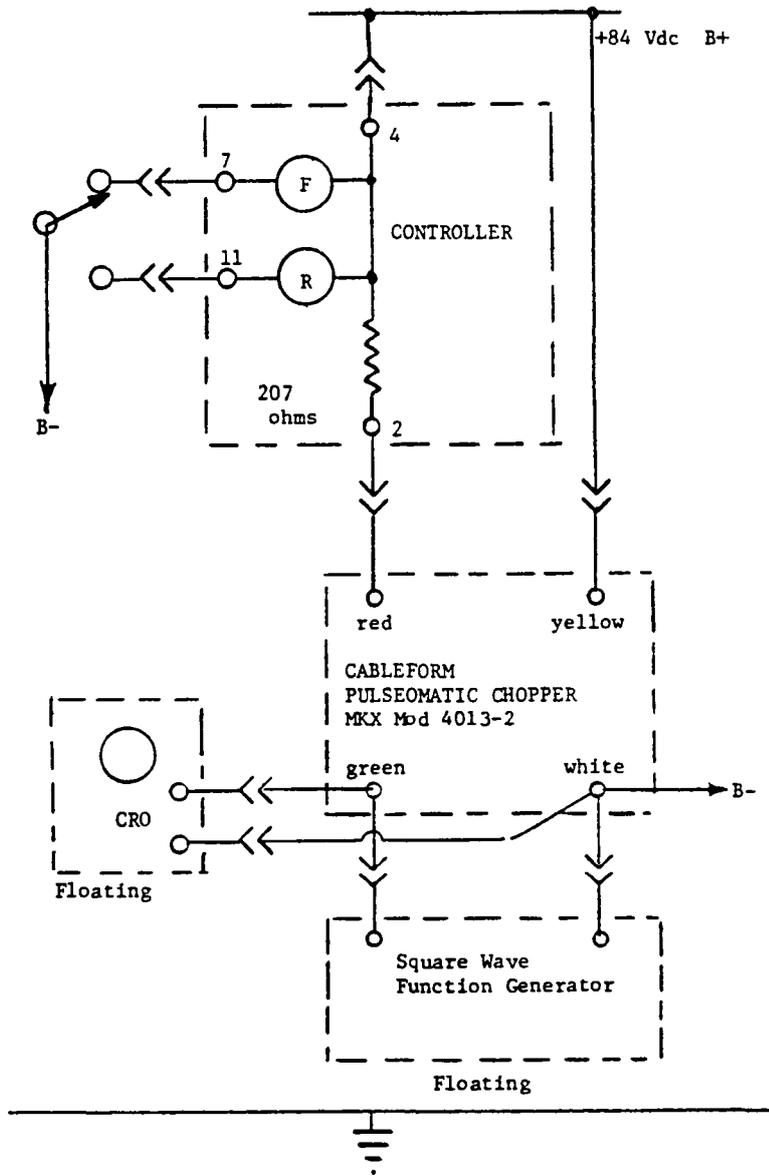
Figure 3   Chopper/Controller Modification

The NIS yields 100 mv for 100 amperes. Thus a multiplying factor of 20 times Watt reading is required.

Instruments and the circuit used in the tests to determine R and L parameters are shown in Figure 4.

Harmonic spectrums were measured using a Tektonix 5L4N Spectrum Analyzer, a storage type cathode ray oscilloscope and a Polaroid Camera.

WAVEFORMS AND THEIR HARMONIC CONTENT

A chopper controlled dc source impresses a step voltage on the armature and field (if a series motor) at regular intervals, determined by the frequency at which the chopper is operating. Neglecting voltage drop in the supply circuit, the voltage wave has a constant value, V, equal to the source voltage during the 'on' time, T_o and is zero during the remainder of the period, T where:

$$T = 1/f$$

and f is the chopper repetition frequency. Such a wave is shown in Figure 5.
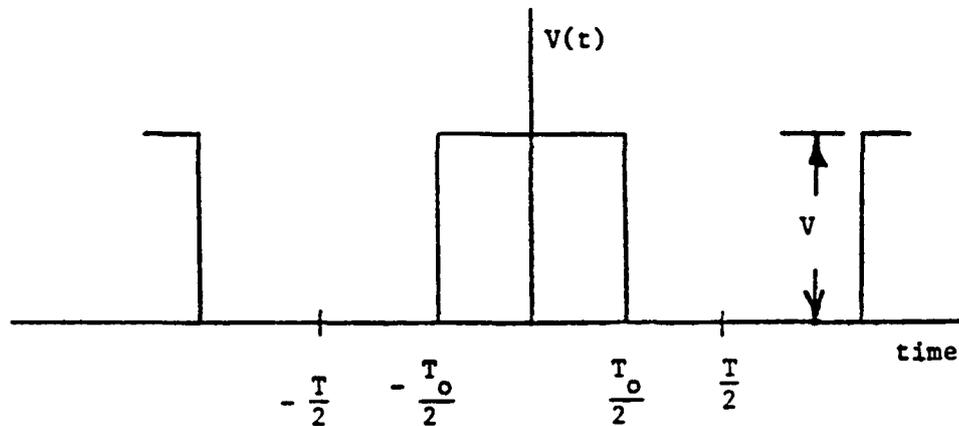
Figure 5 Chopper Controlled Motor Voltage

v(t) can be expressed as a Fourier Series by:

$$v(t) = \frac{V\,T_o}{T} + \frac{2V\,T_o}{T} \sum \left(\frac{\sin n\pi T_o/T}{n\pi T_o/T} \right) \cos \frac{2\pi n t}{T} \qquad (1)$$

-11-
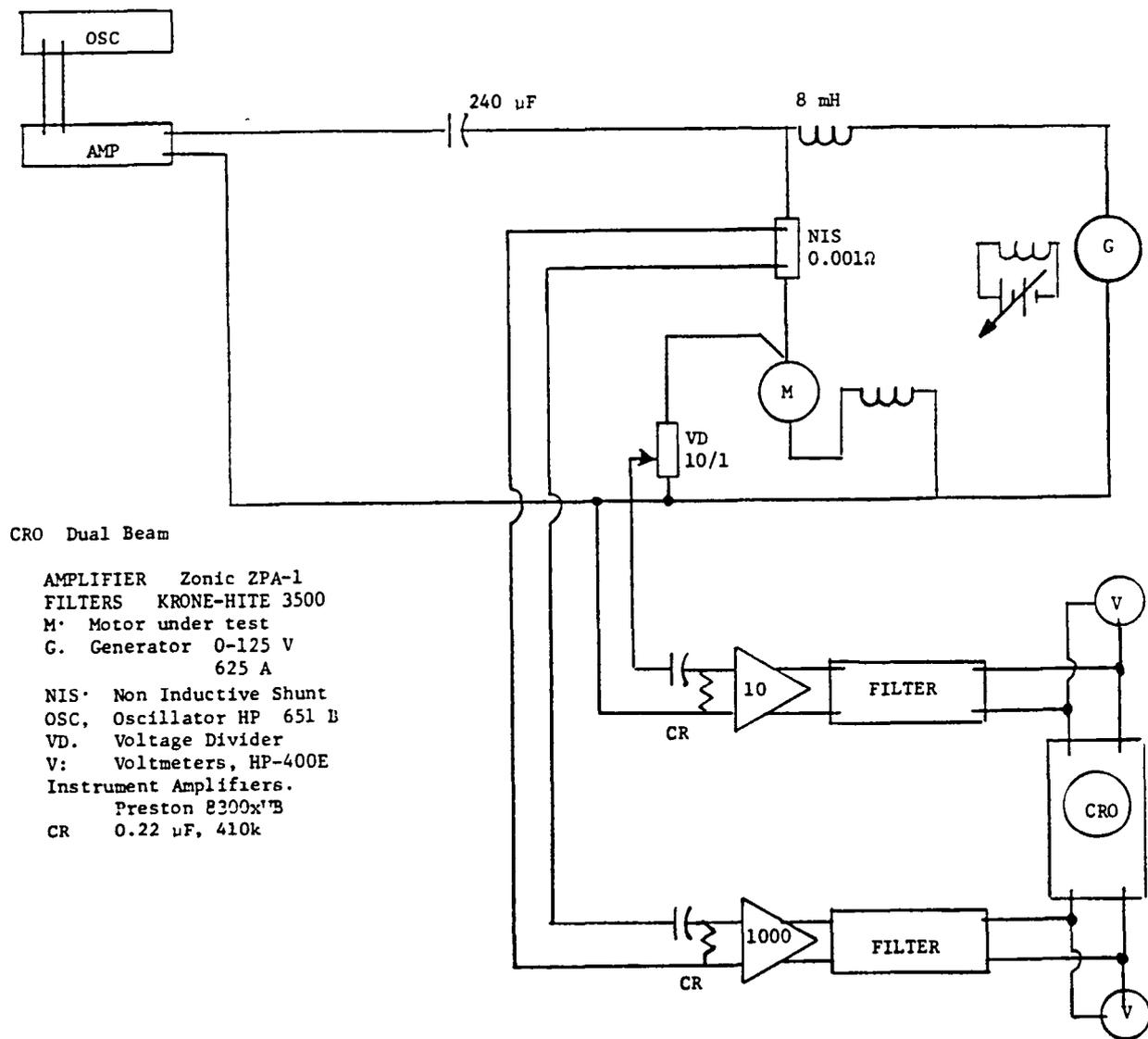
Figure 4   Circuit for Measuring R, L

The current wave forms resulting are as shown in Figure 6 (for continuous conduction).
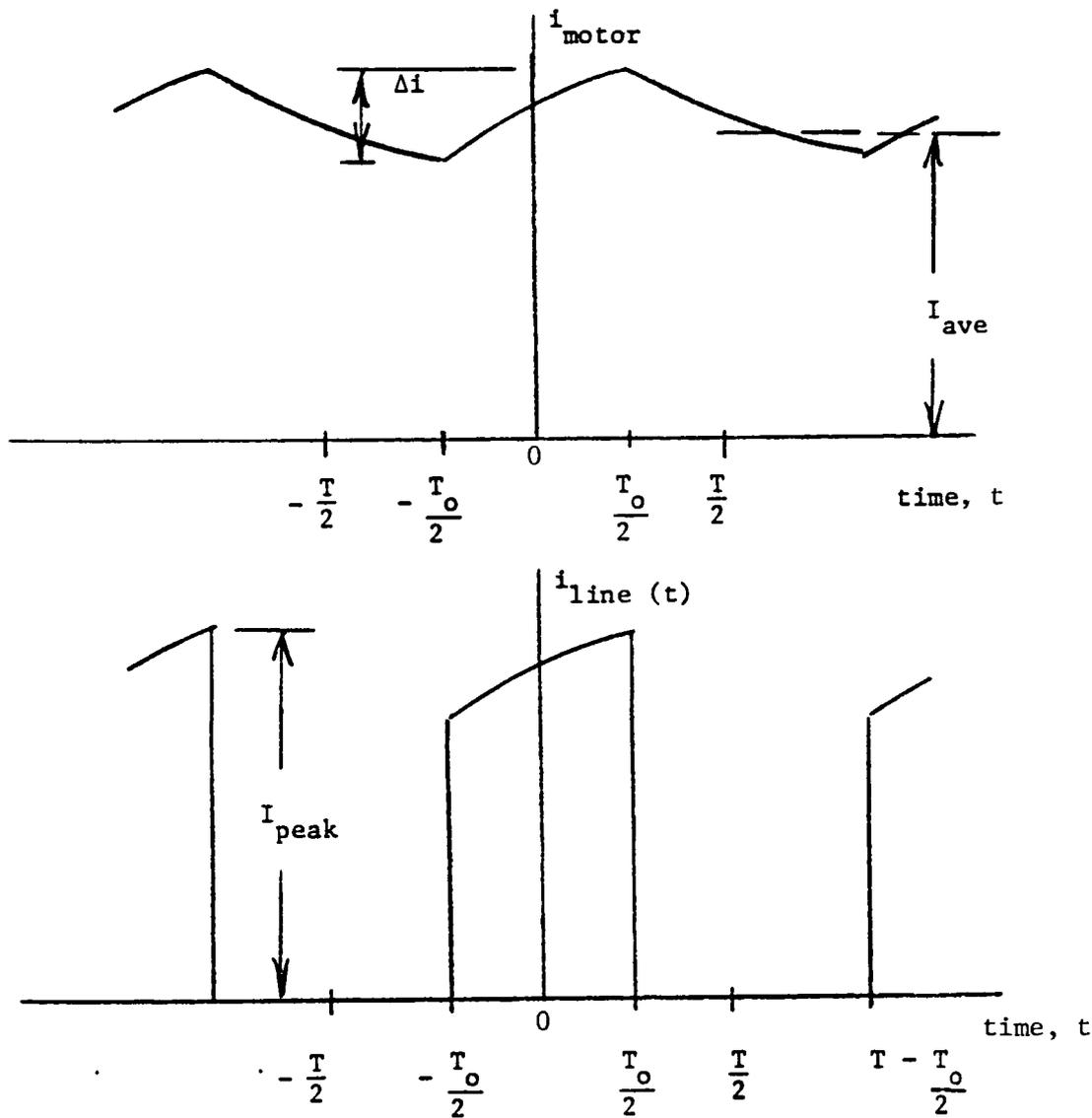
Figure 6   Motor and Line (Source) Current

The motor current flowing from $\dfrac{T_o}{2}$ to $T - \dfrac{T_o}{2}$ circulates through the free wheeling diode (FWD) which is connected back biased and in parallel with the armature and series field.

Franklin (ref. 5) presents the Fourier Series for the motor current as shown. The coefficients are extremely complex and are functions of T, T_o, and V as well as circuit resistance and inductance, and the voltage (or torque constant).

Since the inductance, resistance, and voltage constant are all functions of frequency and saturation of the magnetic circuit, Franklin's Fourier Series does not appear to be widely used nor can it be feasibly used. However, with the use of simplifying assumptions it is possible to obtain an approximate solution for the currents and obtain insight into what may be expected in the way of harmonic content. The assumptions are:

1) constant inductance, L
2) the armature-field time constant (L/R) is long relative to the on-time, T_o, i.e., di/dt is constant. (This was found not to be a reasonable assumption for the motors tested in this investigation).

With these assumptions, the exponential variations become linear and the Fourier Series for the currents becomes:

for line current:

$$i(t) = I_o + \sum \left(\frac{\Delta i}{T_o} \frac{T}{n^2 \pi^2} \sin \frac{n\pi T_o}{T} - \frac{\Delta i}{n\pi} \cos \frac{n\pi T_o}{T} \right) \sin \frac{n2\pi t}{T} +$$

$$+ \frac{2I_o}{n\pi} \left(\sin \frac{n\pi T_o}{T} \right) \cos n \frac{2\pi t}{T} \qquad (2)$$

for motor current:

$$i(t) = I_o + \frac{\Delta iT}{(T-T_o)\pi} \sum \frac{1}{n^2} \left(\frac{\sin n\pi T_o/T}{n\pi T_o/T} \right) \sin \frac{n2\pi t}{T} \qquad (3)$$

It should be noted that an expression for Δi can be derived as follows:

$$\frac{di}{dt} = \frac{\Delta i}{\Delta t} = \frac{\Delta i}{T_o} = \left(V - \frac{VT_o}{T} \right) \frac{1}{L}$$

or,

$$\Delta i = \frac{V}{L} \left(1 - \frac{T_o}{T} \right) \left(\frac{T}{T} \right) T_o = \frac{V}{Lf} \left(1 - \frac{T_o}{T} \right) \frac{T_o}{T} \qquad (4)$$

In order to examine the validity of using the "linearized" equations presented above and to check Franklin's rigorous equation, tests were conducted to obtain the harmonic content under various chopper-motor operating conditions.

The motor used for the tests was the RED* motor, rated 200 amperes with all field windings in series. Harmonic content was measured with a spectrum analyzer, calibrated to read harmonics 1 through 11, in rms values. The CRO display was photographed and values scaled from the photos.

The test overall objectives were:
1) to determine harmonic magnitudes for loss and efficiency calculations,
2) to check for correlation with derived Fourier Series, for both currents and voltage.

To determine, for currents, the variation with respect to saturation and frequency:

3) The percent ripple
4) the ratio of peak to average current, I_p/I_{ave}
5) the ratio of current excursion to average current, $\Delta i/I_{ave}$
6) the ratio of root mean square to average current, I_{rms}/I_{ave}
7) the harmonic amplitudes
8) to determine the error introduced in calculating motor current excursion, Δi, during the duty cycle under continuous conduction situations using the formula that neglects circuit resistance and assumes constant circuit inductance.

Figure 7 presents a typical voltage waveform and its harmonic spectrum. Table 1 tabulates the root mean square (rms) value of the measured harmonics for various frequencies and motor currents.

TABLE 1 Measured Voltage Harmonics (rms)

Harmonic Number

FREQ	I_m	1	2	3	4	5	6	7	8	9	10	11
100	198	31.4	—	10.8	1.6	6.4	1.1	4.4	1.1	3.4	—	—
200	107	32.7	3.3	11.5	2.9	7.3	3.2	5.5	3.1	4.0	2.7	3.6
200	199	31.1	—	10.9	—	6.9	1.6	4.9	1.4	4.4	1.1	4.1
400	110	32.6	4.3	12	3.9	7.6	3.2	5.5	1.9	3.9	.8	2.7
400	199	31.1	1.6	11.5	2.2	7.4	2.7	6	2.5	4.5	2.3	3.8

FREQ   repetition frequency, Hertz

I_m average motor current

*A code name for the wave wound motor. Refer to APPENDIX A for details
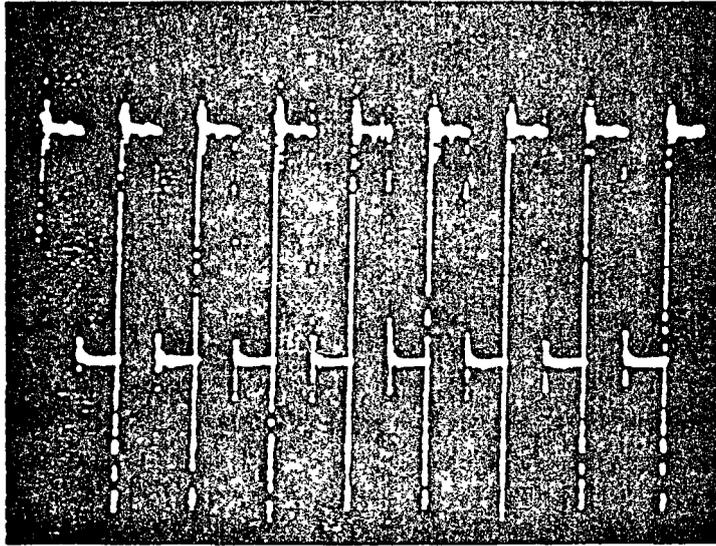
19.2 volt/div
2 ms/div
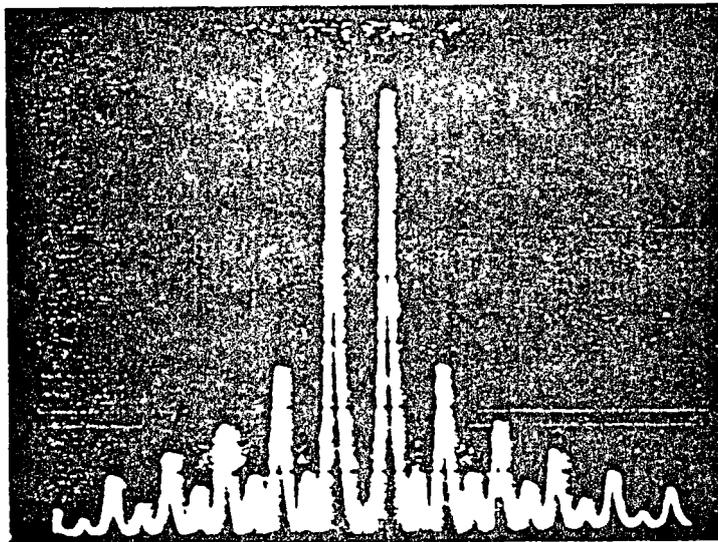
1 kHz/div
4.8 volts/div
(rms)

400 Hz; $T/T_o = 0.5$; I motor = 110; I line = 64

Figure 7   Voltage Waveform and Harmonic Analysis

Although theoretically no even harmonics are generated, they are in fact present. This is explained by the fact that the voltage is a) not a constant during "on time" (due to resistance drop), b) is not zero during "off time", (due to free wheeling diode drop) and c) surges and oscillations are present. Scaling errors are also present.

The rms value of the alternating components of, for example, the test at 400 Hz, $I_m = 110$, is 36.9 volts. The average voltage (based on 80 volts open circuit) was 40 volts. The net rms voltage is $\sqrt{40^2 + 36.9^2} = 54$ volts.

The zero voltage level is at the top of the photos. (For instrumentation reasons voltage-increase is in the down direction.) A typical voltage wave form is reproduced in Figure 8 (inverted, with + upward).
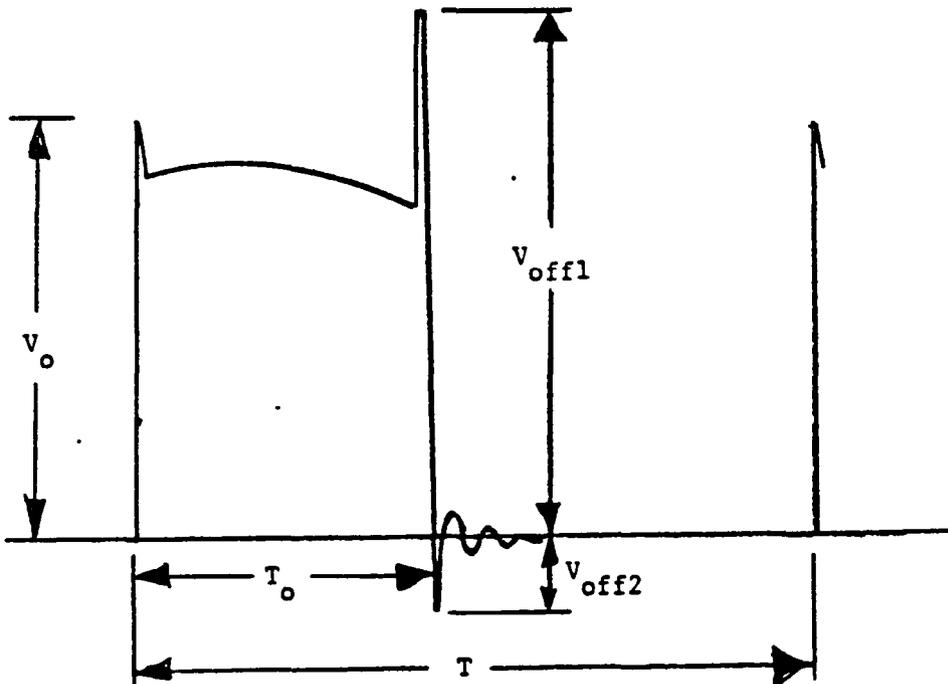
Figure 8   Typical Voltage Waveform

High frequency surge oscillations occur on turn-on and on turn-off due to distributed capacitance interacting with circuit inductance. Typical values of some of the voltage surges V_o, V_{off1}, V_{off2} observed are shown in Table 2.

The observations that can be made here are that the peak surges (up to 1.41 p.u. at turn-off, 400 Hz) are independent of current level but do increase with frequency, approximately to the 0.24 power.

TABLE 2 Turn-Off Voltage Surges

- Voltage Surges -

FREQ	I_m	V_o	V_{off1}	V_{off2}
100	198	77	90	15
200	107	77	107	23.5
200	199	73	107	30
400	110	80	113	15
400	199	80	113	28

The CRO photos shown in Figure 9 are typical of the current waveforms observed. As average motor current increases, or as frequency increases, the waveforms change rather dramatically. Current excursion, Δi, decreases sharply as frequency is increased from 100 to 400 Hz (as expected from equation 4). Also, the excursions tend to become more 'linear' as both frequency and average current are increased (due to decreasing inductance with increasing current level). However, based on measured values of inductance and apparent resistance as a function of frequency and saturation on this motor, L/R of the motor was found to be $0.227f^{-0.94}$.

The tests, for photos shown, were conducted with $T_o/T = 0.45$. Since $T = f^{-1}$, the ratio of on-time to the circuit time constant is:

$$\frac{T_o}{L/R} = \frac{0.45}{f} \frac{f^{0.94}}{0.227} \simeq 2 \tag{5}$$

from which it can be seen that "on time" is nearly 2 time constants in duration and approximately independent of frequency, which indicates the assumption made in deriving the linear relationships is not a valid assumption and considerable error will result if used. Also, it contradicts the increasing Δi linearity with increasing frequency.

The observed fact that current increase and decay becomes more linear with increase in saturation and frequency is apparently due to eddy current effects, which retard the change of flux in the iron surrounding the conductors.

Tests were conducted over the frequency range of 67 to 400 Hz, at brush positions from mechanical neutral ($0°$) to $28°$ against rotation (magnetic neutral) ($-28°$). Data obtained from the photos taken (waveform and spectrum analyzer) is the basis for the results plotted in the following figures.

Figure 10 shows typical harmonic spectra for motor and line current. These spectra are for 100 Hz, with the brushes on $0°$ and on $-28°$. Brush shift has no effect on harmonic magnitude distribution. The average motor current was 200 amperes, the average line current, 104 amperes. Figure 11 is a plot of the
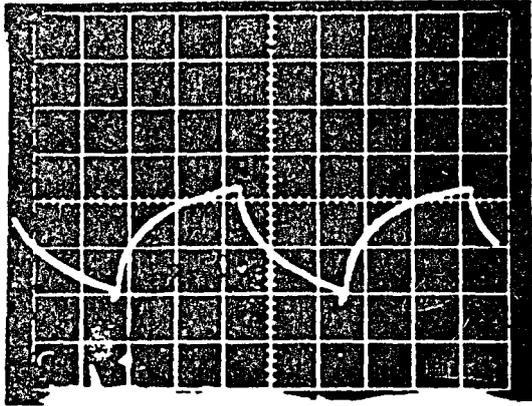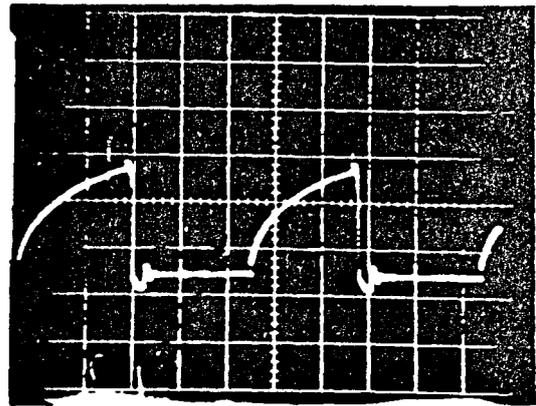
I motor = 62 amperes   I line = 42 amperes

f = 100 Hz, 50 a/div, 2 ms/div, To/T = 0.45
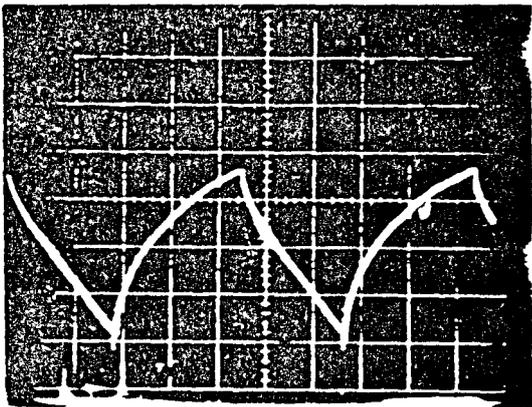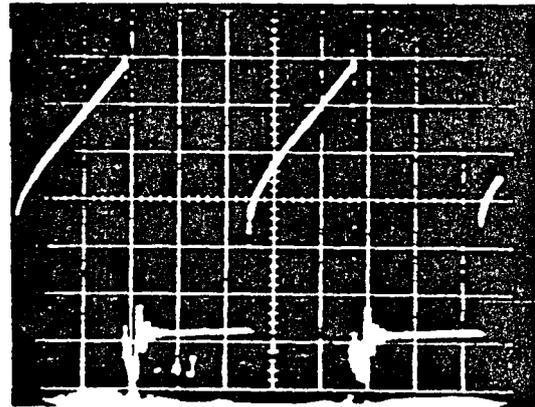
I motor = 201 amperes   I line = 105 amperes

f = 100 Hz, 50 a/div, 2 ms/div, To/T = 0.45
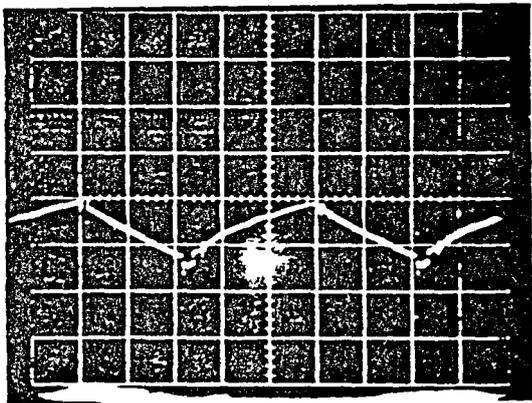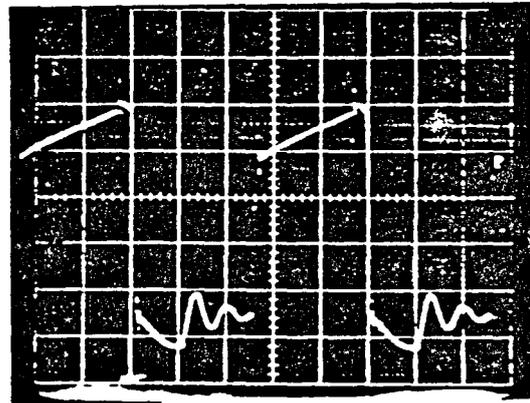
I motor = 208 amperes   I line = 102 amperes

f = 400 Hz, 50 a/div, 0.5 ms/div, To/T = 0.45

Figure 9   Typical Line and Motor Current Waveforms

Amperes (rms)

f = 100 Hz

I_{line} = 104 amp

I_m = 201 amperes
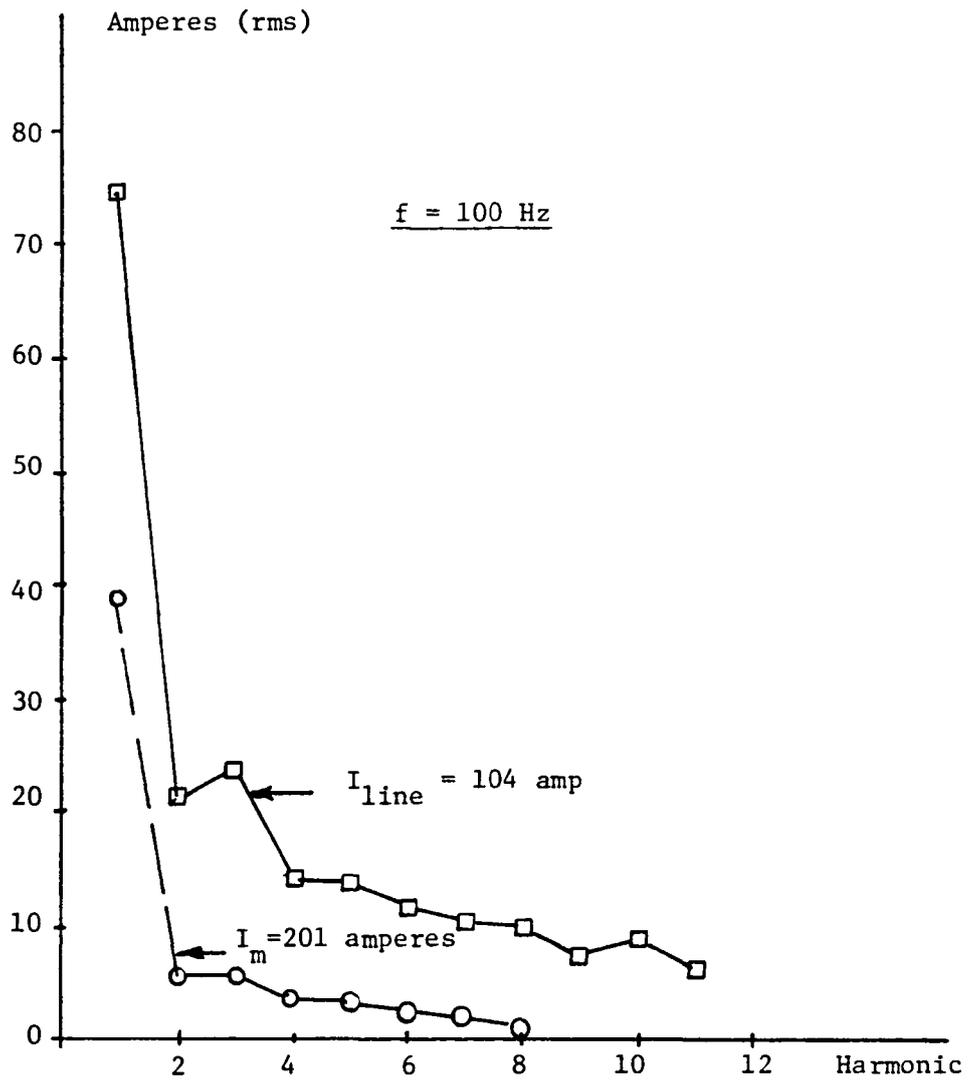
Harmonic

Figure 10 Typical Harmonic Spectrum
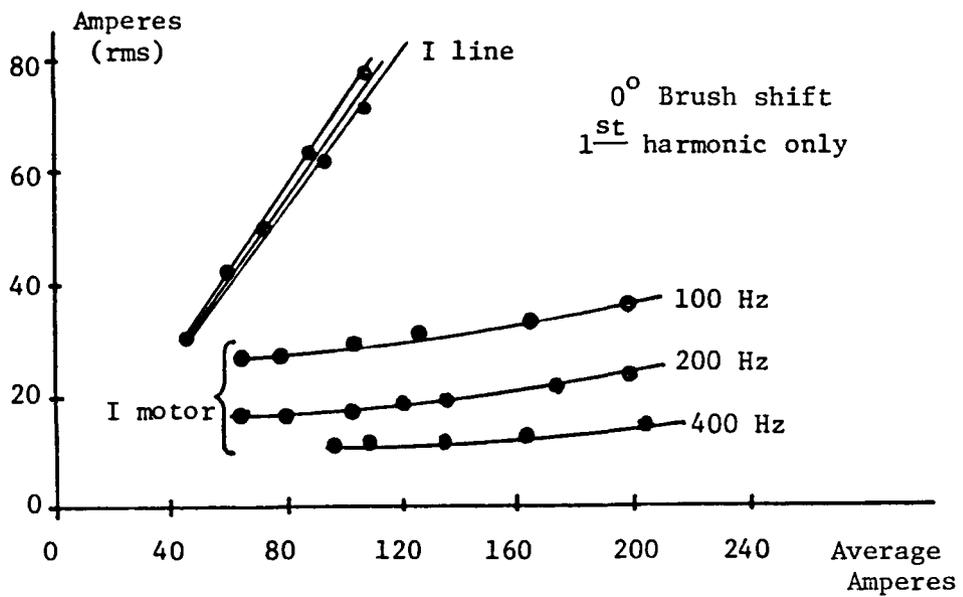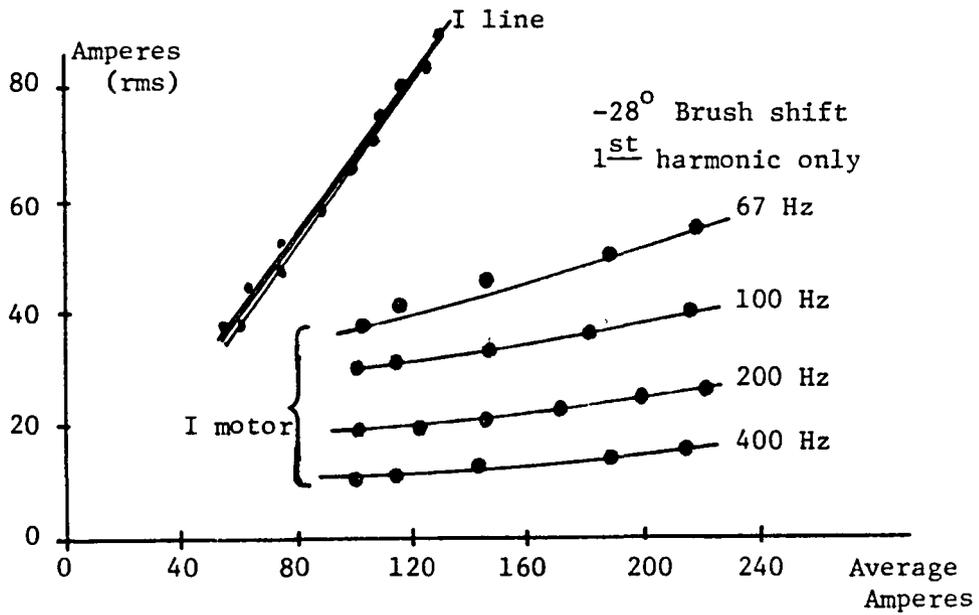
Figure 11 1st Harmonic Variations

1st harmonic magnitude of motor and line current as a function of frequency, average current and brush shift. As can be seen, the 1st harmonic of line current is nearly independent of frequency and is highly dependent upon average current level. The 1st harmonic of motor current, for a given frequency is nearly independent of average current level but highly frequency dependent.

The ratio of root mean square to average value of current was calculated. For all frequencies, the ratio, for line current, varied from 1.25 to 1.2. The variation, for motor currents, $100 < I_m < 210$, was as shown in Table 3.

TABLE 3 Ratio of rms/average Motor Current

Frequency	I_{rms}/I_a (motor)
67	1.03 - 1.07
100	1.02 - 1.05
200	1.01 - 1.02
400	1.002 - 1.008

The percentage or ripple current, calcuated as:

$$\% \text{ Ripple } = \sqrt{\frac{\Sigma I_i^2}{I_{ave}}} \tag{6}$$

is shown in Figure 12 for various frequencies and average amperes. As can be seen, motor current ripple is nearly inversely proportional to frequency (lower Δi) whereas line current ripple is not so heavily frequency dependent. Motor current % ripple decreases considerably (by about 33%) as average current increased from 30-100% of rating. The percent ripple current is independent of brush shift. Figure 13 depicts the variation of the ratio of peak to average motor current; Figure 14 shows the ratio of current excursion (Δi), during a duty cycle, to average line and motor current. These ratios are nearly inversely proportional to frequency. These latter ratios were found to be brush position sensitive (because L decreases about 20% with a -28° brush shift).

Observed values of Δi as T_o/T is varied from 0.1 to 0.6 are plotted in Figure 15. The values are for $T = 0.010$ seconds (100 Hz) speed at 1000 rpm, voltage at 86 volts. The variation in average motor current is also shown.

Equation (4), with L = 0.91 mH (value for 100 amperes, 100 Hz, which occurs at $T_o/T = 0.3$) and V = 86 volts was used to calculate Δi for various T_o/T. This theoretical, linearized variation is also shown in Figure 15. Considerable error is present. For example, at $T_o/T = 0.3$ the calculated value of $\Delta i = 198$

-22-
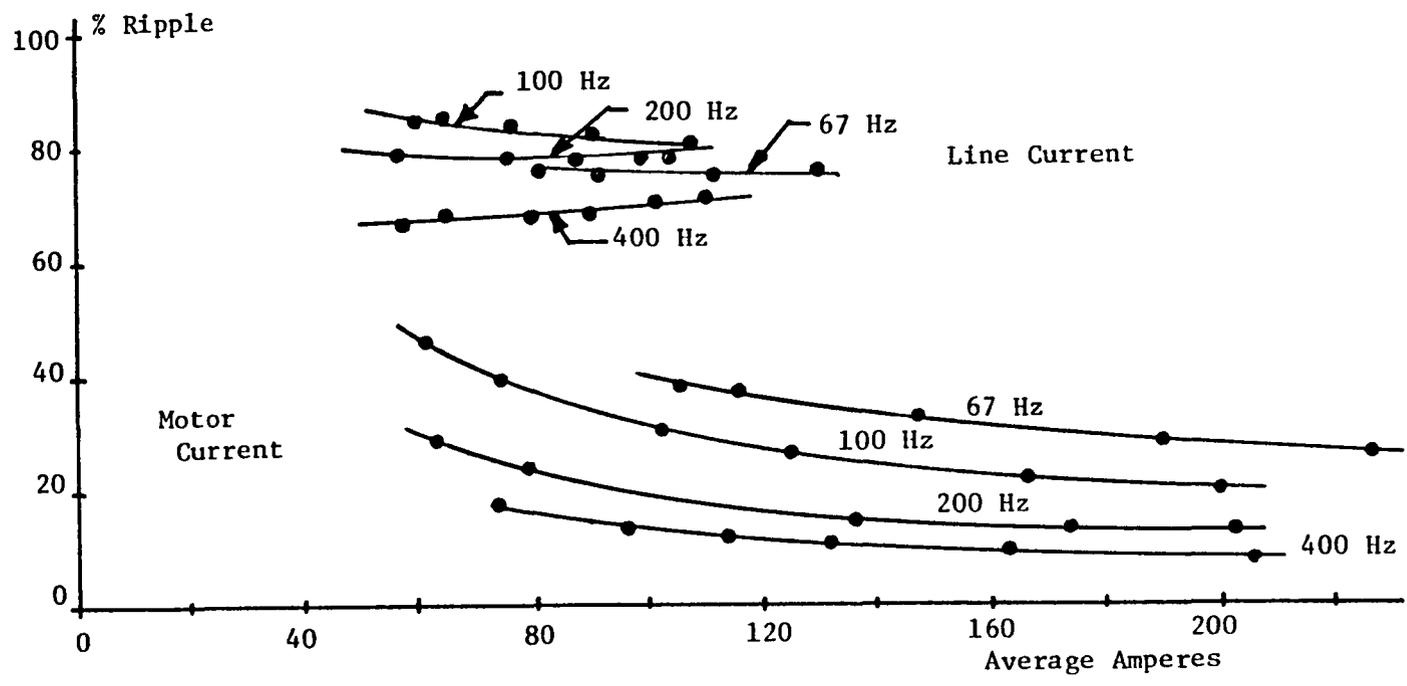
Figure 12   % Ripple Current

$$\% \text{ Ripple} = \frac{\Sigma \sqrt{I_n^{\;2}}}{I_{ave}^2}$$

% Ripple

100 Hz

200 Hz

67 Hz

Line Current

400 Hz

Motor
Current

67 Hz

100 Hz

200 Hz

400 Hz

Average Amperes

Figure 13 $I_{peak}/I_{average}$ vs $I_{average}$

$T_o/T = 0.45$

$0°$ Brush Shift

($-28°$ Brush Shift yields values 20% higher)

100 Hz

200 Hz

400 Hz

Average Motor Amperes
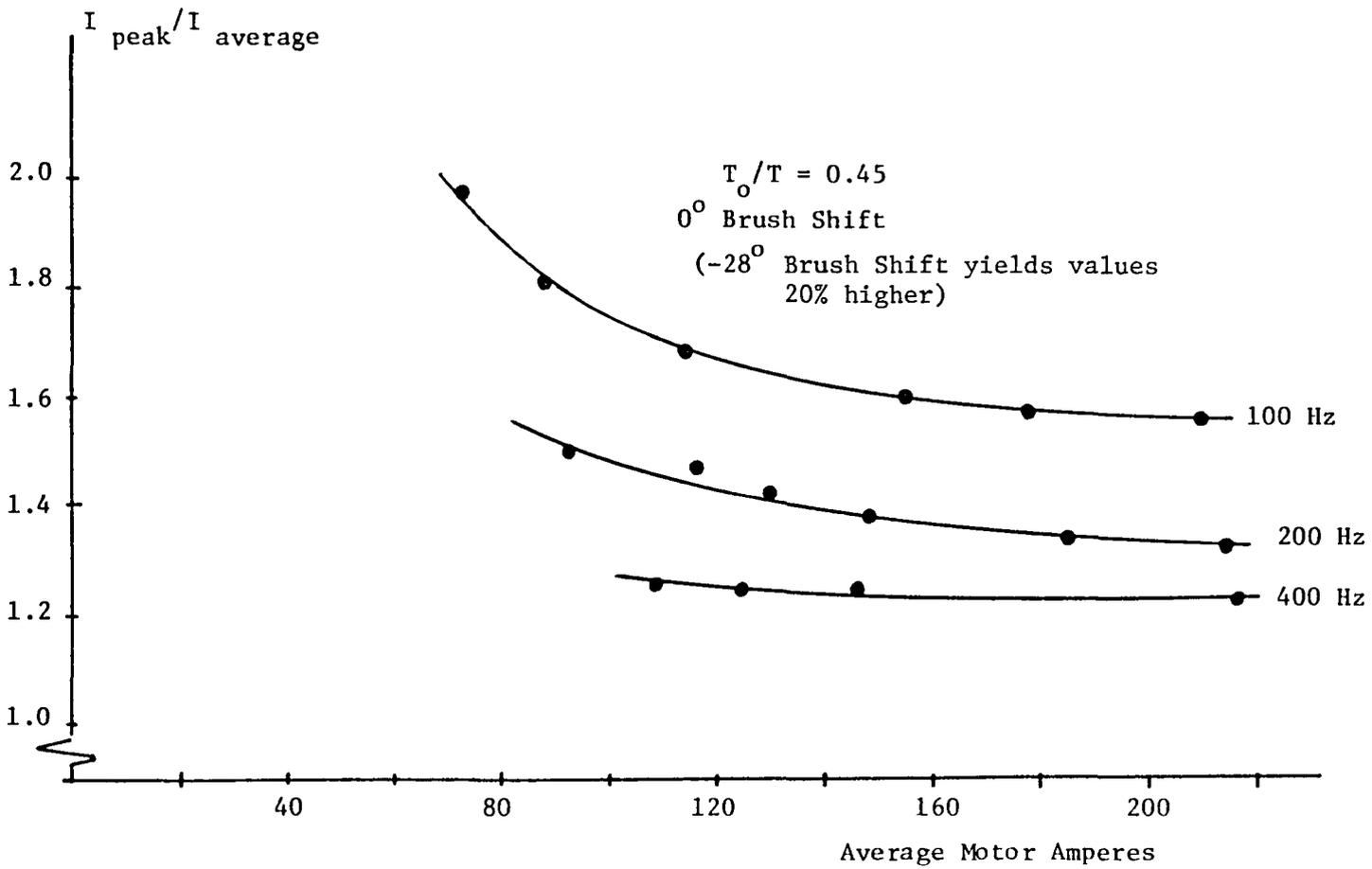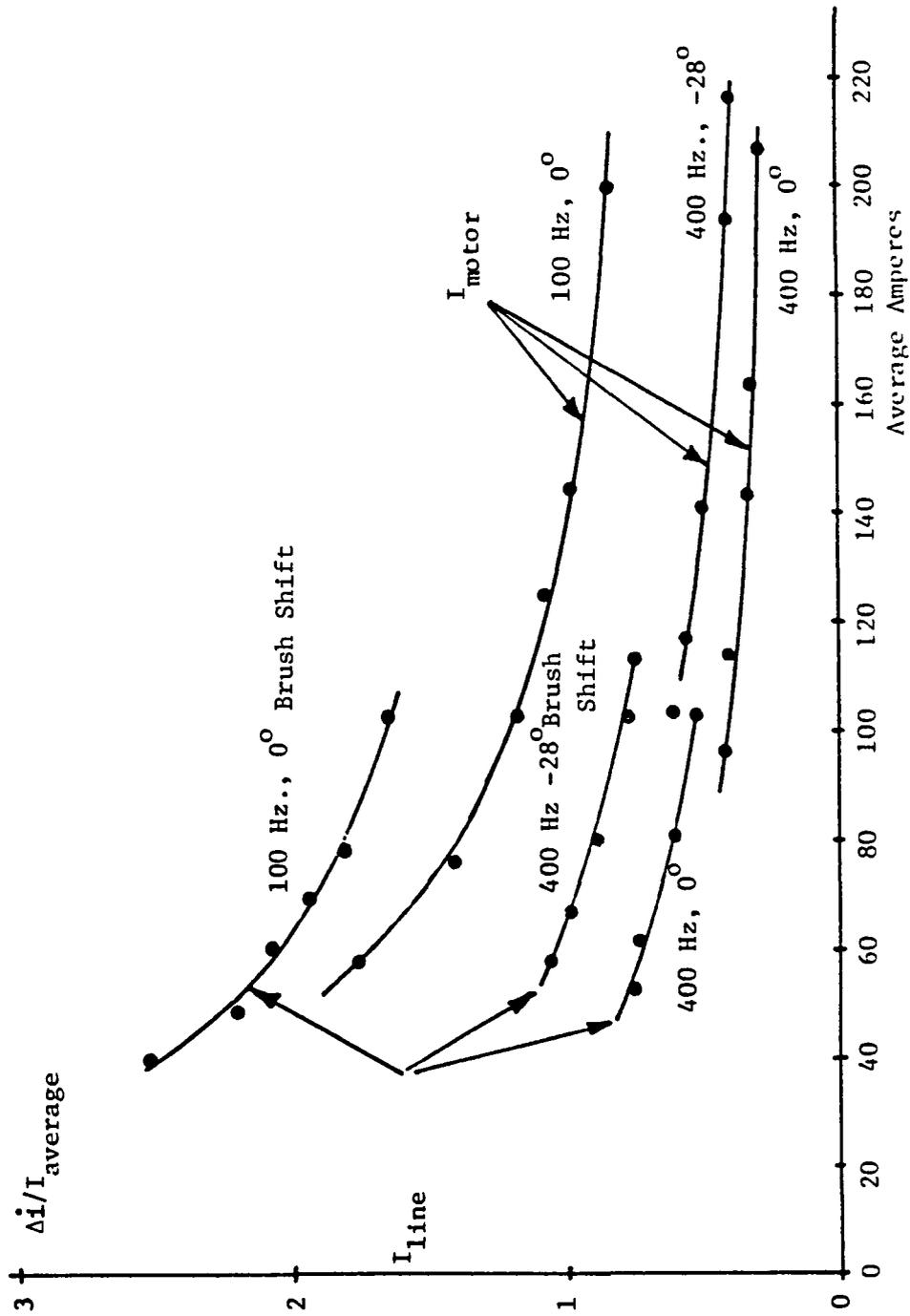
Figure 14   Variation of $\Delta i/I_{average}$ as a Function of
Frequency, Brush Shift and Saturation
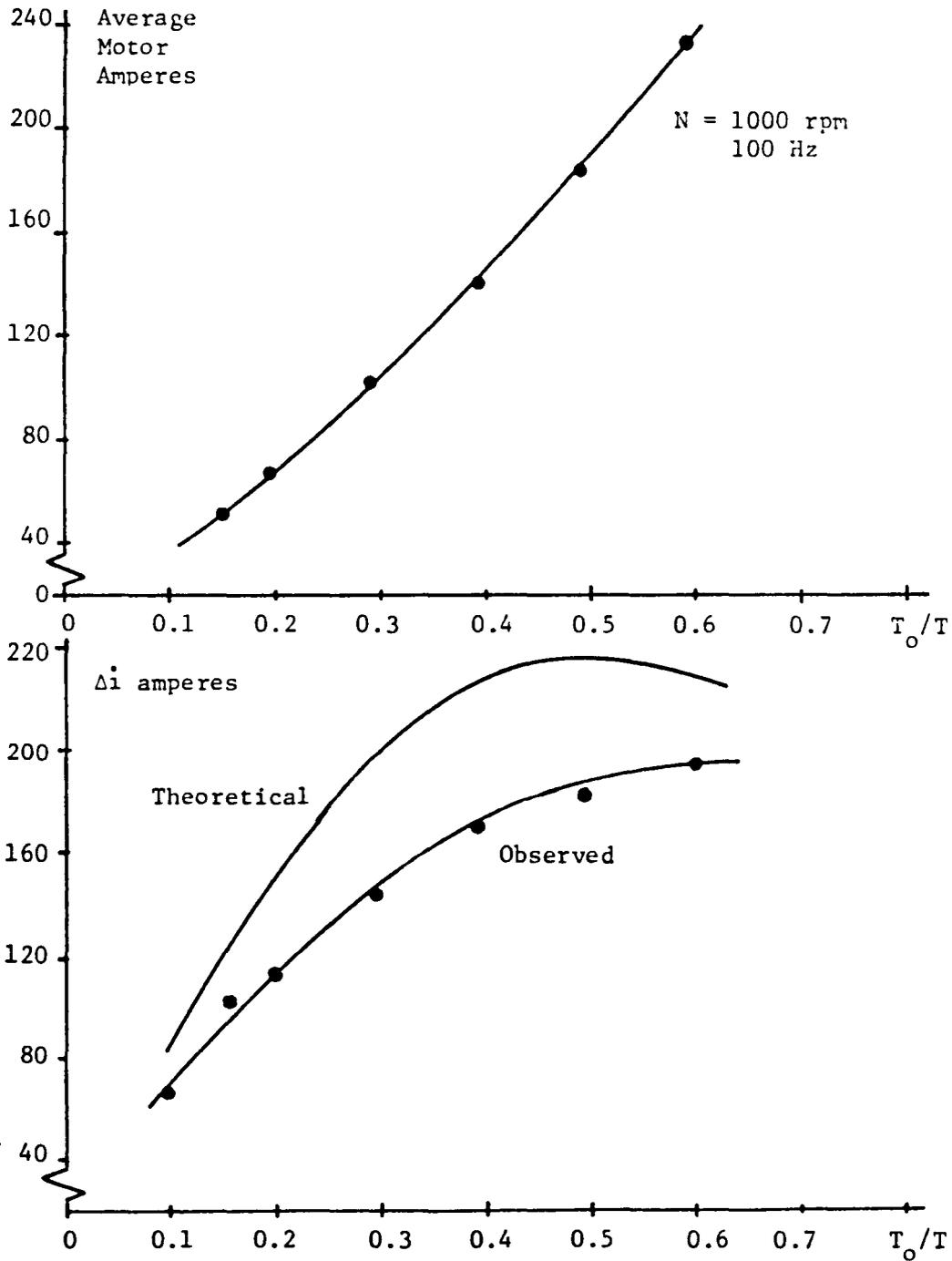
FIGURE 15 Variation of I_{avc} and Δi as a Function of T_o/T

amperes is 1.42 times the observed experimental value of 150 amperes.

According to equation (4) the value of Δi at $T_o/T = 0.5$ should be the same as the value at 0.4. The actual value at 0.6 is 1.14 times greater than the value at 0.4. This is no doubt due to the heavy level of saturation (230 amperes) and lower inductance than at $T_o/T = 0.4$ (140 amperes).

Typical measured harmonic values for 100, 200 and 400 Hz $T_o/T = 45$ and saturated and relatively unsaturated conditions are presented in Table 4 (page 28). The values in ( ), beneath the observed values are calculated values, using Franklin's formulae.

Attempts were made to try to correlate calculated values of the Fourier Series representations with observed current waveforms.

Referring to equations (4) and (5), pertaining to the linearized representation of motor current, it can be seen that the motor current harmonics are proportional to the current excursion, Δi and inversely proportional to n^3, where n is the order of the harmonic. Since Δi is inversely proportional to the chopper frequency the harmonic magnitude also has that proportionality.

Table 5 is a tabulation of observed and calculated (from the observed Δi, using equation 4) rms values of the fundamental harmonic of motor current. Harmonic values calculated using the value of Δi from equation (4) were greatly in error.

Table 5 Fundamental Harmonic, Motor Current (rms)

Frequency	Ave. I_m	Obs. Δi	-1st Harmonic - Observed Value	Calculated Value	% error
100	201	173	36.5	49.6	36 %
100	104	123	29.6	36	21.6%
200	204	125	22.7	35.7	57.3%
200	106	77	18	22	22 %
400	208	57	13.9	16.3	17 %
400	98	41	11.9	11.7	2 %

Higher harmonic values are not listed because they are grossly in error. For example, at 100 Hz, 201 amperes, a second harmonic current of 6.5 amperes rms was observed. The value calculated from the linear version was 1.9 amperes.

It can be generalized that the linearized current Fourier Series is useful only in yielding insight into the variational trend of harmonic component magnitudes with the variation of f, L and T_o/T, but calculated values are higher than actual values.

Finally, an attempt was made to correlate harmonic magnitudes calculated using Franklin's formulae, with observed results. Franklin's equations do take into account the variation of voltage constant with saturation but are based on a

TABLE 4 Observed Motor and Line Current Harmonics (rms)

-Harmonic-

HZ	AVE. LINE	AMPS MOTOR	Δi	1	2	3	4	5	6	7	8	9	10	11
	104			75	21.6	23.9	14.1	14.8	11.8	10.2	10.5	8.2	9.1	5.7
		201	173.5	36.4	6.5	6.6	3.1	3.4	2.3	1.7	-	-	-	-
				(13.5)	(7)	(4.9)	(3.9)	(2.9)	(2.7)	(2.2)	(1.7)	(1.5)	(1.5)	(1.5)
100	61		123	43	13	13	8.2	8.2	6	5.7	5.7	4.6	4.7	3.6
		104		29.6	4.3	5.9	2.8	3.2	1.9	-	-	-	-	-
				(4.2)	(2.1)	(1.4)	(1.4)	(.83)	(.7)	(.8)	(.83)	(.79)	(.71)	(.61)
	102		125	61.2	11.8	25	8	15.5	5.7	10.2	3.4	-	-	-
		204		22.7	2.1	3.6	1.1	1.7	1.3	1	1	-	-	-
200				(11.9)	(6)	(4.2)	(3.1)	(2.8)	(2.4)	(2.1)	(1.8)	(1.5)	(1.3)	(1.2)
	59		77	38.6	7	13.6	4.6	8.3	3.4	4.8	1.6	-	-	-
		106		18.2	.7	3.1	.6	1.7	-	1.0	-	-	-	-
				(2.9)	(1.6)	(1.3)	(.9)	(.6)	(.47)	(.38)	-	-	-	-
	101		57	71.6	9.6	25.5	2.7	11.8	5.7	13.4	-	7.73	2.7	7.3
		208		13.9	1.7	2.4	1.3	1.1	.9	-	-	-	-	-
400				(13.1)	(6.3)	(4.5)	(3.3)	(2.5)	(1.9)	(1.5)	(1.3)	(1.1)	(.93)	(.82)
	54		41	33.5	7.4	10.5	5.7	4.6	4.6	3.4	3	3	1.9	4.6
		98		11.9	.91	2.4	.4	1.5	.7					
				(.95)	(.12)	(.06)	(.1)	(.15)	(.17)					

NOTE: T_o/T = 0.45 Throughout, RED MOTOR

constant value of L and R. Use of the dc resistance of 0.0254 ohms and the value of L, at 100 Hz, saturated, of 0.91 mH were chosen as representative values which should yield maximum value of harmonics. The calculated results are shown, for motor current, in ( ), immediately below the observed values in Table 4. As can be seen, the calculated values are grossly in error and predict only a fraction of the magnitude of hamonic observed – especially for the lower harmonics. The magnitude of lower harmonics may have some error due to error in magnitude measurement. The error is much greater than that resulting from calculations using the linearized version of motor current!

The inescapable conclusion of these tests is that accurate analytical prediction of harmonic current magnitude is not possible with either representation and that accurate values can be obtained only by actual measurement.

Instrumentation Requirements

Average values of current and voltage can be measured using noninductive shunts (NIS) and variable sample rate digital voltmeter (DVMs). The NIS shunt used in this test program was 0.001 ohm, 275 amps continuous with a 6.5 MHz bandwidth.

Tests were conducted to compare voltage drop waveforms and average values of the response from the noninductive shunt, a "conventional" off-the-shelf instrument shunt and a conventional shunt modified to attempt to cancel the field established by the shunt itself. The modification was not noticeably effective. A difference of about 2% was noted in the average readings of the conventional shunt and NIS and as much as 2-to-1 difference in observed magnitude of high frequency oscillations after thyristor cut-off. If accuracy of waveforms and current values is required, it is essential to use noninductive shunts.

Power measurements also require consideration due to the complex waveforms of voltage and current. The necessity for a wattmeter with a wide bandwidth response is portrayed graphically in Figure 15, which shows the ratio of power indicated by the Clark-Hess electronic wattmeter (with 0.6%fs accuracy over the frequency range dc to 30 kHz) and the product of motor current and voltage as read by the average reading DVMs. Errors shown range from 4% at 400 Hz, with reduced current excursion, Δi, to 33% at 100 Hz (increased $i\Delta$).

A theoretical insight into wattmeter bandwidth can be obtained by multiplying equations (1) and (2) to obtain the product of instantaneous, linearized, voltage and line current which yields instantaneous power. When this is integrated over a complete period, true power is obtained as:

$$P_{true} = V I_o \frac{T_o}{T} + \sum_{n=1}^{\infty} 2 V I_o \left(\frac{T_o}{T}\right)^2 \left(\sin \frac{n\pi T_o/T}{n\pi T_o/T}\right)^2 \qquad (7)$$
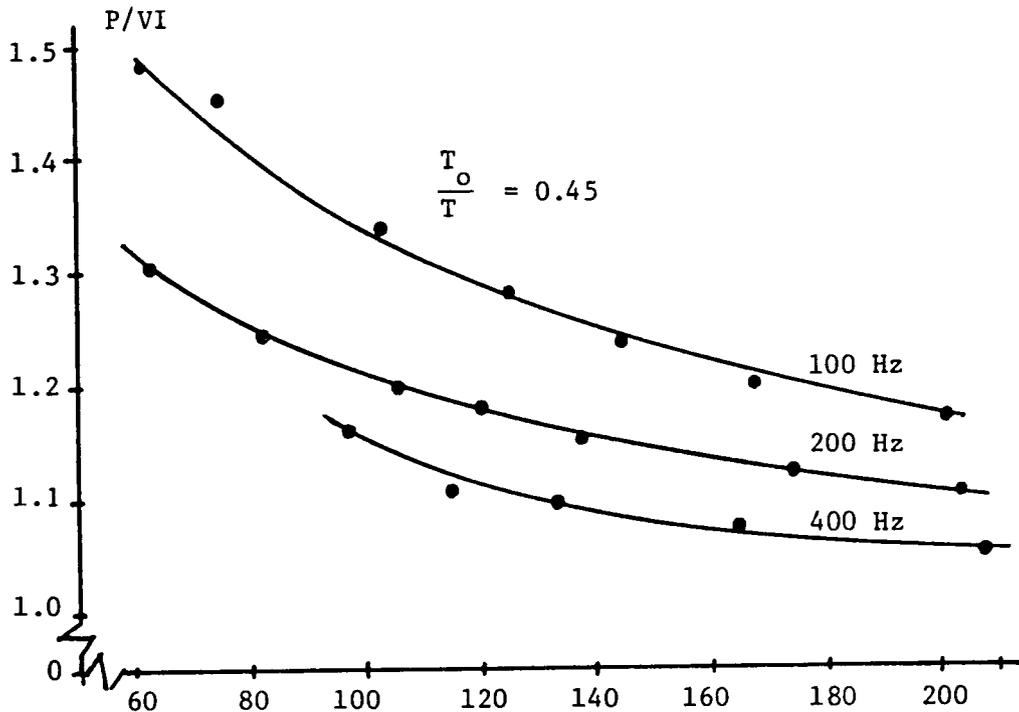
Figure 16 Ratio of Power to Volt-ampere Product

whereas actual power, P_{act} measured is, with a wattmeter with bandwidth to the $k\underline{th}$ harmonic, the same except the summation is form n = 1 to n = k.

The precentage error is:

$$\% \text{ error} = \frac{P_{true} - P_{act}}{P_{true}} \tag{8}$$

The error for values of T_o/T = 0.5, 0.25 and 0.10 for values of harmonic up to 10 are plotted in Figure 17. Theoretically, using the linearized relationships, error is independent of frequency and load current; however, in reality, as seen by the results in Figure 16, which is observed error as a function of motor current, the actual error is both average current and frequency dependent.
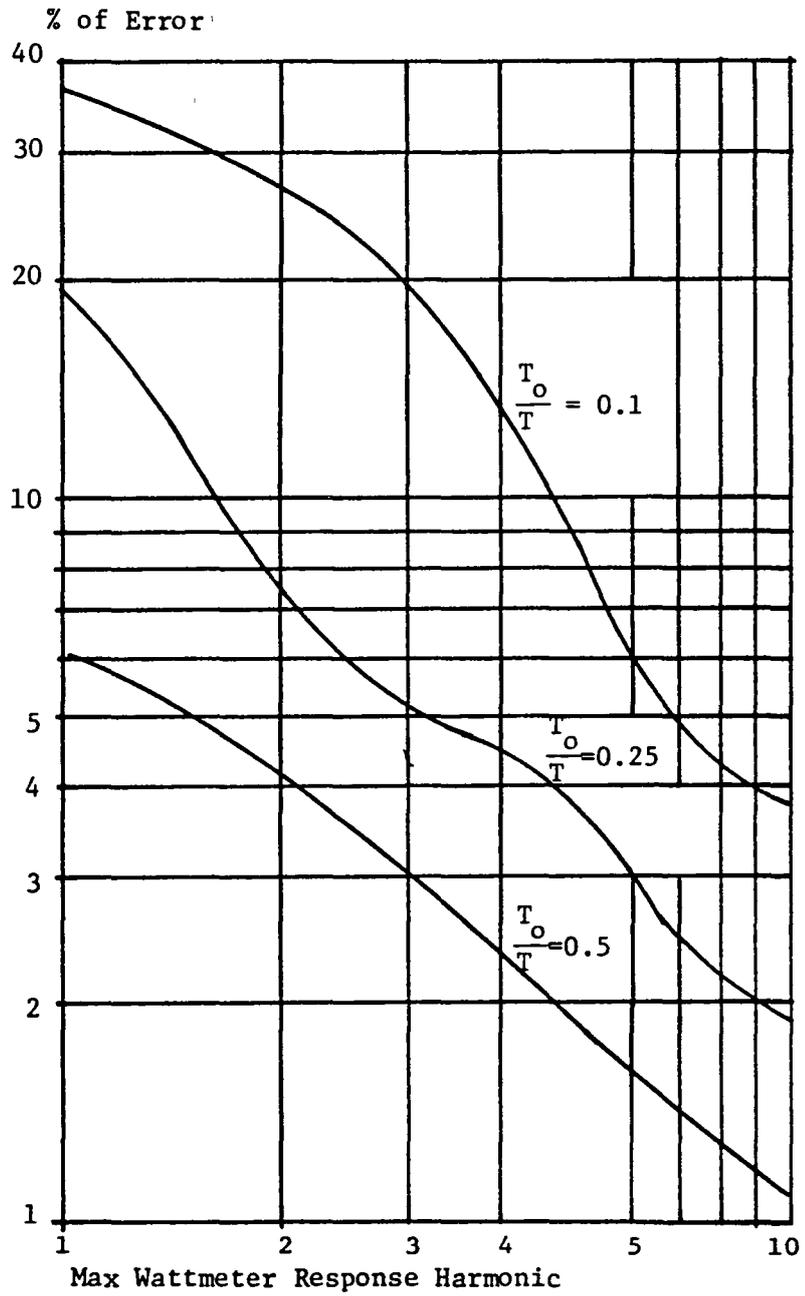
Figure 17 Wattmeter Error

THE CONVENTIONAL MOTOR MODEL

Figure 18 depicts, in circuit form, the model that has been traditionally used for calculating performance and efficiency of dc motors.
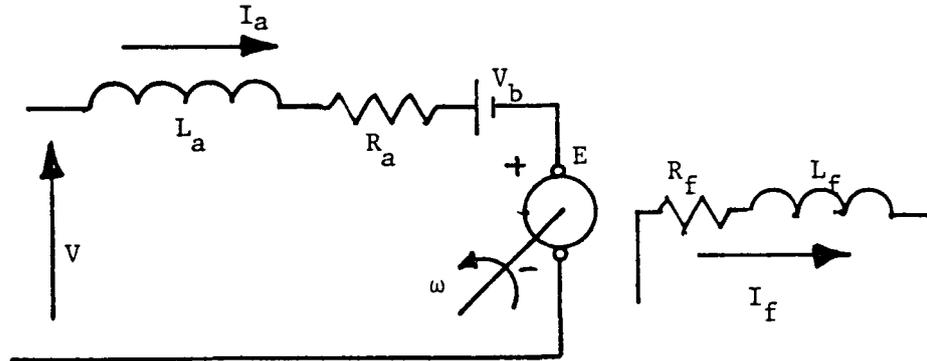
Figure 18   DC Motor Model

For the series motor, $i_f = i_a$ and the field and armature resistance and inductance combine as lumped values, R and L. V_b represents voltage drop across the brush system, E is the counter emf and ω the shaft speed in rad/s.
Equations representing electrical performance can be written as follows:

$$V = R \, i + L \frac{di}{dt} + V_b + E \tag{9}$$

$$E = \frac{Z \, p}{2\pi a} \phi \, \omega = K'\phi \, \omega \tag{10}$$

$$M_e = \frac{E \, i}{\omega} = K'\phi \, i_a \tag{11}$$

where   Z = number of inductors
      p = number of poles
      a = parallel paths in the armature
      ϕ = total flux per pole, Wb.
     M_e = electrical torque, Nm developed
      V = applied voltage.

Since ϕ is proportional to i, $K'\phi$ can be expressed as

$$K'\phi = K \, i_f \tag{12}$$

if it is understood that K is not a constant, but rather a function of excitation, i_f (saturation).

Efficiency can be expressed as:

$$\eta = \frac{P_{out}}{P_{in}} = 1 - \frac{P_{loss}}{P_{in}} \tag{13}$$

where P_{in} is average power input and P_{loss} is the sum of the losses involved in the energy conversion process.

IEEE #113 (ref. 1) details procedures for parameter and performance determination based on ripple free dc or, to a limited extent, dc from a rectifier type supply. The losses addressed consist of:

Joule (I^2R) type losses
Brush contact loss (V_bI)

Rotational Core loss
Stray load loss
Friction, windage and ventilating loss.

Losses are discussed in detail in CHAPTER 3; however, in this brief overview of the use of the conventional model and in presenting its limitations as applied to the motors investigated in this program, the above listed losses are categorized as follows:

a. Joule loss is the I^2R loss in the armature and series field, based on measured circuit resistance.
b. Brush contact loss is based on measured voltage drop across the brush-commutator, including the non-linear carbon resistance and is considered constant.
c. The brushes are supposedly on magnetic neutral and no rotational core loss is present.
d. Stray load loss cannot be calculated or measured directly and is, in accordance with IEEE #113 (ref. 1), taken as 1% of the output power.
e. The brush and bearing friction and windage are determined experimentally and designated as $p_{f\omega}$.
f. Ventilating requirements are not considered.

Parameter Measurement

Section 4.2, IEEE #113 specifies various methods of armature and field resistance measurement and Section 5.5.3 provides values for V_b for various brush types. In the motors tested, brush (material) types were not known with certainty and therefore a "non-standard" test was utilized to determine V_b and total circuit resistance.

This test is based on the relationship shown in Figure 19.

Armature resistance is, of course, linear (at constant temperature). However, voltage drop across the brushes commences at zero with zero current, rising to a nearly constant value at somewhere between 20 and 40% of rated current in a reasonably designed brush system. The sum of a linear plus constant volt-ampere characteristic is also linear, displaced from the zero· intercept. The linear slope is the copper circuit resistance; the zero current intercept of the extended portion of the total is the brush voltage drop, V_b.
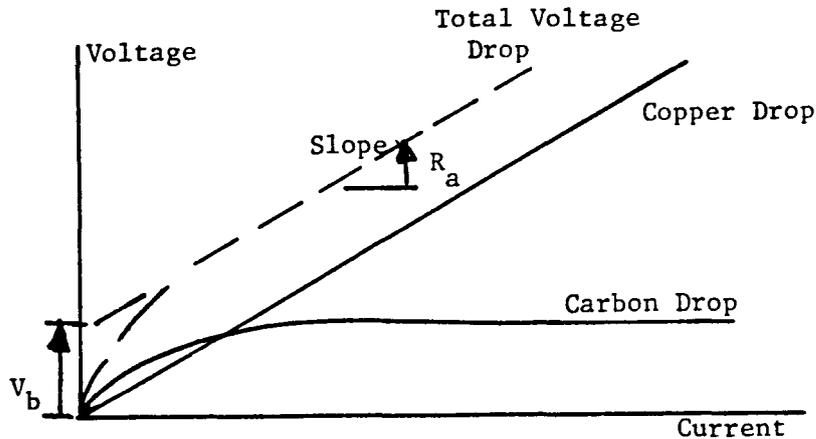
Figure 19 Circuit Resistance and Brush Drop

This technique yielded the following values:

-BLUE* Motor-

Armature, Field and Connectors:	0.0301 ohms
Total Brush Voltage Drop:	0.53 volts

(The manufacturer gave a value of 0.029 ohms)

-RED* Motor-

Armature, Field and Connectors:	0.0354 ohms
Total Brush Voltage Drop:	0.50 volts

The mechanical loss, $P_{f\omega}$, was measured for both the RED and BLUE motors. Curve fit routines were used to establish the following relationships (actual test points are shown in the section of this report where rotating losses are discussed):

BLUE motor: $P_{f\omega} = 0.03 \ (RPM)^{1.18} = 0.43 \ \omega^{1.18}$

RED motor: $P_{f\omega} = 0.072 \ (RPM)^{1.184} = 1.04 \ \omega^{1.184}$

In theory, K can be determined from either torque measurements or from the open circuit saturation (OCS) characteristic, i.e.

$$K = \frac{E}{I_a \omega} \quad \text{or} \quad \frac{M_e}{I_a I_f} \quad\quad (14)$$

If the torque test is made under locked rotor conditions, the measured torque is the electrical torque developed. For a motor without interpoles, the locked rotor test should be made with the brushes located near magnetic neutral. If this is

---

* Code words for the lap wound (BLUE) and wavewound (RED) motors.

-34-

done, the brushes are near, or on, the brush location for proper commutation and are in the normal run location. For a series motor, so locating the brushes accounts for the demagnetizing effect of armature reaction and also for the loss of active conductors due to brush shift, which will exist under running conditions.

K cannot be determined from the OCS curve for a motor to be operated with brushes shifted. Refer to Figures 20, 21 and 22. In Figure 20, two values of K, designated K_v, are shown as calculated from the 2000 rpm OCS curves in Figure 21.

One curve, yielding the highest values of E and K_k, was taken with the brushes on mechanical neutral, i.e. 0° shift. The lower curve is data taken at -28° shift and reflects the loss of active inductors, (since on open circuit, no armature reaction is present). If the brushes are shifted an angle β degrees, the inductors in the region $0 - \beta$ and $\pi-(\pi-\beta)$ have opposite induced voltage in them and this voltage subtracts from the total voltage between brushes. If there are Z' inductors between brushes, the net inductors, for β shift from magnetic neutral, are

$$Z'-Z'(\frac{2\beta}{180}) = Z'(1- \frac{2\beta}{180}) \qquad (15)$$

yielding a ratio of:

$$\frac{K_v \text{ (shifted)}}{K_v \text{ (magnetic neutral)}} = 1 - \frac{2\beta}{180} \qquad (16)$$

In theory, for a 28° shift, this ratio would be 0.68. From Figure 21, the ratio actually observed was between 0.56 and 0.59. The difference is due to inability to precisely determine exact brush position.

If compensating windings, to eliminate and demagnetizing effect of armature reaction, were present, and the brushes were on mechanical neutral, K could be determined from the OCS curve, because magnetic neutral and mechanical neutral coincide.

When the brushes are shifted and the motor loaded, if the brushes are truly on magnetic neutral there is no loss of active inductors; there is a demagnetizing effect due to armature reaction, however. This is the reason why $k_t = K$ is larger at 28° brush shift, than K_v.

The demagnetizing ampere turns per pole are equal to the inductors in the angle of brush shift times the current per armature path,

$$AT_{demag} = \left(\frac{\beta}{360}\right) \left(Z\right) \frac{I_a}{a} \qquad (17)$$

or, the demagnetizing field current is:

$$I_{f \ demag} = \frac{\beta}{360} \frac{Z}{N_f} \frac{I_a}{a} \qquad (18)$$

where N_f = series field turns/pole. For the RED motor, Z = 162, β = 28, a = 2, N_f = 20 (See APPENDIX A).
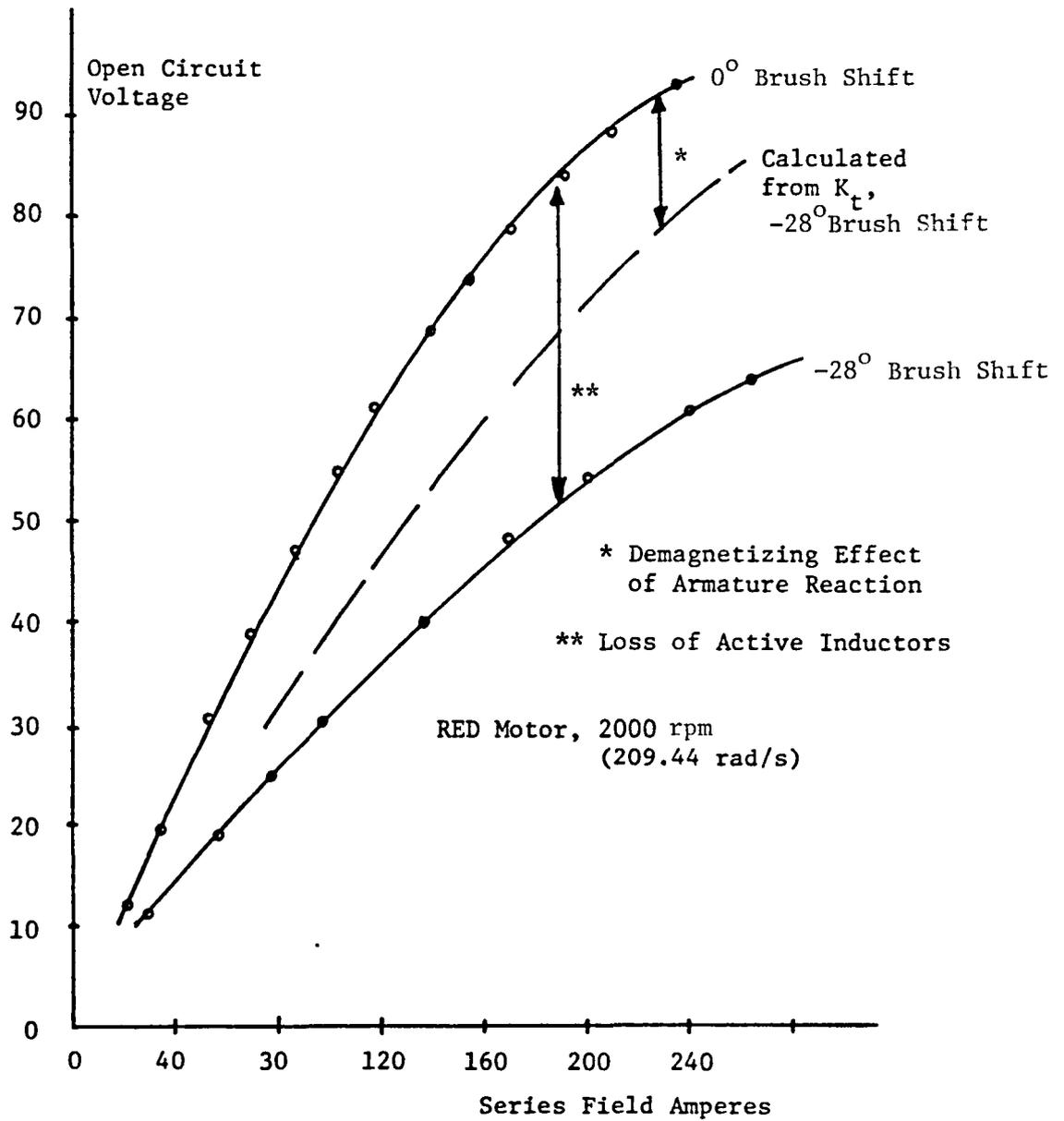
Figure 20 RED Motor Open Circuit Saturation Characteristic

FIGURE 21 RED Motor Torque, Voltage "Constant" Variations

-37-
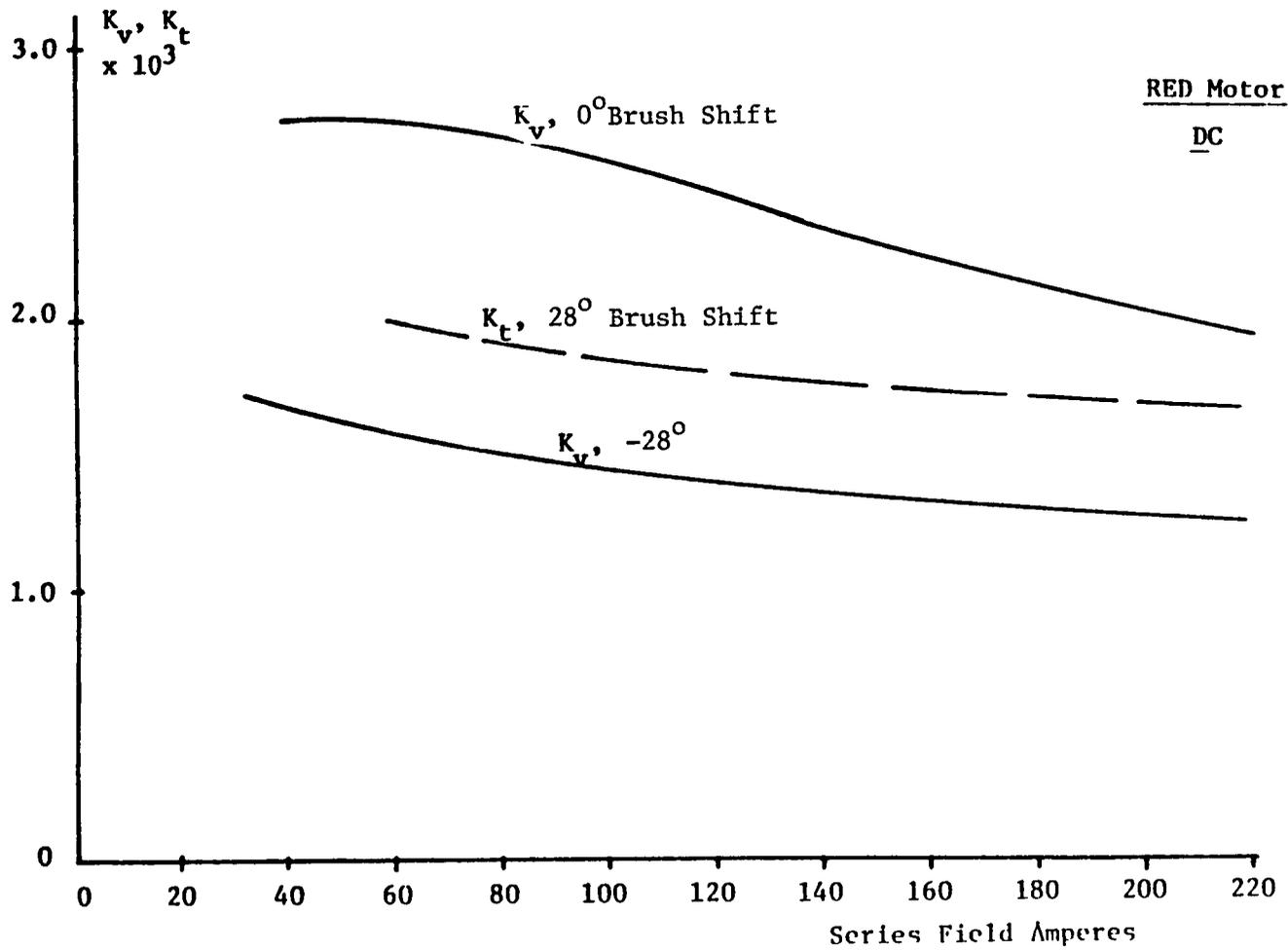
Figure 22 BLUE Motor Torque, Voltage "Constant" Variations

Ripple Free

DC

K_v, K_t

x 10^3

K_v

K_t

-28° Brush Shift

Average Amperes
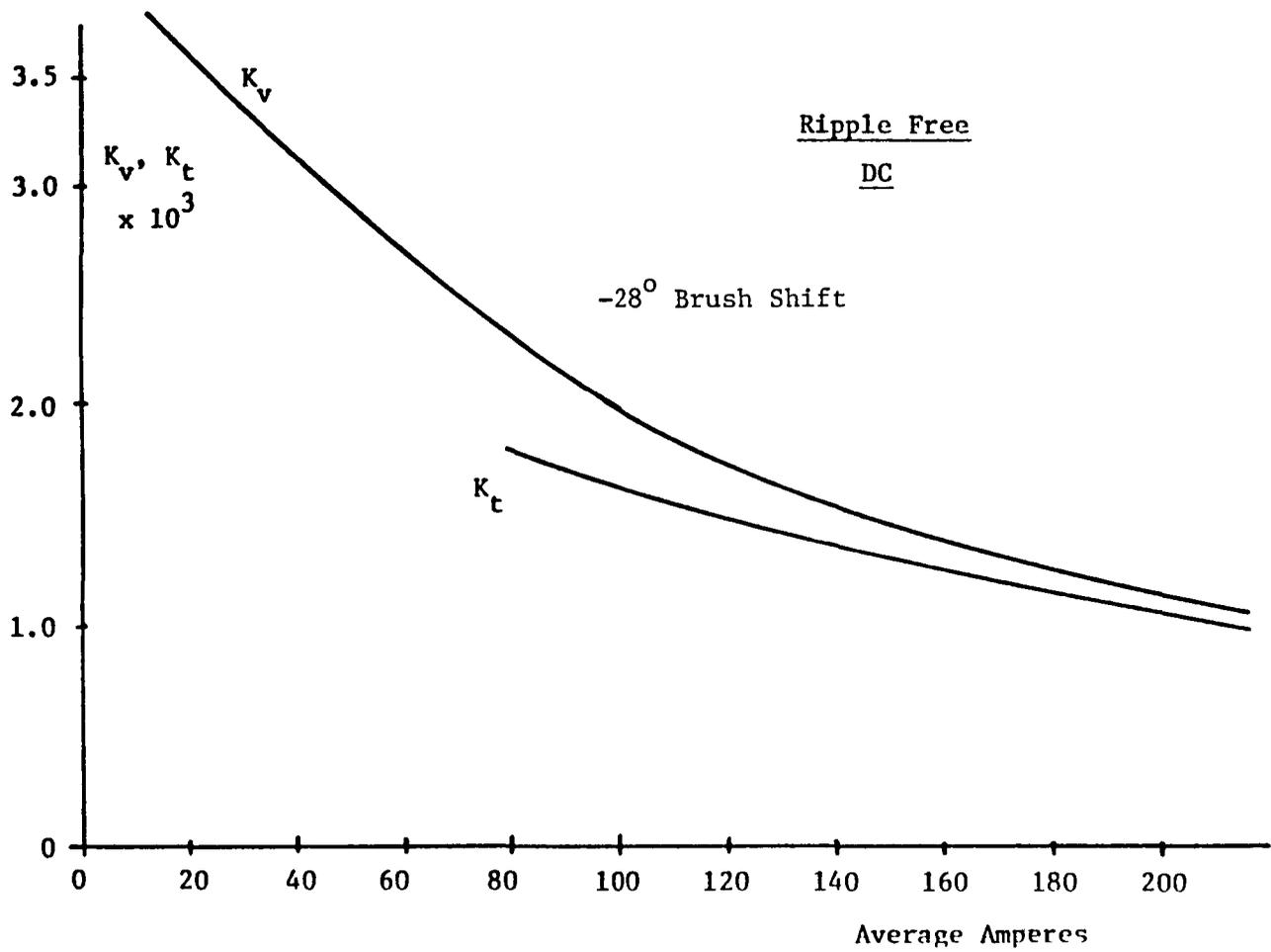
Thus,

$$I_f = \frac{(28)(162)}{(360)(20)(2)} I_a = 0.33\ I_a \tag{19}$$

This relationship indicates that, for $I_f = I_a$, $K_t = (91-0.33)\ K_v$ where K_v is calculated from the OCS curve taken with the brushes on mechanical neutral.

From Figure 21, the ratio K_t/K_v varies from 0.73 at 80 amperes to 0.83 at 200 amperes vs. the theoretical value of 0.667.

The OCS curve calculated from measured vales of K_t is shown dotted in Figure 21.

As can be seen, use of interpoles to avoid brush shift will yield higher torque per ampere, more power output per ampere (higher efficiency) and satisfactory commutation at all speeds, both forward and reverse.

To examine the implications with respect to power, note that for a given current, lower K will yield a higher speed, but a lower torque. If the per unit increase in speed is less than the per unit decrease in torque, the power output per ampere input will be decreased.

From equation (16), the per unit increase in speed is (approximately) (neglecting voltage drops in the circuit):

$$-\frac{1}{1 - \frac{2\beta}{180}} \tag{20}$$

From equation (18) the per unit decrease in torque is:

$$1 - \frac{\beta z}{360}\ N_f a \tag{21}$$

Therefore, since power equals (torque)(speed); if

$$\left(1 - \frac{\beta\ Z}{360}\ N_f a\right)\left(-\frac{1}{1 - \frac{2\beta}{180}}\right) < 1 \tag{22}$$

use of interpoles will yield a higher torque, higher power output per ampere, and a more efficient motor.

For the RED MOTOR, the left hand side of equation (22) is 0.99. For the BLUE MOTOR it is 0.88. Thus, interpoles would improve the performance of these motors.

If interpoles and compensating windings are not used, armature reaction effects can be partially mitigated by increasing the reluctance of the air gap at the pole tips. This was not done in either of the motors tested.

Two other conclusions are readily drawn, i.e. in any event the brushes must be properly located and K can only be determined from tests involving locked rotor torque as a function of current in the field and armature for a machine without interpoles, requiring brush shift.

In obtaining the torque vs. ampere characteristic, three tests, shown in Figure 23 were made for each motor, i.e., runs were made at 120° intervals of the stalled rotor.
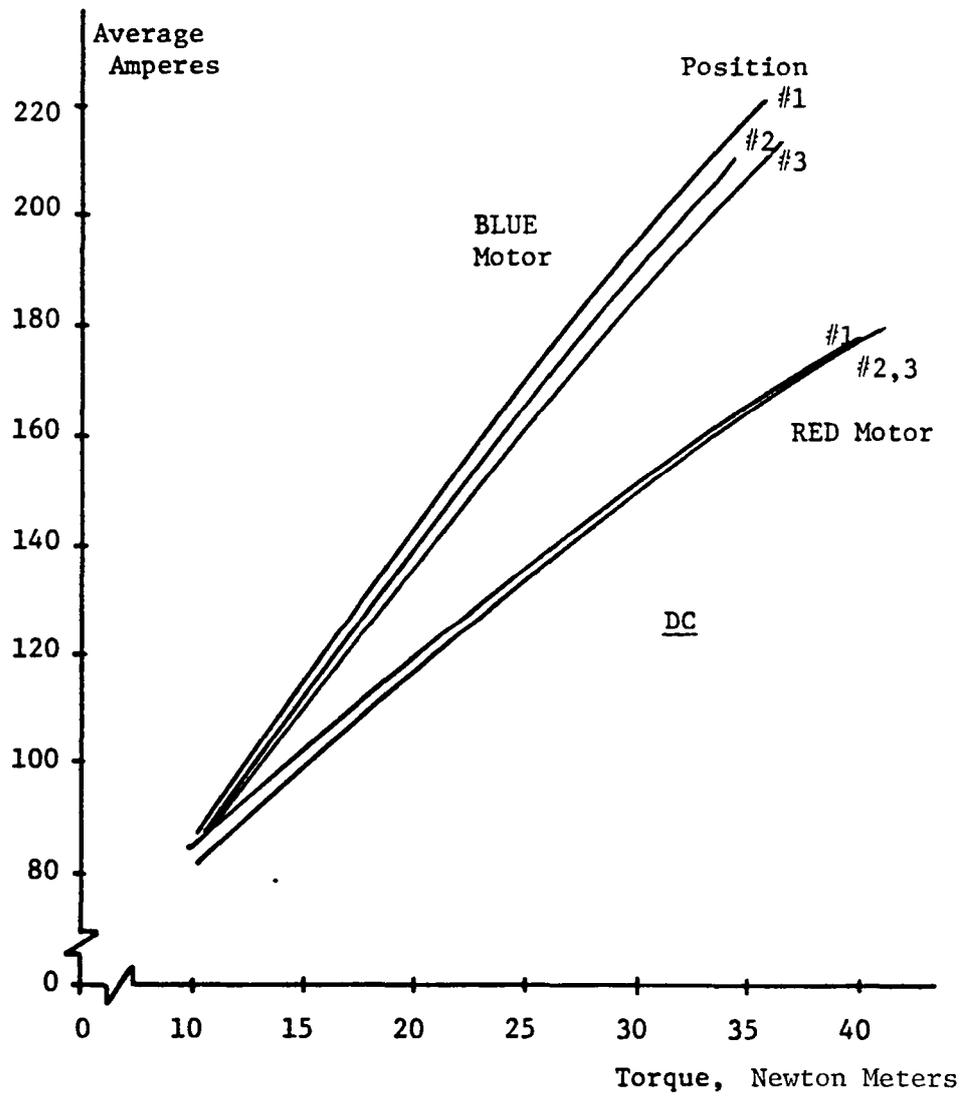
Figure 23   Blocked Rotor Torque Tests
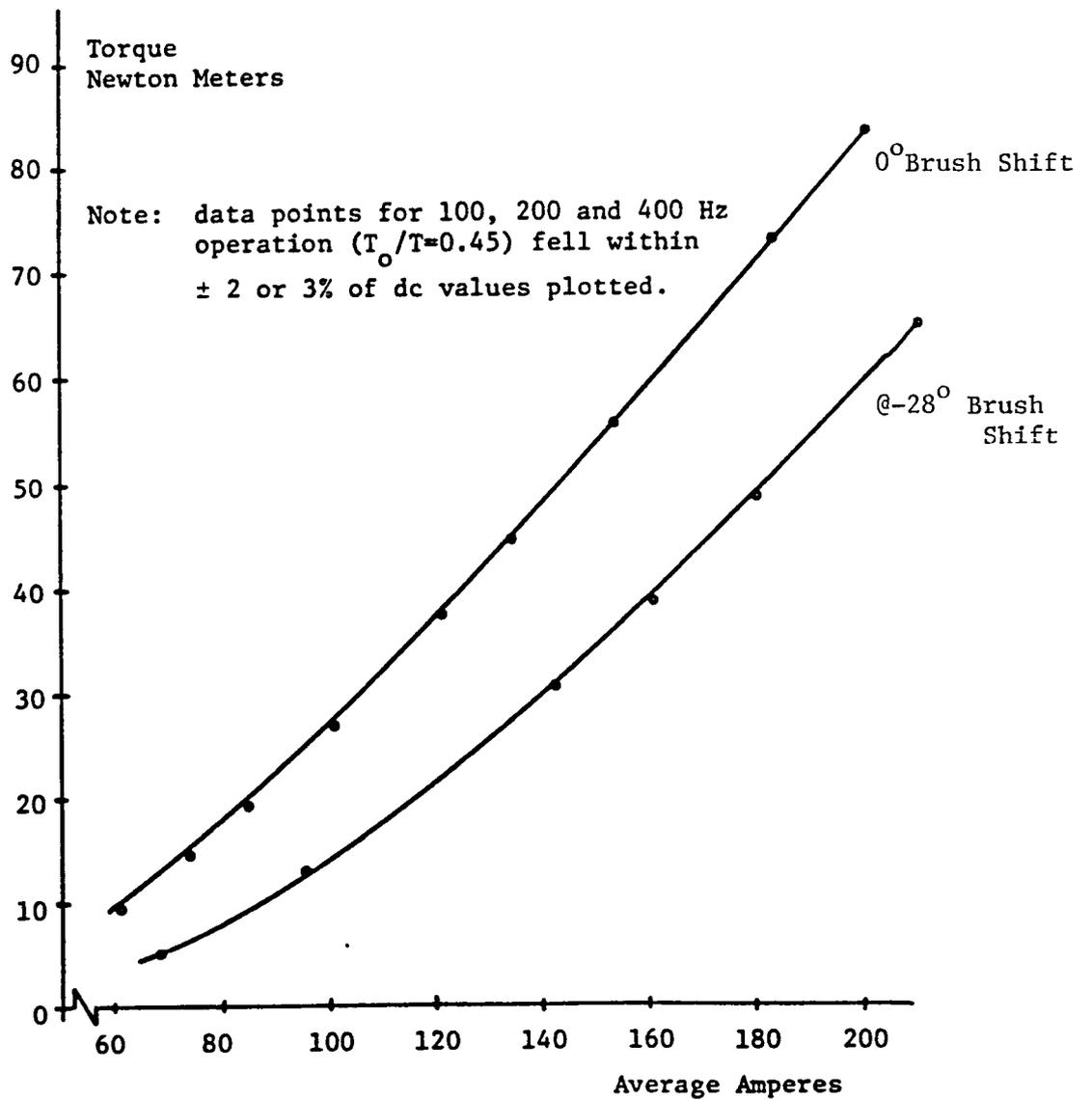
FIGURE 24 RED Motor Torque v. Amperes, Brush Shift Effect

Approximately 10% variation in torque/ampere squared was noted for the 3 positions of the BLUE motor rotor; approximately 3% variation for the RED motor. The readings were averaged to calculate K_t used in this section.

Observed values of torque as a function of current and brush shift during load tests (running) are shown in Figure 24. In this test, the torque with brushes shifted is about 25-30% less than with the brushes on mechanical neutral.

Calculated Performance

Based on measured values of R, V_b, $P_{f\omega}$, and K, steady state torque, speed, power output and efficiency as functions of current, for ripple free dc supply, can be calculated as follows:

$$(K_v = K_t = K)$$

Speed

$$N = \frac{60\omega}{2\pi} = \frac{V - V_b - I_a R}{k\,I_f} \left(\frac{30}{\pi}\right) \text{ rpm} \tag{23}$$

Mechanical Torque Output

$$M = M_e - \frac{P_{f\omega}}{\omega} = I^2 K - \frac{P_{f\omega}}{\omega} \tag{24}$$

Power Output

$$P_o = M\omega \tag{25}$$

Efficiency

$$\% \; \eta = \left(1 - \frac{P_{loss}}{P_{in}}\right) 100 = \left(1 - \frac{(I^2 R + P_{f\omega} + 0.01\,P_o + V_b I)}{VI}\right) 100 \tag{26}$$

also,

$$\% \; \eta = \left(\frac{M\omega}{VI}\right) 100 \tag{27}$$

Actual load tests were conducted on the RED and the BLUE motors in order to evaluate the accuracy of calculated performance equations. Laboratory quality instrumentation, including a digital strobotachometer, were used in the determination of the experimental data. Since data is used in later comparisons, the tests were run at nominal 42 volts, corresponding to many of the chopper supplied tests.

Figures 25, 26, 27, and 28 present the results observed experimentally and as calculated using equations (23) through (27).
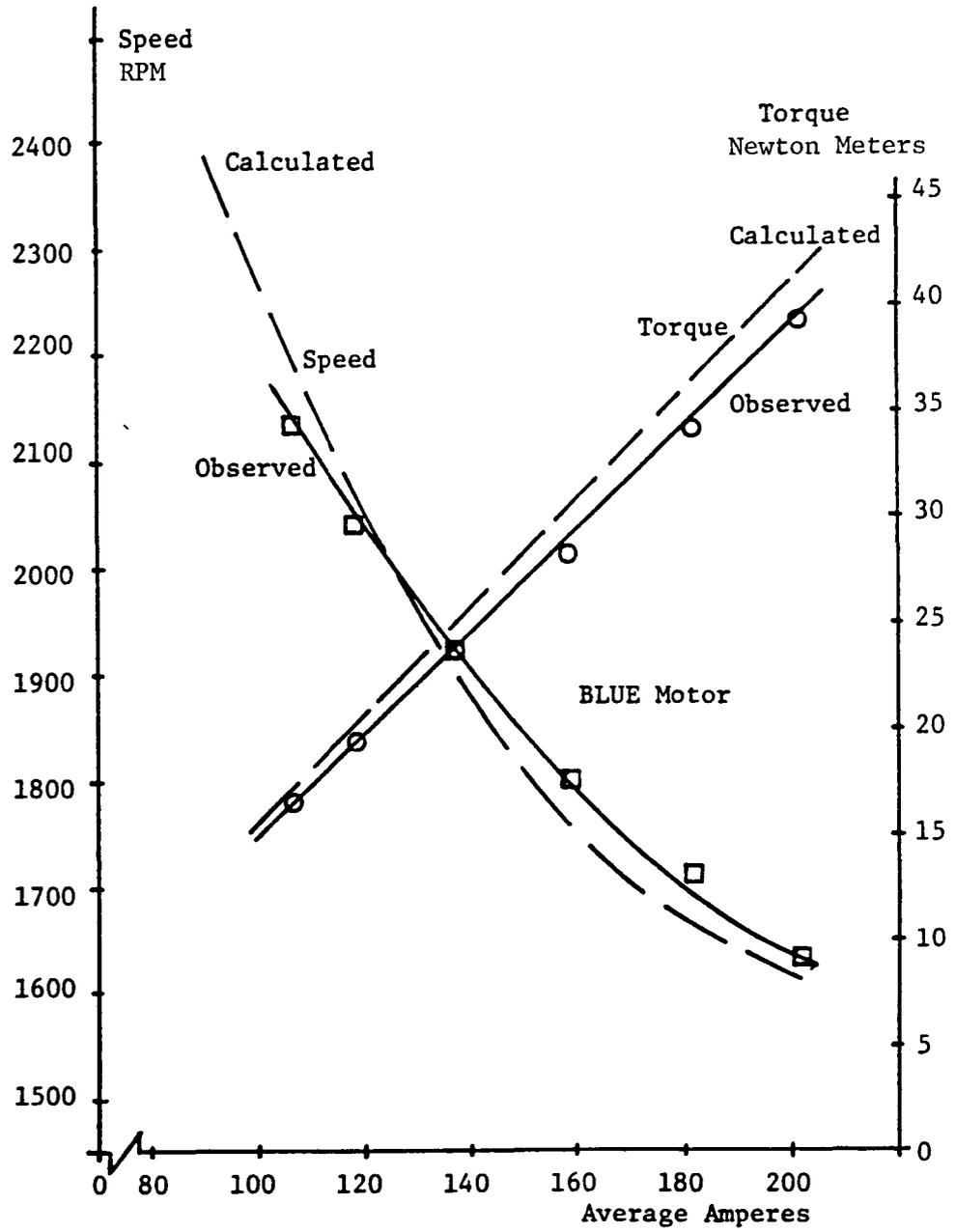
Figure 25   BLUE Motor Torque, Speed v. Current
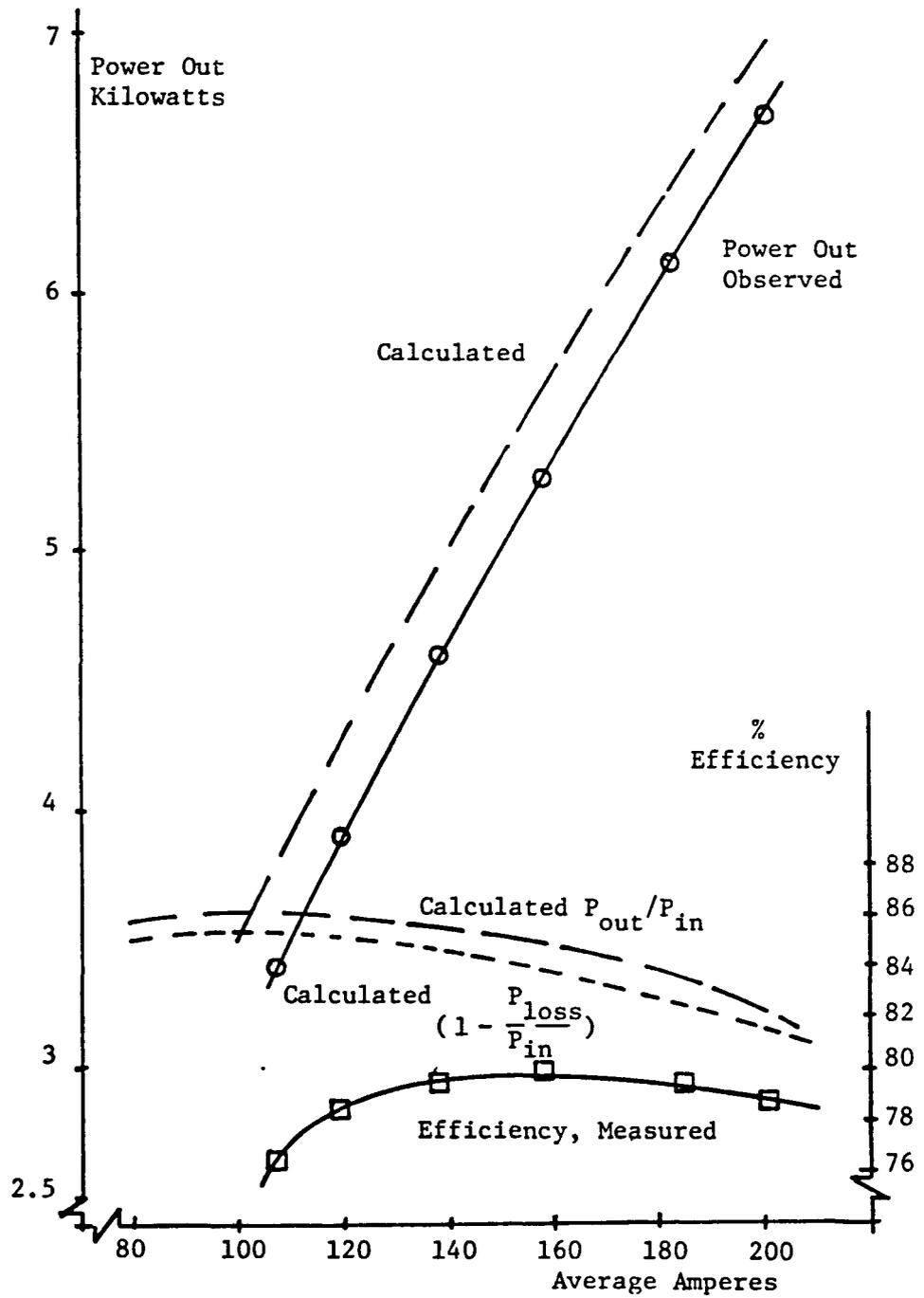
Figure 26   BLUE Motor Power, Efficiency v. Current
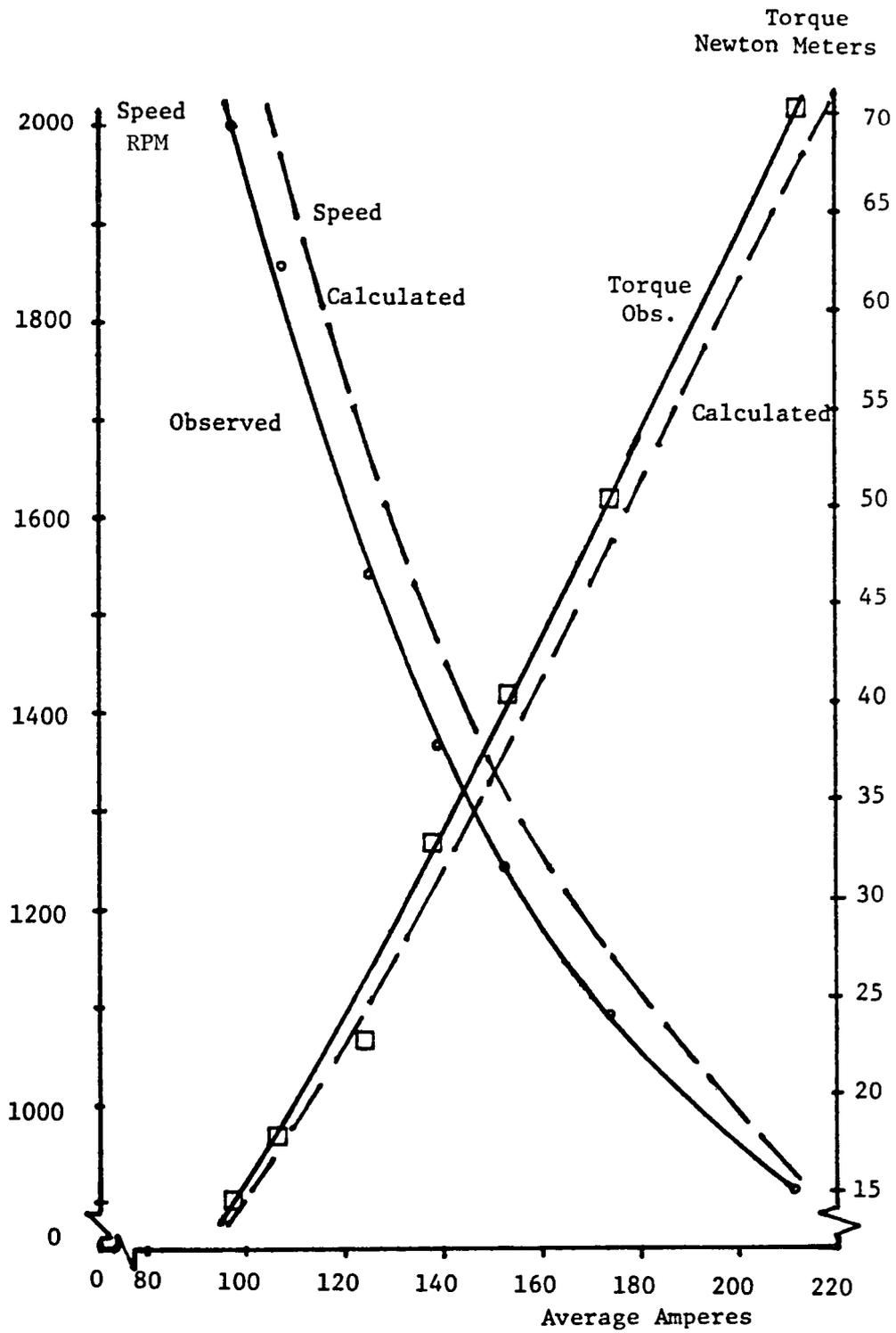
Figure 27 RED Motor Torque, Speed v. Current
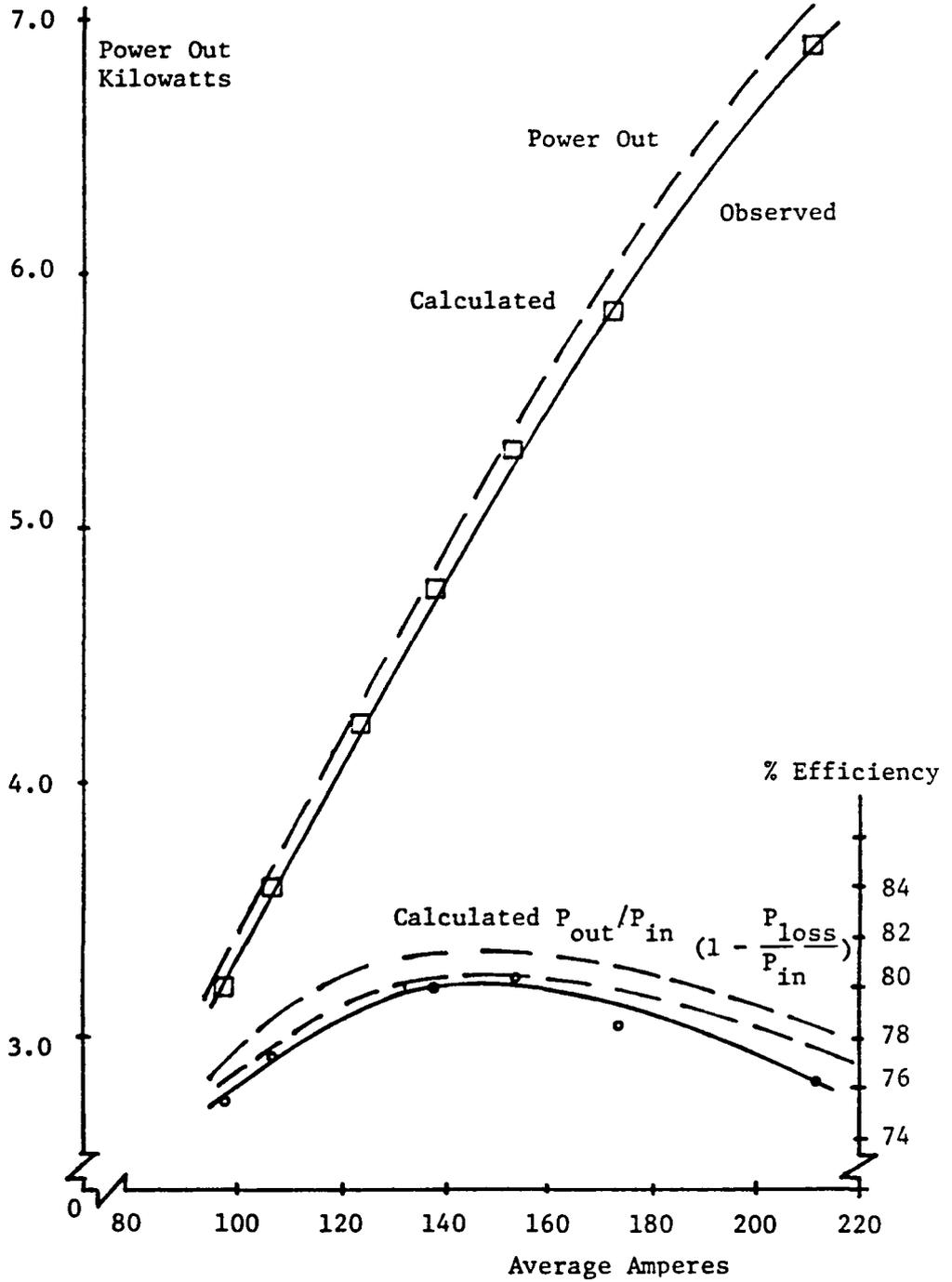
Figure 28 RED Motor   Power, Efficiency v. Current

As can be seen, except for efficiency, there is very good correlation between observed and calculated results. In general, calculated results are within 5% of observed experimental results. Because of the hysteresis effects in the magnetic circuit and due to the fact that the value of K is the average of 3 rotor position measurements, 5% error is considered acceptable, since the value of torque for a given current on stalled rotor varied over a 3-10% range.

For both motors, calculated efficiency was higher than actual efficiency. It is believed that this is due to neglect of "rotating core loss," which results from joule loss in the conductors undergoing commutation if the conductors are not in a position of zero flux density during the process. This is a substantial loss if the brushes are not precisely located or if an excessive number of coils are shorted during the commutation process. The RED motor efficiency calculated was quite close to the observed value; the BLUE motor value was much more in error. This can be attributed to the fact that more coils are shorted during commutation in the BLUE motor and to the fact that the BLUE motor (because it is lap wound) has an equalizer connection which apparently results in a finite joule loss not reckoned with in equation (26).

As will be shown in the following sections there are additional losses introduced if the current and voltage are other than ripple free dc and it should be noted that the conventional model does not account for these effects, which are introduced by virtue of the chopper action.

CHOPPER CONTROLLED MOTOR BEHAVIOR

When the motor is chopper controlled, the performance of the motor is quite different, in some respects, from the performance observed under "ripple free" dc power.

When the motor is chopper controlled, the speed-ampere characteristic is altered and the alteration is both frequency of chopper action and brush position dependent. If the brushes are shifted for proper commutation, the speed, at a given current is increased significantly over the speed, at the same current, with the brushes on neutral, i.e. 0°. The reason for this is the decrease in the number of active inductors in the armature. With the brushes on 0°, there is relatively little effect on speed due to frequency. This is shown in Figure 28, indicating approximately a 10% band covering dc, 100, and 400 Hz. However, when the brushes are shifted, the effect of frequency on the characteristic is quite pronounced. For example, at 150 amperes, brushes on -28°, reference to Figure 21 indicates that the value of K_v changes by 11% when the brushes are shifted, when supplied from ripple free dc. However, from Figure 29, if the motor is chopper controlled, at 400 Hz repetition rate, the speed changes by 48% in shifting brushes from 0° to -28°, and the spread in speed between 100 Hz and 400 Hz is about 18%, with higher speed with higher frequency at a specific current.

The most drastic change in the motor characteristic with chopper control is the efficiency as calculated from observed electrical-power-in/mechanical-power-out values. Power in was measured using the wide bandwidth electronic wattmeter. Note that the efficiency degradation increases with decreasing frequency and decreasing load. Referring to Figure 12, it is noted that % ripple decreases with increasing load and frequency. The iron losses resulting from the harmonic currents would tend to increase with frequency. Another factor associated with harmonics is "skin effect," which increases the apparent resistance of the wind-
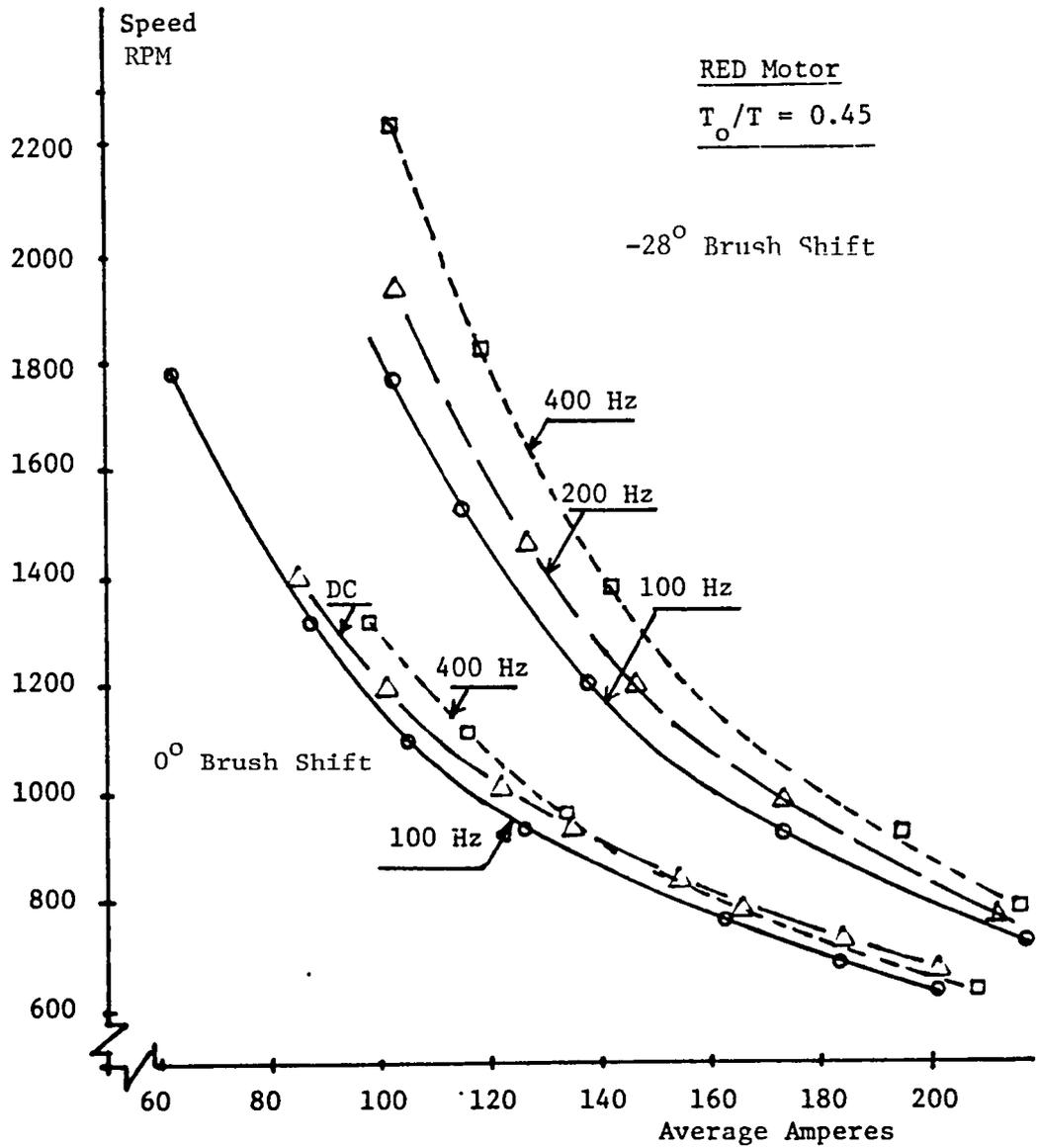
Figure 29 Effect of Brush Shift and Frequency
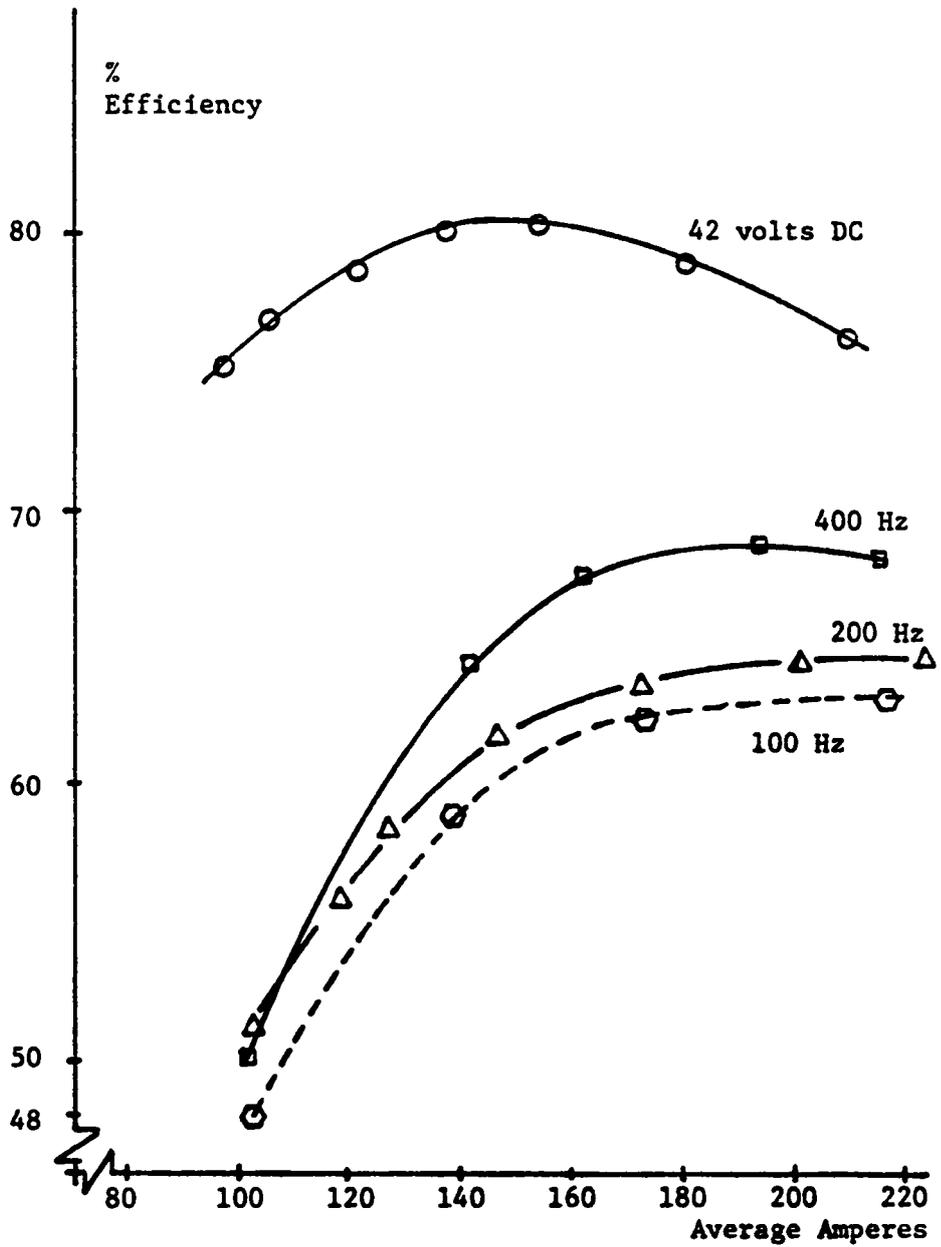
Figure 30   RED Motor   Effect of Frequency on Efficiency

harmonics is "skin effect," which increases the apparent resistance of the windings. The inductance will also change with frequency. The effects were investigated and are detailed in the following section.

Stalled rotor torque tests were conducted on both the RED and BLUE motors, runs being made at 120° intervals. Tests were conducted using ripple free dc and with the chopper control operating at a frequency of 67 Hz. Figure 31 shows the increased torque per ampere observed when the motors were chopper controlled. Figure 32 shows the same variation, in the form of the calculated torque constant as a function of average current. The increase is due to the harmonic current components creating torque due to the "universal" (ac/dc) properties of a series motor. The harmonic current values are not included in the average value of current, as measured.

MEASUREMENT OF RESISTANCE AND INDUCTANCE

As pointed out in the previous section, there is "skin effect" in the conductors due to the harmonic currents. Thus a knowledge of the apparent resistance of the motor armature and field is essential. In addition, knowledge of the inductance of the dc series motor is essential if a meaningful model of the machine, for dynamic studies, is to be configured and it is a necessary parameter in the application of a specific chopper type controller with a particular motor.

IEEE #113 (ref. 1) briefly notes procedures for measuring inductance, although the standard is primarily addressed to the shunt connected machine. The technique for measuring armature inductance involves a 60 Hz supply, with series field out of the circuit and neglecting the resistance of the circuit. Frequency variations and saturation are not addressed. Saunders (ref. 2) proposed a test scheme involving a dc source, through a choke, paralleled with an ac source with blocking capacitor as a scheme to determine, in effect, incremental inductance as a function of dc saturation.

DeWolf (ref. 6) made measurements of armature inductance. He found that the armature circuit inductance of the series wound motor varied widely with frequency and degree of saturation.

Quoting DeWolf, "... it is concluded that both dc and variable frequency ac power supplies... are required to obtain meaningful measurements of armature circuit inductance of series wound machines."

Accordingly, experimental work was undertaken to investigate the techniques and problems involved in series field parameter determination.

The first step was selection of an ac power supply and a rather formidable problem manifested itself. In essence, the problem was that what appeared to be a harmonic free source displayed relative large harmonics in the voltage that appeared across the brushes of the blocked rotor and series field of the series wound motor. This was when a variable frequency single phase generator was tested for suitability as an ac source. Visual observation of the open circuit voltage indicated a relatively harmonic free voltage. Actually, the 3rd and 9th harmonics were measured as 3% and 1% respectively of the fundamental, yielding distortion in the range of 0.05% where:

$$\% \text{ Distortion} = \frac{\sqrt{\Sigma(RMS)^2 - RMS_{fundamental})}}{RMS_{fundamental}} \times 100 \tag{28}$$
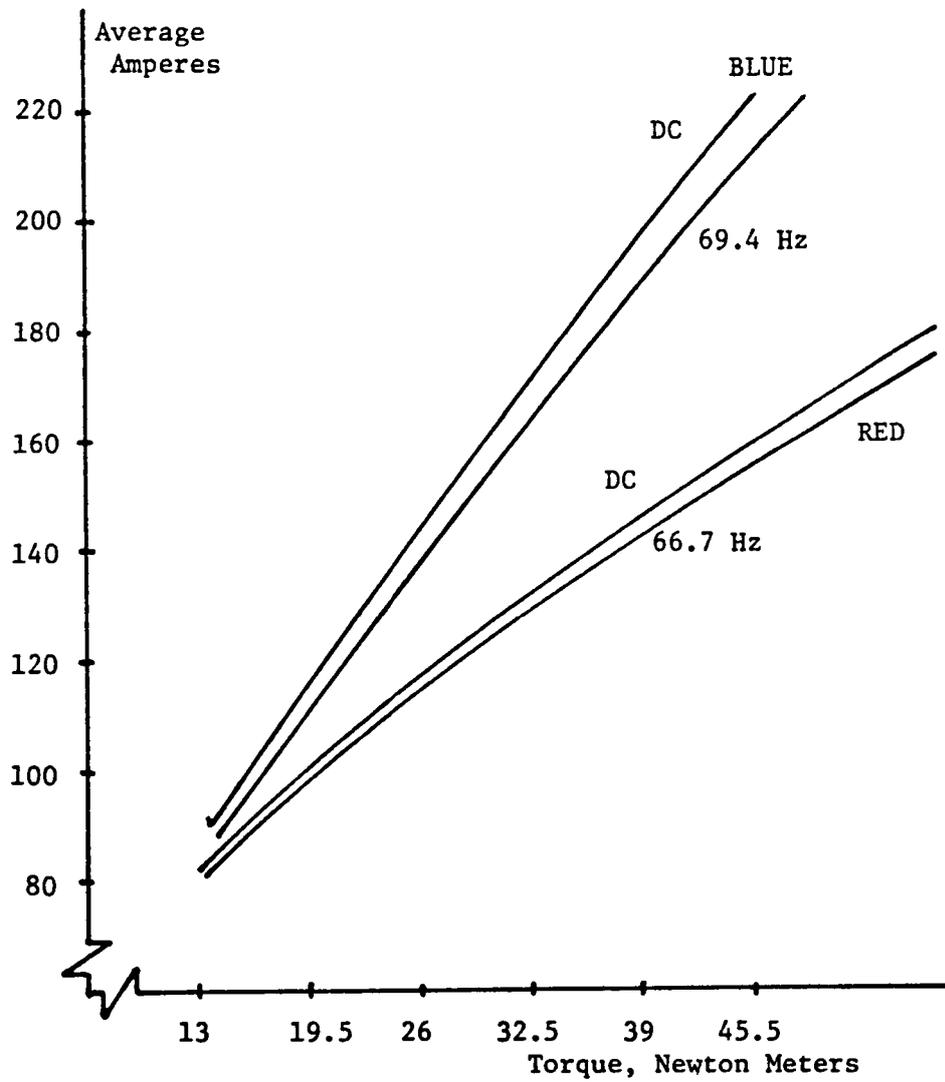
Figure 31   Effect of Frequency on Stall Torque
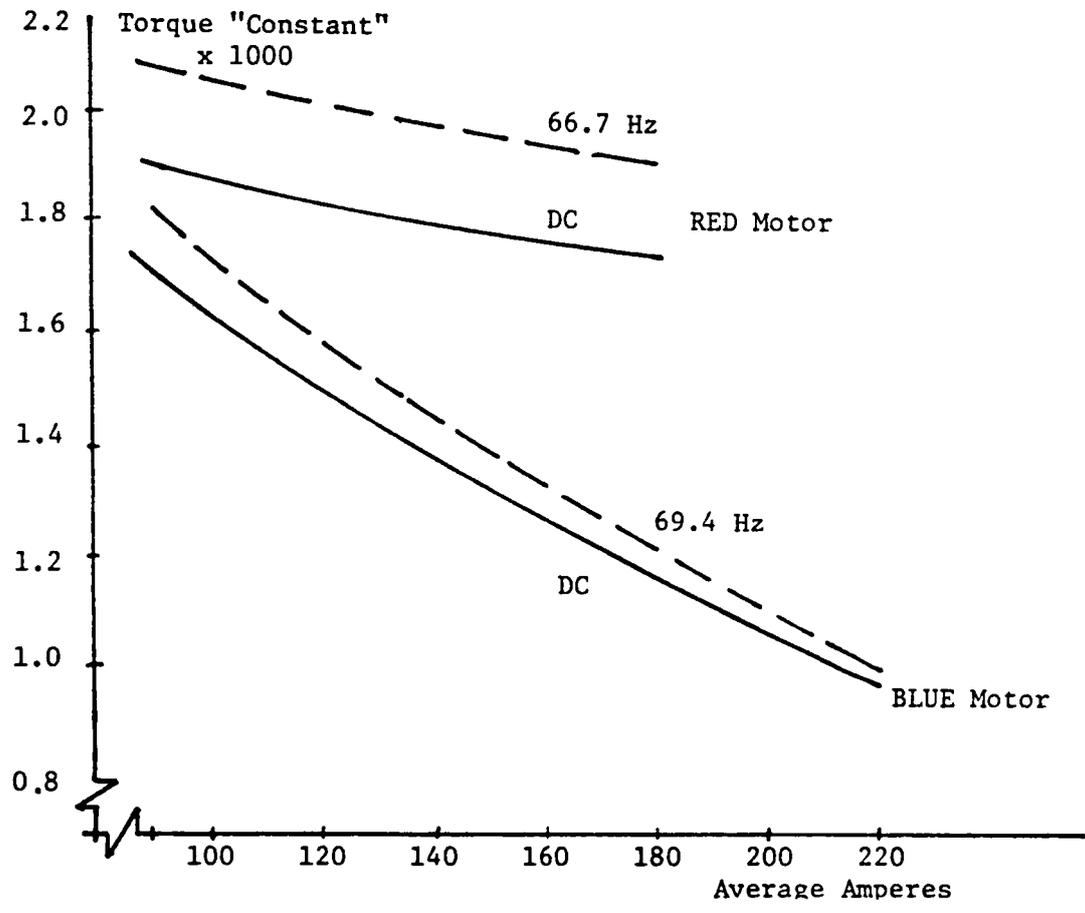
Figure 32 Effect of Frequency on the Torque "Constant"

The generator was connected across the armature and field of the RED motor through a 200 µF capacitor bank. Because the capacitor impedance decreases with increasing frequency and the choke (inductance) in series with the dc source (and shunting the motor under test) increases with increasing frequency, harmonic currents are magnified in the test motor circuit.

To determine R, L at various frequencies and saturation levels, it is necessary to accurately measure voltage, current and the angle between them. The harmonic distortion resulting from the straightforward use of a rotating machine as an ac source was found to be intolerable and was discarded.

The scheme that was developed and from which meaningful data was obtained is depicted in Figure 4. The blocking capacitor was sized to keep the voltage across the capacitance to relatively low values, especially at lower frequencies. The voltage divider is required because of input voltage limitations in the instrumentation amplifiers used. To reject the dc component of current and voltage in the signals, capacitor input filters were utilized. Since the ratio of voltage to current and their phase angle is desired, the slight attenuation and phase shift introduced does not affect results if both signals are equally affected.

After filtering, the voltage and the current signals were amplified using floating differential amplifiers with gains of 10 (for the voltage signal) and 1000 (for the current signal) yielding amplifier outputs, in volts, proportional to the actual current and voltage levels.

In order to isolate the frequency desired for the measurement, band pass filters were placed between the amplifier outputs and the voltmeters and the oscillograph. These filters have dial settings for low and high frequency cutoff, f_ℓ, and f_H.

Some attenuation and phase shift (lead through the low pass; lag through the high pass sections) does occur. From the attenuation characteristic, for these filters, if f/f_H and f_L/f are set at 0.4 for 0 db attenuation, i.e.,

$$f_H = 2.5\ f; \quad f_L = 0.4\ f$$

where f is the pass frequency, the phase shift through the low pass section is $+60°$; the phase shift through the high pass section is $-60°$, yielding zero net phase shift and zero attenuation. Because of the error inherent in dial settings, the final adjustment of the dial settings is made by utilizing a common input signal and trimming for identical band pass filter outputs.

After filter setting adjustments were made, the common input signal was removed and the differential amplifiers with gain setting noted above were connected between the NIS and the voltage divider outputs and the filter inputs. The voltmeters used were wide frequency response, high accuracy, true RMS reading voltmeters.

Tests for R and L were conducted using a 1.5 - 2 ampere ac current derived from the oscillator-amplifier source, at various frequencies from 30-1500 Hz and at various levels of dc current.

Readings of voltage and current were made and the phase shift was measured on the CRO. From the data, R and L can be calculated as:

$$R = \frac{V}{I} \cos \phi; \quad L = \frac{V}{2\pi f I} \sin \phi \tag{29}$$

Inherent errors are introduced in making the length measurements. The magnitude of the errors can be visualized from:

$$\Delta R = (\frac{V}{I} \sin \phi) \Delta\phi \tag{30}$$

the % error, in determining R is:

$$\%R = (\frac{\Delta R}{R}) \, 100 = 100 \tan \phi \, (\Delta\phi) \tag{31}$$

where ΔR is the calculated error based on a measured angle error of $\Delta\phi$.

Similarly, % error in determining L is:

$$\%L = 100 \cot \phi \, (\Delta\phi). \tag{32}$$

Actual ϕ is in the range 55-65 degrees.

Assuming $\phi = 60$;

$$\%R = 173 \, \Delta\phi \qquad \%L = 58 \, \Delta\phi \tag{33}$$

For a cycle length of 60 mm on the CRO, and an error in measurement of 0.5 mm (trace width), about 10% error in the calculation of R and a 3.5% error in the calculation of L can result.

The carbon brushes were replaced with radiused copper blocks in order to eliminate the non-linear resistance effect of carbon. The rotor was blocked to prevent rotation.

The current level of the ac current injected was 2 amperes or less; thus the inductance calculated is incremental inductance. Test results are described in detail in reference 7. Both the RED and BLUE motors were tested and the nature of the variations of R,L were found to be identical, although the actual values were, of course, different. The initial series of tests were conducted over the frequency range from 30 to 1500 Hz to gain an overview of the variations. After the frequency trends were established from these tests, tests were run at 400 Hz to isolate other phenomena.

Inductance Variations

Figure 33 shows the variation in inductance measured, for the RED motor over the frequency range from 30 to 1500 Hz from the unsaturated to full saturation condition. Figure 34 presents the variation of inductance of the RED motor as frequency is varied and current is held constant at values of 50, 100 and 175 amperes. Figure 35 depicts the effect of brush shift and shows the division of inductance between the armature and field in the RED motor. As can be seen, brush shift does not affect the armature to any extent but it does have a noticeable effect, over all. This result was obtained at 400 Hz, and two field windings series connected. The difference between measurements made with carbon brushes and copper blocks is shown for the RED motor, in Figure 36.

Figure 33 L as a Function of Frequency and Saturation

-55-
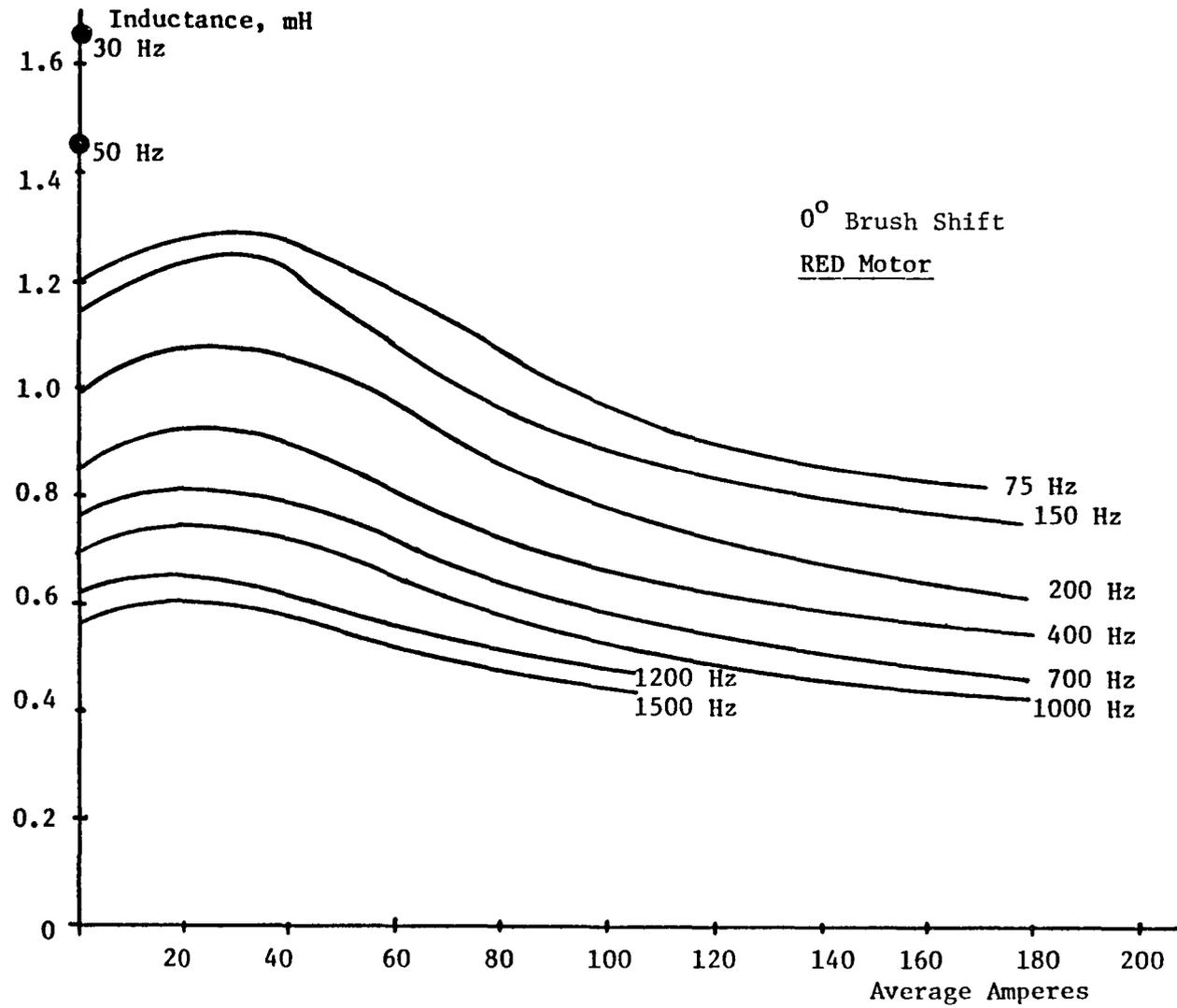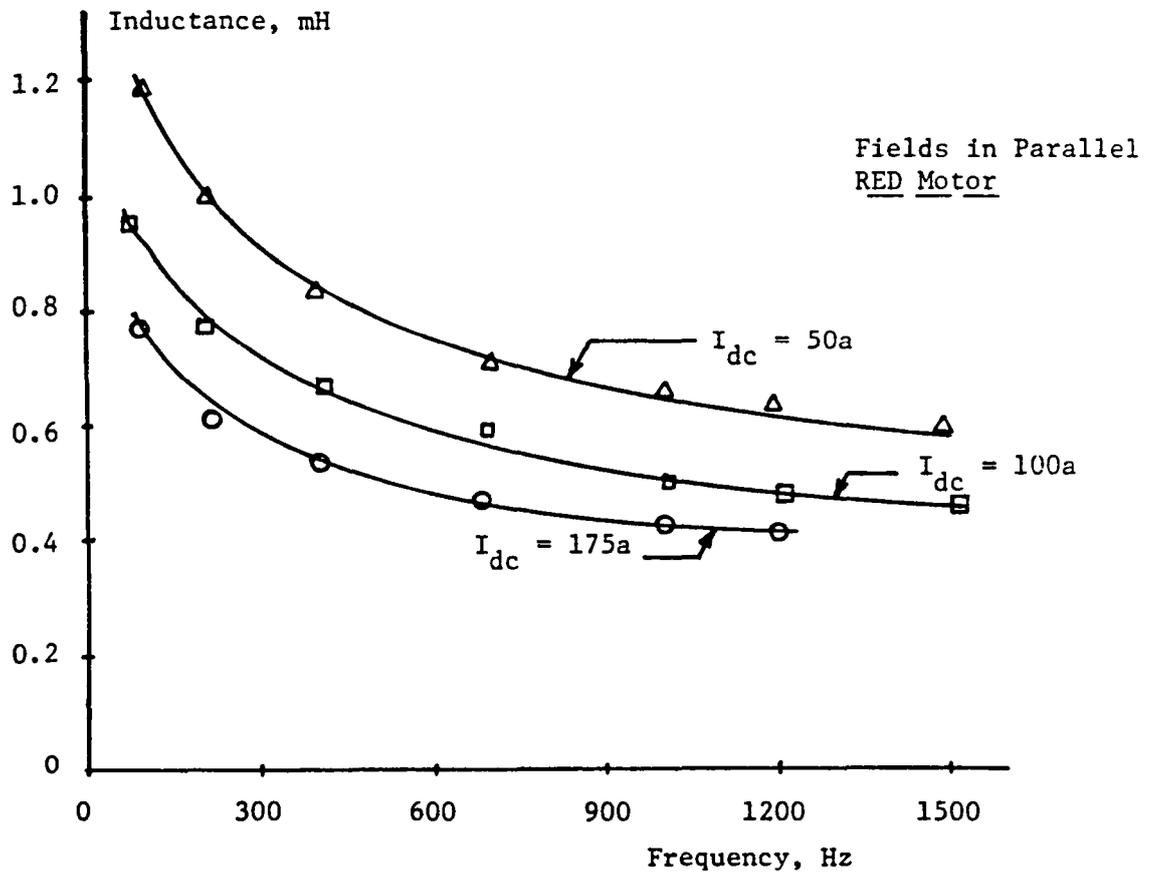
Figure 34, L as a Function of Frequency and Saturation
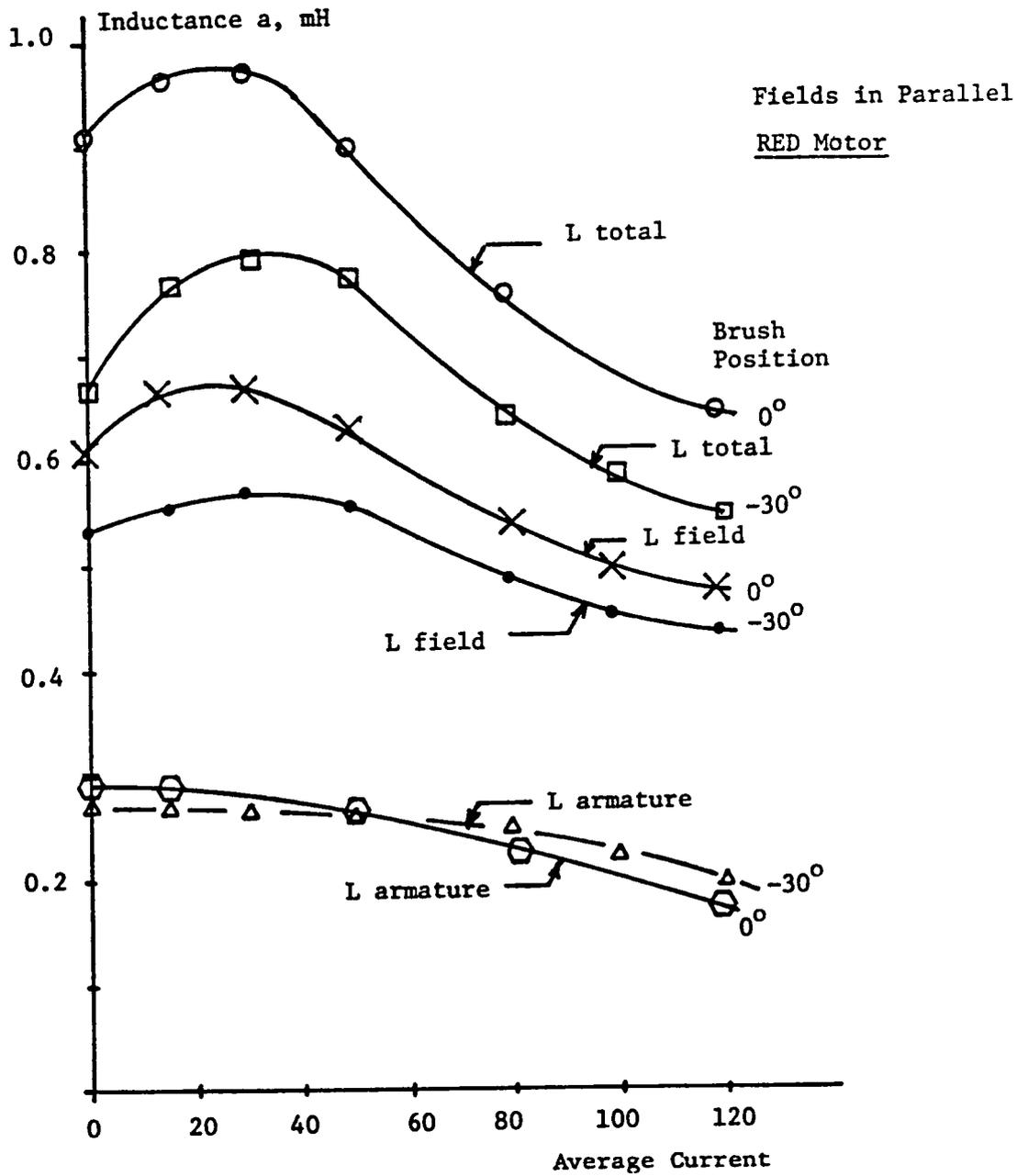
Figure 35   Field and Armature Inductance
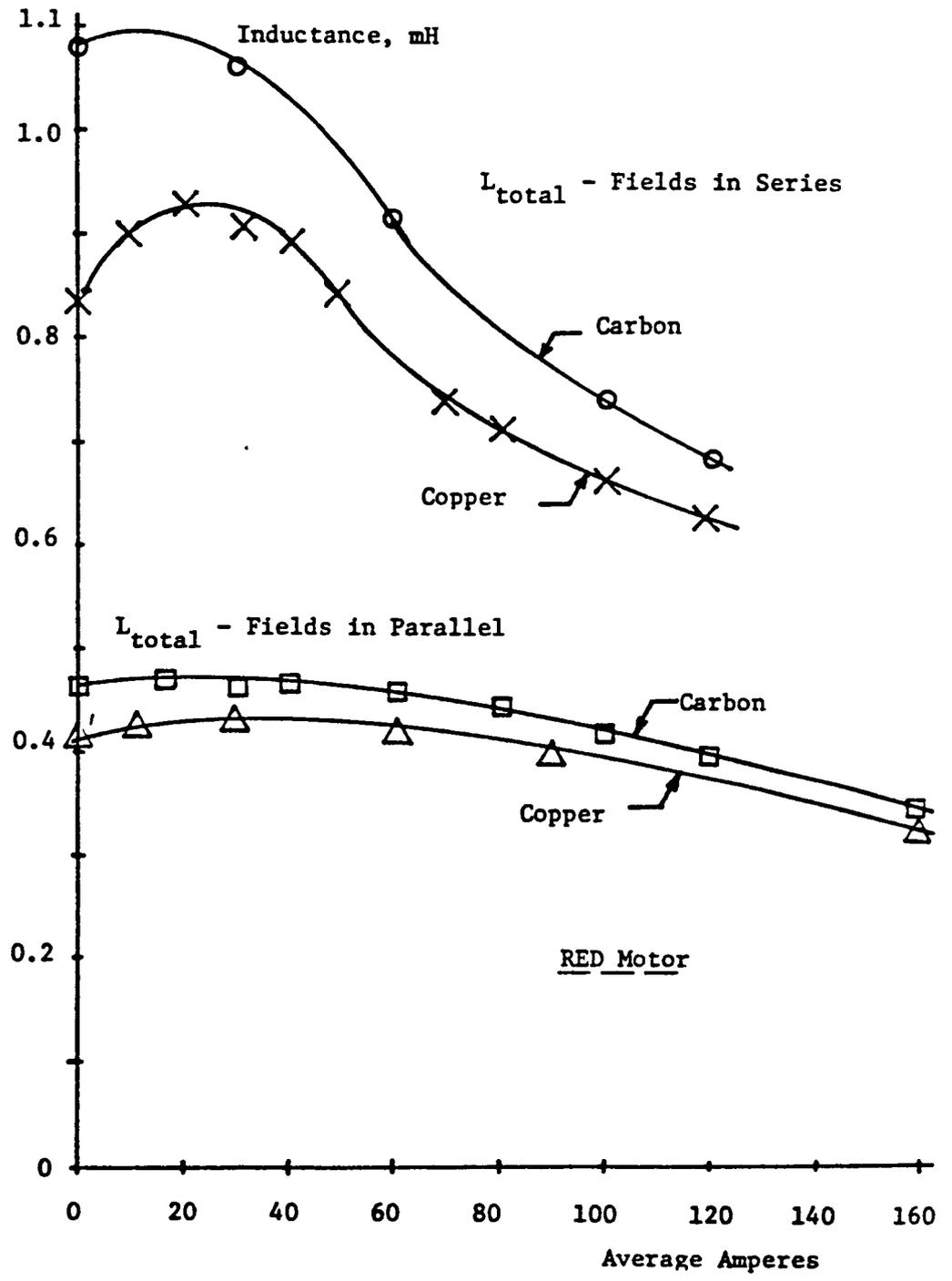
Figure 36   Effect of Carbon Brushes on L Measurement

Apparent Resistance Variations

The apparent resistance, as seen by the current fundamental and harmonics, changes with both frequency and saturation (since the variations are due to eddy current, skin and proximity effects).

Figure 37 presents apparent resistance variation for the RED motor with frequency and level of saturation changes, and Figure 38 depicts the same type of information in a different fashion. The effect of brush shift and the division between series fields and armature for the RED motor at 400 Hz are shown in Figure 39. As can be seen, since the vast majority of the apparent resistance is in the field windings, use of fine stranded wires (rather than solid conductors) appear to hold promise of reducing the apparent resistance (and the harmonic current joule losses) appreciably.

## $\omega L/R$ Variation

A curve fit routine, applied to the experimental data obtained for both motors indicates that R and L, as functions of frequency and saturation, varied in an identical fashion, although the actual values for the two motors were different. (One had a solid frame, the other a laminated frame). Total variations in L and R were found to be, for the RED motor:

$$L = 3.8 \ f^{-0.24} \ I^{0.063} \ mH$$

$$R = 0.0167 \ f^{0.7} \ I^{-0.07} \ ohms$$

from which:

$$(2\pi f) \ \frac{L}{R} = \frac{\omega L}{R} = \frac{X}{R} \simeq constant \qquad (34)$$

Summary and Conclusions on R,L Variations (ref. 7).

Inductance Variations:

The armature inductance is independent of brush position and armature-only excitation. It accounts for about 1/3 of the total armature circuit inductance. The armature circuit, including the series field, is about 30% less under saturation conditions than unsaturated, decreasing approximately as the -0.06 power of the dc current level. Also, it decreases proportional to the -0.24 power of frequency (over the frequency range tested, i.e. to 1500 Hz). The armature circuit inductance is dependent upon brush position, decreasing in proportion to the angle of the shift against rotation. For the motor tested, with the brushes located for proper commutation, it decreased by 15%. It should be noted that, in a constant inductance circuit, higher frequency current harmonics are suppressed in magnitude; but in the motors tested, with decreasing inductance with increasing frequency the suppression (or decreasing trend) is not as pronounced.

Resistance Variations

For the motor with results detailed here, the dc resistance of the armature and fields was measured as 0.0189 and 0.0165 ohms respectively for a total of 0.0254 ohms. The ratio of armature to field dc resistance is 1.15. From Figure 39, at 400 Hz, this resistance ratio is only 0.15; thus about 90% of the resistance to ac harmonic current is associated with the series field winding. This indi-
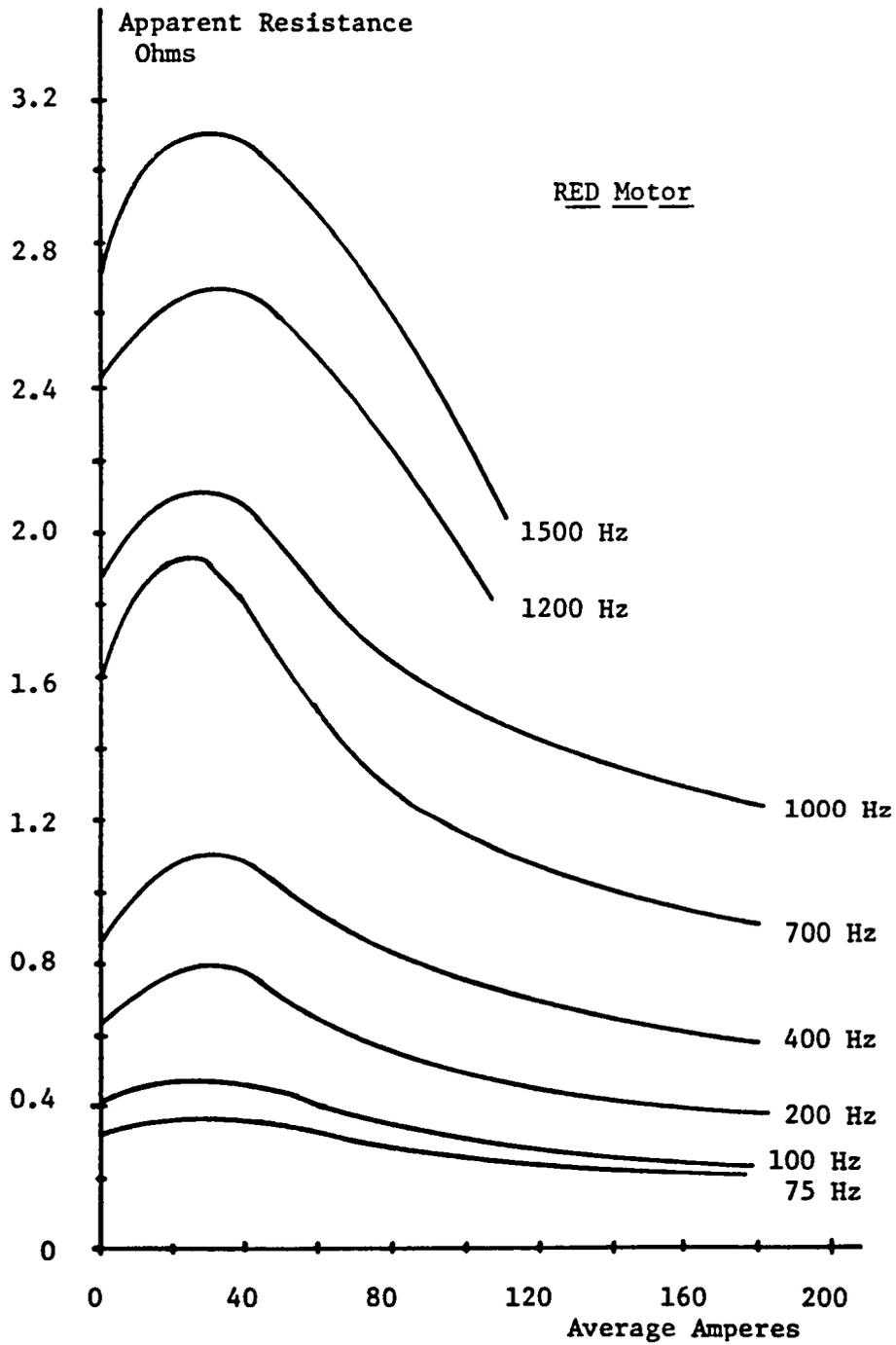
Figure 37   Apparent Resistance as a Function of
Frequency and Saturation
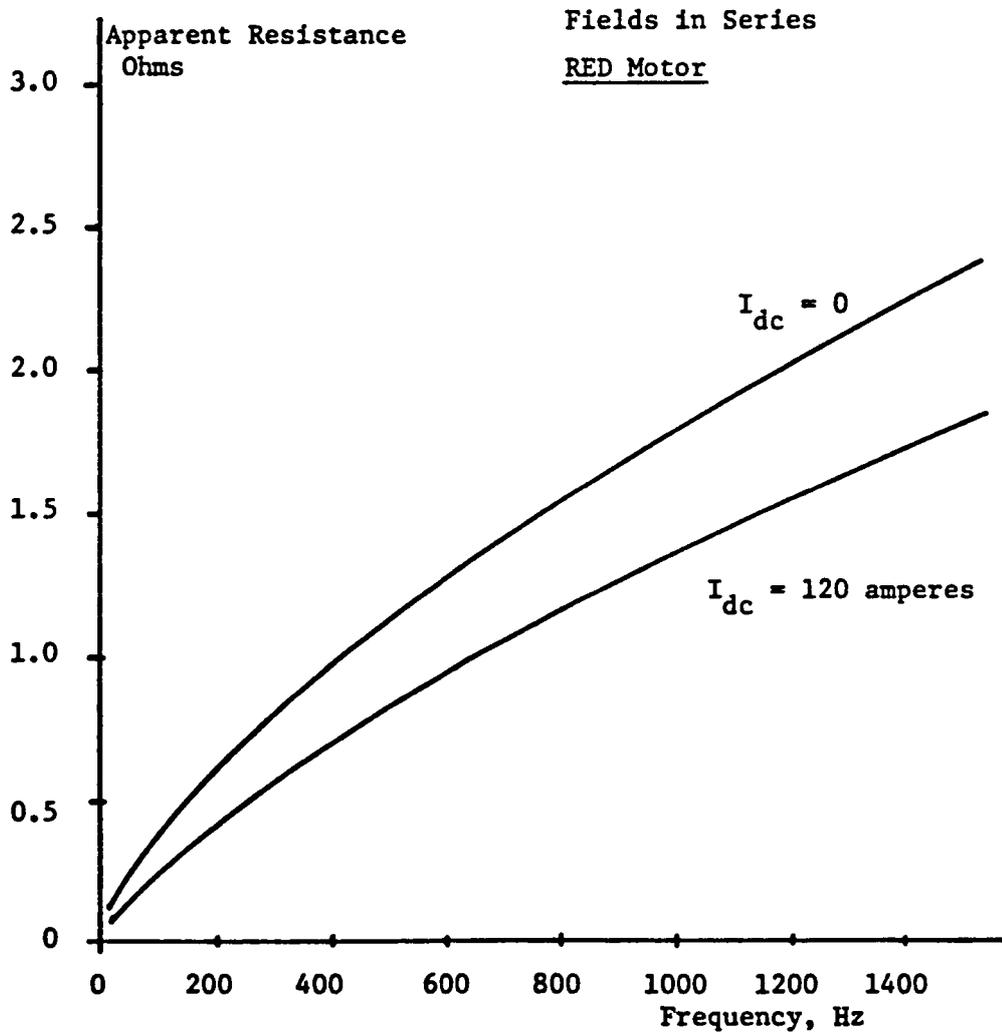
FIGURE 38   Apparent Resistance as a Function of Frequency and Saturation
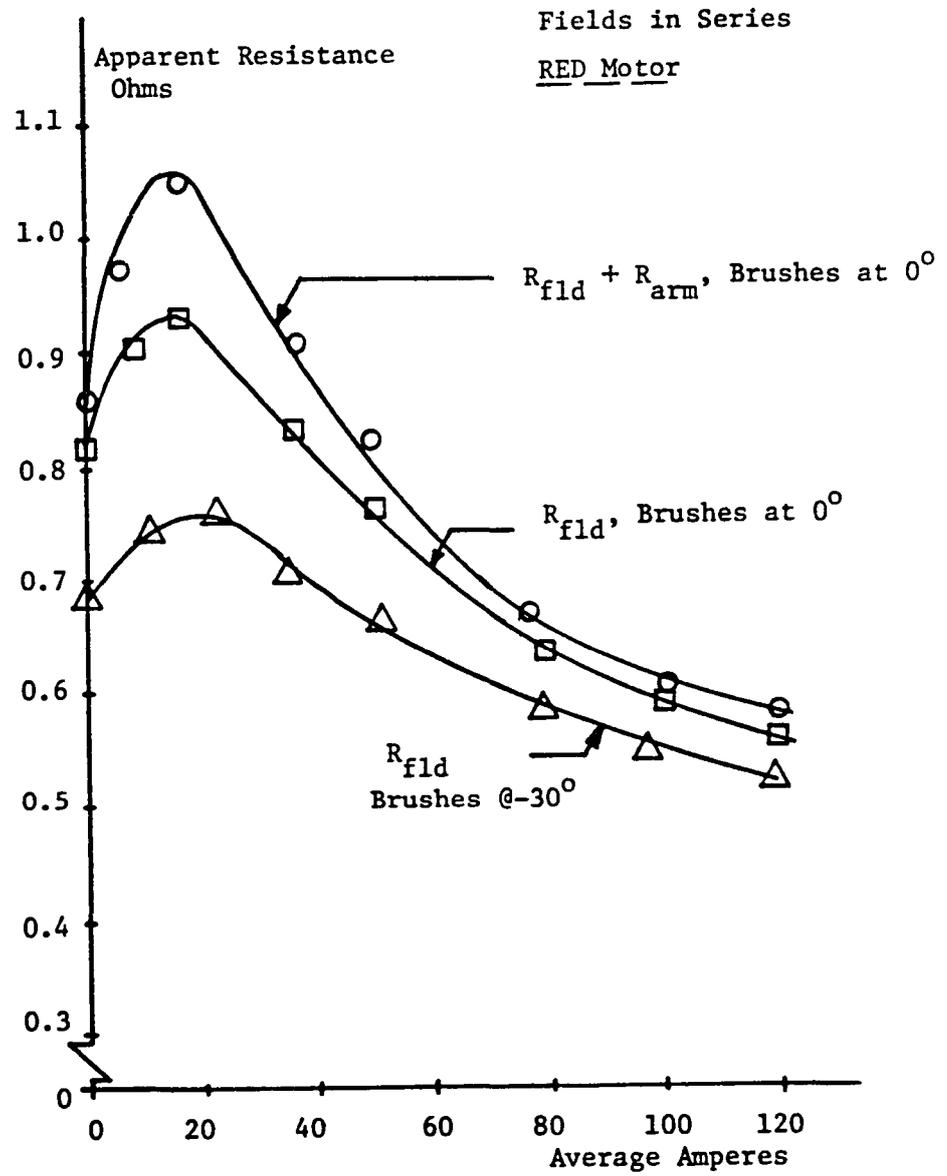
Figure 39 Field and Armature Apparent Resistance

cates that this loss could be decreased by using multiple insulated small wires in parallel rather than fewer heavy strands for the series field winding. Apparent resistance decreased about 15% with brush shift. The values observed under saturated conditions were 20-30% less than the unsaturated values (depending upon frequency). For a given degree of saturation, the apparent resistance increased with the +0.7 power of frequency. For a specific frequency, the resistance decreased approximately as the -0.07 power of the average current level.

Carbon Brush vs Copper Block Values:

(1) The value of inductance measured using copper blocks was found to be about 6% less than values from measurements with carbon brushes.

(2) Measurement of apparent resistance with carbon brushes in place yielded a value of approximately 75% greater than found using copper blocks.

Magnitude of Losses:

The combination of relatively high harmonic currents and the apparent resistance (reflecting hysteresis and eddy current skin and proximity effect losses) yields a loss component which should be included in any efficiency determination.

Motor/Chopper Interface Influence:

Since the chopper is sensitive to the amount of inductance in the circuit, care should be taken to use the saturated value of inductance, obtained at the maximum operating frequency, when evaluating the interface details.

On Measurement Techniques:

The circuit used in this test does yield accurate values of R and L. Because of the harmonic effects, special care must be used in the selection and application of the variable frequency power supply and instrumentation to be used. Copper blocks should be substituted for the carbon brushes.

It was noted that, for the motors tested, the ratio of reactance to apparent resistance is nearly independent of frequency and level of saturation.

Conclusion

The dependence of circuit parameters on frequency and saturation indicate the need for inclusion of these factors in a model of the motor from which performance is to be calculated.

CHAPTER 3

LOSSES

Losses were discussed in a general fashion in the previous chapter. This chapter discusses the losses in a more quantitative manner, presents the results of experimental tests and observations and presents some suggestions as to means to decrease the losses through design methods. The losses can be classified as follows:

-Joule Losses-

1. Load current losses in the field and armature windings due to normal ohmic resistance and skin effect.
2. Eddy current losses in the following:
    (a) the armature winding, due to flux distortion under the pole faces
    (b) the armature winding, due to tooth saturation and the main flux
    (c) the armature conductors, due to slot leakage flux during commutation
    (d) the iron of the pole face due to the variation of air gap flux density due to slot openings
    (e) throughout the magnetic circuit (armature, poles, yoke) due to chopper action.
    (f) in the steel banding wire used to secure the armature winding.
3. Losses in the equalizer connection, if present.
4. Loss in the coils undergoing commutation due to the short circuit current flowing.
5. Loss due to the carbon brush and the brush-to-commutator contact resistance.
6. Loss due to the free wheeling diode, if chopper controlled.
7. Loss due to current circulating in the shaft, housing and bearings resulting from shaft induced emf due to:
    (a) unsymmetrical distribution of flux between the poles resulting in a net flux encircling the shaft
    (b) capacitive coupling between windings and the magnetic core in conjunction with the current harmonics.

-Iron Hysteresis Losses-

8. Throughout the magnetic structure due to current harmonics resulting from chopper action.
9. In the pole face due to variation of air gap flux due to slot openings.

-Mechanical Losses-

10. Frictional Losses due to:
    (a) bearings
    (b) brushes
11. Losses due to windage (or drag).
12. Losses due to ventilation requirements.

In performance calculations involving ripple free dc supplied motors, the term "stray-load" loss is applied to 2a, b, c, d, f, 3, 4, 7 and 9, and is commonly taken as 1% of the output power. This is not an appropriate value to use if current harmonics are present, as shown in Figure 30. It should be noted that these types of losses cannot be either measured (except by other loss elimination) or accurately calculated. The method of dealing with these losses is for the motor designer to incorporate design features which minimize these types of losses. The same approach is true for many of the other loss types, also, such as 2e and 8.

Joule Losses

1. Load Current Losses

Joule losses occur in the armature and field winding and are typically 3-5% of the rated power output at rated output of the motor, if supplied from ripple free dc. However, if harmonics are present, this type of loss is increased substantially due to skin effect and eddy current losses resulting from the current harmonics associated with chopper action. It should be noted that even when a motor is supplied from ripple free dc, skin effect in the armature inductors is present, although less than the skin effects resulting from chopper current harmonics. The reason for this skin effect, and steps to take to mitigate it, can be visualized if it is noted that armature inductor current is alternating in nature (prior to commutation) at a frequency:

$$f = \frac{np}{120} \qquad (35)$$

where n = rev/m; p = number of poles.

There is a cross slot leakage flux associated with each conductor and the current which flows therein. The slot leakage flux passes across the slot, through the teeth and around the bottom of the slot, as shown in Figure 40.
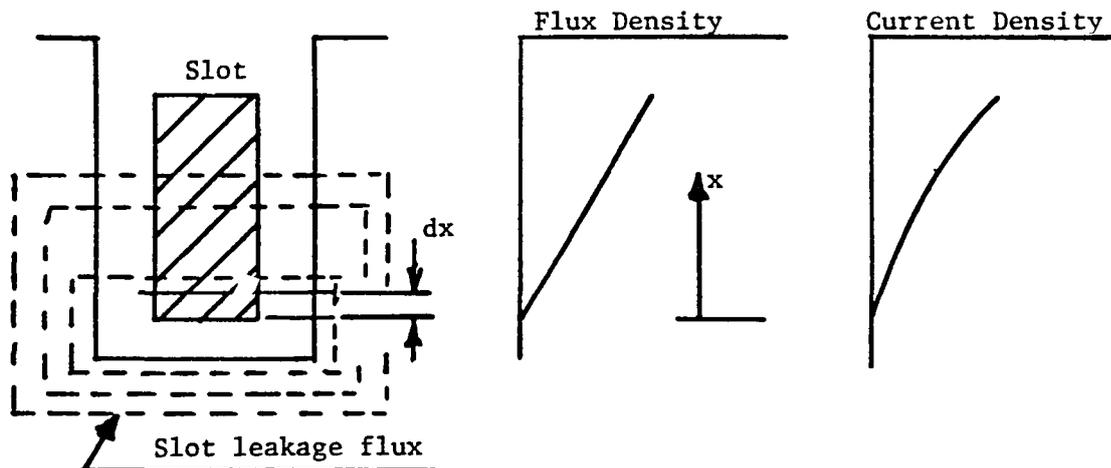
Figure 40. Inductor Skin Effect

Applying Ampere's law, it can be seen that the magnetizing force increases as distance x increases; thus the flux density of the cross slot flux increases linearly (if the permeability of the iron is very much greater than that of air) toward the top of the slot. The bottom element (shown as dx) is linked by all of the flux; the uppermost element by only the flux due to current in that element. Thus, the inductance of the elements decreases with increasing x. The voltage drop in all elements must be the same; therefore, because of the L di/dt voltage drop, the current is crowded into the upper portion of the conductor and the current density is as shown in Figure 40, reaching a maximum at the top of the inductor. Thus, a skin effect phenomenon, even with ripple free dc, exists. This skin effect can be reduced if multiple strands insulated from each other are used, since the skin effect increases with the square of the height of the conductor.

The skin effect loss in the armature is estimated (ref.8) at 5-25% of the "dc" copper loss, based on the dc ohmic resistance, depending upon how finely the inductors are stranded.

The previous chapter detailed static tests made to determine the variation of resistance and inductance with frequency. The apparent resistance measured accounts for skin effect in the conductors (loss #1) and for eddy current loss effects due to harmonic currents (loss #2e), but does not account for other eddy and hysteresis effects present when the motor is loaded and running.

Based on R,L tests made on the BLUE and RED motors (ref. 7), it was established that R and L, as functions of frequency and saturation, varied in an identical fashion for the two motors, although actual values for the motors were different. A curve fit routine applied to the RED motor measurements yielded (with the two field windings in series with the armature) the following apparent resistance and inductance, as seen by harmonic currents:

$$R = 0.0167 \ f^{0.7} \ I^{-0.07} \ \text{ohms} \tag{36}$$

$$L = 3.8 \ f^{-0.24} \ I^{-0.063} \text{mH} \tag{37}$$

These expressions point up the difficulty of applying a model, consisting of R,L,C, components, to the analysis of the behavior of the motor when subjected to chopper control and the resulting current, voltage harmonics.

Table 6 presents calculated losses due to observed harmonic currents for conditions of approximately 100 amperes and 200 amperes for chopper frequencies of 100 and 400 Hz and using the values of apparent resistance measured for those frequencies and currents.

Figure 30 compares the efficiency calculated from test results on the RED motor for conditions of ripple free dc and chopper controlled at chopper frequencies of 100, 200 and 400 Hz. Efficiencies from these curves are utilized in Table 6 to determine total losses for the conditions presented. Data tabulated includes:
- (a) the increase in losses using the chopper control over the ripple free dc
- (b) the calculated sum of the losses due to the harmonic currents
- (c) the difference between (a) and (b), denoted as "non-accounted for increase"

TABLE 6   RED Motor Calculated I^2R Losses $T_o/T = 0.45$

A. – Condition.   T = 0.01, f = 100 Hz, I_m = 103 amperes, P_o = 3500 watts (dc supplied)

I (Harmonic)	f	R	I^2R	LmH	wL/R
29.6	100	.303	265.5	0.94	1.95
4.3	200	.492	9.1	0.8	2.03
5.9	300	.654	22.8	0.72	2.08
2.8	400	.8	6.3	0.67	2.11
3.2	500	.935	9.6	0.64	2.14
1.9	600	1.062	3.8	0.61	2.3

Total 317 watts

$I_{DC}^2 R_{DC}$ = 371   (calculated) watts

From Figure 28, 30, For same Pin

100 Hz Eff: 48.2%, P_{Loss} = 2367 watts

DC Eff. 76.6%, P_{Loss} = 1069 watts

Increase·   1298

– Harmonic Calc·   −317

non accounted for increase= 981 watts

B. – Condition: T = 0.01, f = 100 Hz, I_m = 201 amperes, P_o = 6660 watts

36.4	100	.289	383.1
6.5	200	.470	19.8
6.6	300	.624	27.2
3.1	400	.763	7.4
3.4	500	.892	10.3
2.3	600	1.013	5.4
1.7	700	1.13	3.3

Total 457 watts

$I_{DC}^2 R_{DC}$ = 1414   (calculated) watts

100 Hz Eff· 63.2%, P_{Loss} = 3167 watts

DC Eff   77.4%, P_{Loss} = 1945 watts

Increase = 1222

– Harmonic Calc   = −457

non accounted for increase= 765 watts

C. – Condition.   T = 0.0025, f = 400 Hz, I_m = 98 amperes, P_o 3393 watts

11.9	400	.762	107.9
.91	800	1.238	1.0
2.4	1200	1.644	9.5
.4	1600	2.01	0.3
1.5	2000	2.351	5.3
.7	2400	2.671	1.3

Total 125 watts

$I_{DC}^2 R_{DC}$ = 336   (calculated) watts

400 Hz Eff. 49%, P_{Loss} = 2289 watts

DC Eff: 75.6%, P_{Loss} = 1095 watts

Increase   = 1194

– Harmonic Calc   = −125

non accounted for increase= 1068 watts

D. – Condition·   T = 0.0025, f = 400 Hz, I_m = 208 amperes, P_o = 6840 watts

13.9	400	.723	139.7
1.7	800	1.174	3.4
2.4	1200	1.56	9.0
1.3	1600	1.907	3.2
1.1	2000	2.23	2.7
.9	2400	2.534	2.0

Total 160 watts

$I_{DC}^2 R_{DC}$ = 1514 (calculated) watts

400 Hz Eff. 68.5%, P_{Loss} = 2805 watts

DC Eff: 76.8%, P_{Loss} = 2066 watts

Increase = 739

– Hamonic Calc. = 160

non accounted for increase= 579 watts

(d) the joule loss due to a ripple free dc current and the measured dc resistance.

(e) in condition (a), the values of L and $\omega L/R$ were calculated to verify the near constant ratio discussed in Chapter 2.

For each condition, the observed power output, P_o is shown. Using the dc efficiency, power input is calculated and the losses under chopper operation are calculated from this same input power and the efficiency from Figure 30.

The following observations can be made:

(a) Efficiency of a conventional motor is sharply reduced when chopper controlled. The higher the chopper frequency, the less the reduction in efficiency.

(b) The decrease in efficiency is more pronounced at lower values of average current, because the ripple (and magnitude of the harmonics) is a higher percentage of the average current, I_m. For example, refer to Figures 14 and 15 which show an increase of $\Delta i/I_{average}$ as $I_{average}$ decreases and as frequency decreases.

(c) Chopper control introduces additional losses not accounted for by consideration of harmonic currents and apparent resistance, as measured.

2. Eddy Current Losses

2.(a) In the Armature Due to Distorted Pole Face Flux

Eddy current losses occur in the armature inductors as they pass under the pole face if the flux density is not uniform. Non-uniformity results from the cross field component of armature reaction. The armature mmf is triangular in shape, with zero crossing midway between the brushes. If the brushes are on mechanical neutral, the flux density resulting from the armature mmf can be decreased by increasing the reluctance of the air gap under the pole tips. This is accomplished by designing the arc of the pole face with a radius much larger than the radius of the armature (chamfered pole shape), causing armature and pole face to be non-concentric, with air gap length at the pole tips larger than at mid pole. Another approach if laminated poles are used is to have the laminations with only one tip at each pole and stack the laminations such that the tip is in the opposite directions for adjoining laminations. The effect here is to decrease the permeability by decreasing the area of pole tip iron.

The above approaches merely modify (decrease) the magnitude of the loss. The armature reaction effect can be (theoretically) completely suppressed by the use of compensating windings embedded in the pole face.

The magnitude of this loss cannot be ascertained by measurement nor accurately calculated. In a motor operated on ripple free dc, it is estimated (ref. 8) to be 0.05-0.06% of the power output in a non-compensated motor and to be negligible if compensating windings are present. If the motor is supplied from a chopper source, the losses will most certainly be considerably higher because of the pulsations of the armature current due to the chopper action and resulting harmonics.

Compensating Winding Design

If armature current is to be passed through the compensating winding, the cross sectional area of the compensating winding must be "a" times greater than that of the armature conductors which carry a current of I/a amperes (a is the number of parallel paths in the motor). If Z_c is the number of compensating conductors per pole and the compensating winding is to provide the same mmf as that of the armature (ref. 9):

$$Z_c I_a = \left(\lambda\right)\left(\frac{Z}{p}\right)\left(\frac{I_a}{a}\right) \qquad (38)$$

$$\text{or} \qquad Z_c = \frac{\lambda Z}{ap} \qquad (39)$$

where:

Z = total inductors
λ = pole arc/pole pitch
p = number of poles

For the BLUE motor, with $Z = 256$, $a = 4$, $p = 4$, $\lambda = 53/90$ and 4 - #15 wire coils   (See Appendix A)

$$Z_c = 9^+ = 10$$

The cross sectional area required, for Z_c, is calculated as 0.01 square inches. Based on each Z_c equal to three times armature length (4-3/4 inches), this would add 1.83 lbs copper to the weight of the motor. For the RED motor, $Z_c = 5$, of area 0.023 square inches, yielding an added weight of copper of 1.67 lbs.

The conductor Z_c should be stranded to reduce eddy current losses. It appears that the increase in efficiency would offset the added weight of the winding.

2.(b)   In Armature Due to Tooth Saturation

Eddy current losses occur in the armature inductors due to tooth saturation and the main flux. Most dc machines are highly saturated, magnetically (refer to the nearly linear torque vs. ampere curves, Figure 27) with the armature teeth being the most saturated. A portion of the main flux passes through the slots and conductors. As the armature rotates and a tooth passes under a pole tip, the saturation level changes and the flux linking the conductors changes, and eddy currents are induced in the conductors (especially those conductors lying in the top part of the slot) and losses result. These losses have been estimated (ref. 8) to be on the order of 10-30% of the copper losses due to armature current in a motor supplied from ripple free dc.

Liwschitz-Garik (ref. 8) presents an empirical method of calculating these losses by expressing them as equivalent losses produced by a current flowing in the embedded part of the total winding. The current density corresponding to this current is:

$$J_m = 2.48 \left(\frac{hf}{\rho} \right) (10.2 \, B' - 16) \quad \text{amperes/cm}^2 \qquad (40)$$

Where: h = conductor height, cm

ρ = resistivity, micro-ohm cm = 1.724

$f = \frac{Np}{120}$, N = rev/min, p = # poles

B' = flux density at tooth root (taken as saturation level, approximately $1.83/\text{w/m}^2$

Let: K_1 = this loss as a % of dc copper loss at rated current

J = Current density at rated load

λ = net core length/1/2 mean turn length

Then:
$$K_1 = \left(\frac{J_m^2}{J^2} \right) (\lambda) \ 100 \qquad (41)$$

For the RED motor: $J = 224$ amperes/cm^2

$\lambda = 0.325$

$f = \frac{N}{30}$; $h = 0.787$ cm

then: $J_m = 0.1N$

and: $K_1 = \frac{2}{10^5} \ N^2 \%$

For $N = 2000$ $K_1 = 81\%$ of rated I^2R loss

   $N = 1000$ $K_1 = 20\%$ of rated I^2R loss

For the BLUE motor this loss is negligible because of the relatively small height of the conductor (i.e. 0.145 cm, which is 18% of height of RED motor conductor) and K_1 is proportional to the square of the height.

The following observations can be made:

The·losses can be mitigated by:

 a. reducing conductor height

 b. using deeper slots (with the top inductors further from the air gap)

 c. by using more iron in the motor (less saturation) which will improve the torque/ampere characteristic also but which adds weight and cost to the motor.

2.(c)   In the Armature Due to Cross Slot Leakage Flux

Eddy current losses are present in the conductors undergoing commutation (current reversal). The current reversal causes the slot cross leakage flux to collapse and then build up in the opposite direction. It is not possible to measure this loss, which is the principal constituent of stray load loss in a motor running on ripple free dc. It is possible to perform an analysis which gives insight into the loss, however.

Liwschilz-Garik (ref. 8) and Rudenburg (ref. 10) present methods of calculating (empirically) the increase in loss, due to eddy current effects, in conductors, due to cross slot leakage flux. The empirical equations yield different results, as will be shown in this section.

-Redenburg Method-

(Revised to apply to multiconductors in the slot)

Figure 41 portrays the slot, the conductors and the value of flux density, calculated by Ampere's law and assuming the iron is infinitely permeable.
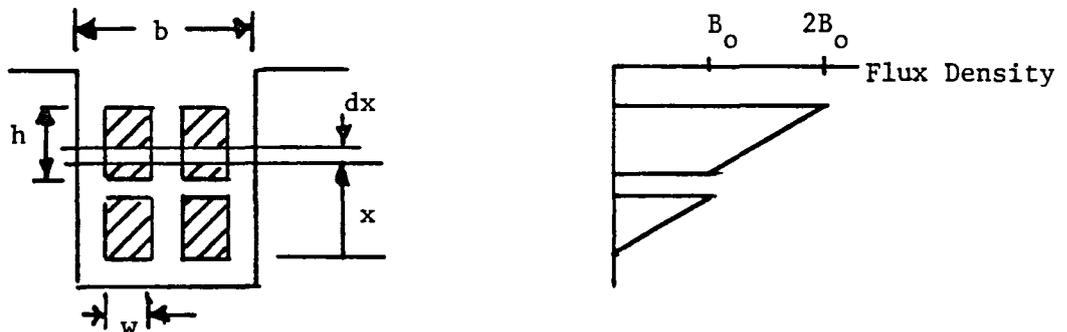
Figure 41.   Slot Cross Leakage Flux Density

Rudenburg shows that flux density, B, and current density, J, within the conductors are, assuming instantaneous current reversal:

For the Bottom Conductors

$$B = \frac{2}{\pi} B_o \sum_1^\infty \pm \frac{1}{n} \, \varepsilon^{-\alpha t} \, \sin \frac{n \pi x}{h} \tag{42}$$

$$J = 4 \, J_o \sum_1^\infty \pm \, \varepsilon^{-\alpha t} \, \cos \frac{n \pi x}{h} \tag{43}$$

For the Upper Conductors

$$B = \frac{4B_o}{\pi} (\varepsilon^{-\beta t} \sin \frac{\pi x}{h} + \varepsilon^{-9\beta t} \sin \frac{3\pi x}{h} + \ldots) \qquad (44)$$

$$J = 8J_o (\varepsilon^{-\beta t} \cos \frac{\pi x}{h} + \varepsilon^{-\beta t} \cos \frac{3\pi x}{h} + \ldots) \qquad (45)$$

where: n = harmonic number, $\alpha = n^2/T$ and $\beta = 1/T$

$$T = \left(\frac{\mu_o}{\pi^2 \rho}\right)\left(\frac{yw}{b}\right)\left(\frac{h}{n}\right)^2 \qquad (46)$$

w = conductor width, meters
y = number of conductors per layer
b = slot width, meters
h = conductor height, meters
ρ = resistivity, ohm-meter
x = distance from bottom of conductor

$$B_o = \mu_o \left(\frac{2yI}{b}\right) = \left(\frac{2\mu_o}{b}\right)\left(\frac{I_a}{a}\right) \qquad (47)$$

$$J_o = \frac{I}{wh} \qquad (48)$$

where:

$$I = \text{current per conductor} = \frac{I_a}{ya}$$

I = armature current
a = number of parallel paths

The above equations are based on a current collapse from a current of 2I to zero, simulating a change from + I to - I.

The loss produced by one current reversal can be determined from the initial energy, W, stored in the conductors and slot from consideration of the energy density. (Iron eddy current losses are neglected because the armature iron is assumed laminated.)

$$\text{energy density} = \frac{B^2}{2\mu_o} \qquad (49)$$

from which:

$$W = \frac{1}{2\mu_o} \int B^2 \, dv \tag{50}$$

where dv is the volume element, $\ell b dx$, with ℓ the length of the stack, and B, the flux density defined as shown in Figure 40.

$$W = \frac{1}{2\mu_o} \int_o^h (B_o \frac{x}{h})^2 \, \ell \, b \, dx + \frac{1}{2\mu_o} \int_o^h (B_o + \frac{x}{h} B_o)^2 \, \ell \, b \, dx$$

$$= \frac{B_o^2}{2\mu_o} \, \ell \, b \int_o^h (1 + \frac{2x}{h} + \frac{2x^2}{h^2}) \, dx \; .$$

$$= \frac{4 \, B_o^2 \, \ell \, b \, h}{3\mu_o} = \frac{16}{3} \, \mu_o \frac{\ell h}{b} \, (\frac{Ia}{a})^2 \frac{joules}{slot} \tag{51}$$

For ripple free dc, the frequency of current reversal will be

$$f = (\frac{N}{60}) \, (\frac{P}{2}) \tag{52}$$

and total joule losses, W_t, is (since W is lost twice each cycle)

$$W_t = 2 \, fW = \frac{32}{3} \, \mu_o \frac{\ell h}{b} \, (\frac{Ia}{a})^2 \, f \qquad watts/slot \tag{53}$$

The "dc ohmic resistance" loss, W_{DC} in 2 y conductors (2 layers of conductors) is: (where k is half the coil length/slot length)

$$W_{DC} = \frac{\rho \ell k}{wh} \, (\frac{Ia}{ay})^2 \, (2y) \, k \quad watts/slot \tag{54}$$

Of course, the "dc skin effect" due to non-uniform current distribution results in an actual joule loss greater than this value, but insight into the effect can be gained by finding the ratio:

$$\frac{W_t}{W_{DC}} = \frac{16}{3} \frac{\mu_o}{k} \, (\frac{w}{b}) \, \frac{h^2 y}{\rho} \, f = \frac{16}{3} \frac{\pi^2 f}{k} \, T \tag{55}$$

where T is the fundamental time constant, equation (46).

Applying the foregoing to the RED motor for which:

$w = 1.88 \times 10^{-3}$ meter   81 commutator bars
$y = 3$
$b = 7.63 \times 10^{-3}$ meter $\ell = 0.096$ meter
$h = 7.9 \times 10^{-3}$ meter $k = 5.8$
$\rho = 1.67 \times 10^{-8}$ ohm-cm
$a = 2$ parallel paths

-73-

$$I = \frac{Ia}{2 \times 3} = \frac{Ia}{6}$$

$$T = \frac{\mu_o}{\pi^2 \rho} \left(\frac{yw}{b} \right) h^2 = 0.35 \text{ ms}$$

The motor was tested over the speed range 930-2000 rpm, for a current reversal frequency range of 31-67 Hz, or periods of 15-32 milliseconds. Thus, the fundamental time constant, $T = 0.352$ ms is short, compared with the 15-32 ms time to the next commutation of that particular conductor, and the transient slot flux and eddy currents will have decayed prior to the next current reversal.

The validity of the assumption of instantaneous commutation can now be examined.

For 81 commutator bars, the time, t_c, for a bar to pass under a brush and accomplish current reversal will be, at the slower speed;

$$t_c = \left(\frac{1}{81} \text{ rev.} \right) \left(\frac{60}{930} \frac{\text{sec}}{\text{rev}} \right) = 0.8 \text{ ms}$$

and at the higher speed;

$$t_c = 0.37 \text{ ms}$$

These times are on the same order of magnitude as the fundamental time constant. Therefore, the eddy currents will decay within the commutation period and their magnetic fields will follow the reversing current. Thus, the energy will be dissipated in conductors and in brush-commutator contact resistance.

For the RED motor, from Figures 27 and 28:

$$I = 200, \quad N = 960, \quad f = 32 \text{ Hz}, \quad P_o = 6640 \text{ watts}$$

$$\frac{W_t}{W_{DC}} = \frac{16}{3} \frac{\pi^2 T f}{k} = \frac{0.018}{5.8} f = 0.099$$

$$I = 100, \quad N = 1940, \quad f = 65 \text{ Hz}, \quad P_o = 3320 \text{ watts}$$

$$\frac{W_t}{W_{DC}} = 0.202$$

The measured dc resistance was 0.0189 ohms. For a 200 ampere load;

$$W_{DC} = (200)^2 \times .0189 = 756 \text{ watts}$$

and:

$$W_t = (0.099) \times W_{DC} = 75 \text{ watts}$$

which is $\frac{75}{6640} \times 100 = 1.13\%$ of P_o

For the 100 ampere load

$$W_t = \frac{756}{4} \times 0.202 = 38.2$$

and this is 1.15% of P_o.

Since this loss is the major component of the stray load losses, commonly taken as 1% of P_o for ripple free dc current input, the theory presented here agrees reasonably well with the 1% figure arrived at through elimination of known losses to segregate the overall stray load losses.

When the motor is supplied from a chopper source, under the assumptions previously made, the effect of the harmonic currents, I_1, I_2, I_3, etc. of frequency f_1, f_2, f_3, etc. can be superimposed upon the current of the commutation frequency, using equation (55) to obtain;

$$W_t = \frac{16}{3} \frac{\pi^2}{k} T \{p \frac{N}{120} + f_1 \left(\frac{I_1}{I_{DC}} \right)^2 + f_2 \left(\frac{I_2}{I_{DC}} \right)^2 + f_2 \left(\frac{I_2}{I_{DC}} \right)^2 +$$

$$+ \ldots f_n \left(\frac{I_n}{I_{DC}} \right)^2 \} I^2_{DC} R_{DC} \qquad (56)$$

This equation neglects the retarding effect on flux build up due to eddy currents in the iron.

Equation (56) was used to calculate W_t for the average current and the additional W_t due to the various harmonic currents for four conditions, i.e. approximately 100 and 200 amperes average and at chopper frequencies of 100 and 400 Hz. Results are tabulated in Table 7.

The same calculations were performed for the BLUE motor, yielding a time constant, T, of 0.014 ms (1/25 of the constant for the RED motor) resulting in a negligible ratio W_t/W_{DC}. The reason for the extremely short time constant for the BLUE motor is that the coils are wound with 4-#15 wires paralleled. Each #15 is only 1.446 mm in height, whereas for the RED motor, the conductor height is 7.9 mm, a ratio of 5.5, and the loss effect is proportional to the square of the height.

-Liwschitz-Garik Method-

This method consists of the use of empirical equations for finding the skin effect losses in the conductors due to cross slot leakage flux, commencing with the "depth of penetration" equation:

$$\xi = 0.227 h \sqrt{\frac{wy\ f}{b\rho}} \qquad (57)$$

where: w = conductor width, cm
                y = # of conductors per layer
                b = slot width, cm
                ρ = resistivity of conductor, micro ohm - cm
                h = conductor height

                $f = \dfrac{N\ p}{120}$, N = rev/m

                p = # of poles

Find:

$$\sigma = \frac{b\ +\ (y\ -\ 1)\ \Gamma_c}{\Gamma\ (\dfrac{D_c}{D})\ \xi^2} \tag{58}$$

where: b = brush width, cm.

                Γ_c = commutator pitch, cm.

                Γ = pole pitch, cm.

                D_c = commutator diameter, cm.

                D = armature diameter, cm.

Find $$F\ =\ \frac{0.116}{0.13\ +\ \sigma} \tag{59}$$

Let: K_2 = skin effect loss as a % of dc copper loss at rated current

        λ = core length / 1/2 mean turn length

        m = # of layers of conductors in the slot

then: $$K_2\ =\ (\frac{4}{3\pi}\ m^2\xi^2\lambda F)\ 100 \tag{60}$$

K_2 was calculated for the motors with the following results:

RED MOTOR K_2 = 6.7%

                    $I^2 R_{dc}$ loss = 756 watts

                    Skin effect loss = 51 watts

BLUE MOTOR K_2 = 0.39%

                    $I^2 R_{dc}$ = 440 watts

                    Skin effect loss $\cong$ 2 watts

-76-

The value of 51 watts for the RED motor as calculated here corresponds to W_t calculated for dc current, 200 amperes, conditions B and D, Table 7, which were calculated by Rudenburg's procedure (modified by this investigator) yielding 52 watts for 201 amperes and 55 watts for 208 amperes.

The following observations can be made and conclusions drawn:

   (a)   at light loads, the "stray load" loss, with the chopper increased
         about 27% over the calculated dc value,
   (b)   for the 100 Hz, 100 ampere condition the loss increase was calculated
         at 20%, whereas for 400 Hz, 200 amperes it was only 4%. The variation
         is attributable to the fact that the fundamental harmonic current for
         the 400 Hz condition is only 7% of I_m, whereas for the 100 Hz condi-
         tion it is 18%.
   (c)   since the skin effect is proportional to the square of the height of
         the conductors, insulated strands built up to necessary conductor
         cross section are highly recommended for use.

2.(d)   In the Pole Face Iron Due to Slot Effect

Eddy current losses occur in the pole face by virtue of the variation of the air gap flux density due to slot openings. This loss cannot be measured. However, an empirical procedure for estimating the loss has been developed (ref. 8), and the results reproduced here. (This loss phenomenon is independent of current variation within the conductors; it is due only to permeability variations in the air gap.)

In order to determine the magnitude of the flux density ripple, B_o, the Carter coefficient, k_c is used to correct for slot opening.

$$k_c = \frac{g + (slot\ width/5)}{g + (slot\ width/5)(1 - slot\ width/slot\ pitch)} \qquad (61)$$

where: g = gap length.

then: $B_o = k_c \beta B$ (62)

B is average flux density in the air gap, β is a function of b/g and can be determined from Figure 42. (b is slot width at the air gap).
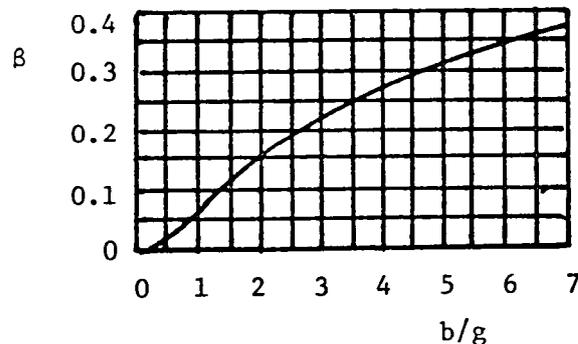
Figure 42. The quantity β as a function of b/g

TABLE 7   RED Motor, Calculated Slot Leakage Flux Loss
(Rudenburg Method) $T_o/T = 0.45$

A. - Condition: $T = 0.01$, $f = 100$, $I_m = 103$, $N = 1770$ rev/mm, $P_o = 2327$ watts

I	f	W_t
104	DC	38
29.6	100	8.1
4.3	200	.34
5.9	300	.97
2.8	400	.3
3.2	500	.5
1.9	600	.2
		48.4

due to chopper harmonics.

$$\% \text{ increase} = \frac{48.4 - 38}{38} \times 100 = 27\%$$

B. - Condition: $T = 0.01$, $f = 100$, $I_m = 201$, $N = 645$ rev/m, $P_o = 5562$ watts

I	f	W_t
201	DC	52.2
36.4	100	8.0
6.5	200	.5
6.6	300	.8
3.1	400	.2
3.4	500	.4
2.3	600	.2
1.7	700	.1
		62.5

$\%$ increase = 20%

C. - Condition: $T = 0.0025$, $f = 400$, $I_m = 98$, $N = 1380$ rev/m, P_o 3393 watts

I	f	W_t
98	DC	26.5
11.9	400	5.9
.91	800	.1
2.4	1200	.7
.4	1600	—
1.5	2000	.5
		34

$\%$ increase = 27%

D. - Condition: $T = 0.0025$, $f = 400$, $I_m = 208$, $N = 632$ rev/m, $P_o = 5659$

I	f	W_t
208	DC	54.7
13.9	400	1.8
1.7	800	.1
2.4	1200	.2
1.3	1600	.1
1.1	2000	.1
		5.7

$\%$ increase = 4%

B, the average flux density can be determined from:

$$E = \frac{Z \phi p N}{60a} \quad \text{or} \quad V\frac{T_o}{T} \cong \frac{Z B A p N}{60a} \qquad (63)$$

neglecting armature/field circuit resistance. (V is source voltage, T_o/T is ratio of chopper on time to chopper period).

The pole face loss is then estimated from:

$$\text{Loss} = (p)(A) \; k_s \; (\frac{QN}{1000})^{1.5} \; (\frac{B_o 1}{1000})^2 \times 10^8 \text{ watts} \qquad (64)$$

where:

p	=	# of poles
A	=	area of pole face, cm^2
Q	=	# of slots
N	=	rev/min
B_o	=	peak flux density ripple, webers/meter^2
1°	=	lamination thickness, cm., or if solid pole face, it is slot pitch
k_s	=	24×10^{-4} for solid steel
	=	6×10^{-4} for 0.06" sheet steel
	=	5×10^{-4} for 0.04" Dynamo steel

For the RED motor, with 26 gauge, 0.0457 cm laminated poles, the loss, calculated using equation (64), at 960 rev/m, yields a loss of 0.27 watts, which is negligible. However, if the poles were not laminated, for the same conditions, the loss would be 593 watts.

This is an insignificant type of loss if the pole faces are laminated, but would be a major loss if solid poles are utilized.

2.(e) In the Magnetic Circuit Due to Harmonics Resulting From Chopper Action

The apparent resistance increase with frequency (ref. 7), described in Chapter 2, is a measure of skin effect in the conductors, with frequency. There are insufficient ampere turns available in the measurement technique for a series motor to force the harmonic flux throughout the magnetic circuit; thus this loss is not accounted for in the change in apparent resistance detailed earlier.

2.(f). In Steel Banding Wire Used to Secure the Armature Winding.

This loss is highly dependent upon longitudinal location of the banding, the resistivity of the wire used and the amount of wire used. The loss can be eliminated by using a non-metallic high tensile strength, high modulus of elasticity material, such as Dupont Kevlar, an Aramid which has a high modulus of elasticity (low stretch), very good tensile strength and stability, even at temperatures in excess of 280^oC, and is non-conducting.

3. Losses In The Equalizer Connection:

In a lap wound (parallel) machine, with p poles, p/2 voltage polygons exist. (A voltage polygon is obtained if the phases, representing the amplitude of the emf's of the winding elements, are shifted with respect to each other by an angle corresponding to a slot pitch and arranged in succession in the same order in which they follow one another.) Since it is a parallel winding, the points on the voltage polygon, when the p/2 polygons are placed one above the other, should coincide. If the pole system is not symmetrical, or if armature bearings are eccentric, the voltages at the points where they should coincide do not in fact coincide. Since some of the points are connected by brushes of the same polarity, circulating currents will flow through the brushes, and sparking at the commutator (and some loss) results. The same problem arises if the armature windings are not symmetrical. Since each two parallel paths make one voltage polygon, the number of winding elements (commutator bars) must, for symmetry, be an integer, i.e.

$$\frac{\# \text{ of bars}}{a/2} = \text{integer} \tag{65}$$

and,

$$\frac{\# \text{ of slots}}{a/2} = \text{integer} \tag{66}$$

Those two conditions must be met for a lap winding for $p \geq 4$. For the simplex wave (series) winding, no symmetry requirements (or equalizer winding) are required. The equalizer winding improves commutation but does introduce an un-measureable joule loss in the winding. The BLUE motor does have an equalizer winding. For it,

$$\# \text{ of bars} = 64$$
$$\# \text{ of slots} = 32$$
$$a = 4$$

Thus, the conditions for winding symmetry are met. However the pole system is not symmetrical and thus the equalizer winding is necessary and undoubtedly contributes to joule loss in the motor. The RED motor winding is wave wound (simplex) and thus does not require an equalizer winding. However, since it has 81 bars, 27 slots it would require an equalizer if it were duplex, or triplex wound (a > 2). If the duplex or triplex wave winding is utilized, it must not only satisfy the criteria of equations (65) and (66) but must also fulfill the additional criteria of:

$$\frac{p}{a} = \text{integer} \tag{67}$$

if an equalizer winding is not to be required.

4. Losses in Commutated Coils.

As the commutator segments pass under the brushes and the direction of current in the coils connected to the segments short circuited by the brush reverses,

joule losses occur in the coils. These losses are an unavoidable aspect of dc machines and are minimized if the brushes are on magnetic neutral. If the brushes are not on magnetic neutral, the losses are considerably larger because the short circuited coils have a rotational emf induced in them due to the dc component of flux and a transformer emf induced due to the time varying flux, if harmonic currents are exciting the field.

The magnitude of the loss depends on:

    a.   the number of turns/coil, and the conductor resistance,
    b.   the number of coils shorted (commutator segments shorted by the brush),
    c.   the number and position of the brushes,
    d.   whether lap or wave wound,
    e.   the flux present (excitation current),
    f.   the speed of the motor,
    g.   the frequency of the harmonic currents.

The wave wound RED motor brushes span 3 commutator segments; there are 2 pairs of brushes, resulting in 6 turns short circuited. The lap wound BLUE motor, with skewed commutator, has 4 segments shorted by each brush. For the 2 turns/coil, 3 coils shorted and 4 brushes, there are a total of 24 turns shorted.

Since these motors rely on brush shift to achieve satisfactory commutation and location of proper brush shift is not an exact science, it is highly probable that the brushes will not be on magnetic neutral.

To investigate the effects of brush shift, as well as those of speed, average current and frequency effects on this type of loss, several tests were conducted with the field excited at various levels of current, both ripple free dc and chopper controlled. Since there was no current in the armature, the brushes on 0° (mechanical neutral) correspond to magnetic neutral. Previously measured brush and bearing friction and windage loss were subtracted from the shaft power input to the motor, yielding the loss in the coils:

$$P_c = \omega T - P_{rot} \tag{68}$$

where P_c = commutating loss

                 ω, T = speed, torque

                 P_{rot} = mechanical rotating loss

Figures 43 and 44 depict P_c as a function of speed, series field current and brush position for the BLUE motor, from ripple free DC supply. Figures 45 and 46 show the same information for the RED motor. For the brushes on magnetic neutral, the losses for the RED motor increase nearly linearly with speed (for constant current) (Figure 45) whereas theoretically (since emf is proportional to speed and P_c is proportional to the emf squared) they should increase by the square of speed. For the BLUE motor, the increase with field current is linear at 1000 rpm, but approaches a second order variation at higher speeds. This leads to the belief that the contact resistance between brush and commutator varies with speed and current density. (The motors have different brush material, so the variation is different between the two motors.)

Figure 43 BLUE Motor Losses in Commutated Coils As a Function of Speed and Saturation

Watts Loss

700

600

500

400

300

200

100

0

3320 rpm

Armature on Open Circuit
I_f from Generator DC
Brushes at 0°

2000 rpm

1000 rpm

0   20   40   60   80   100   120   140   160   180   200   220

field Amperes
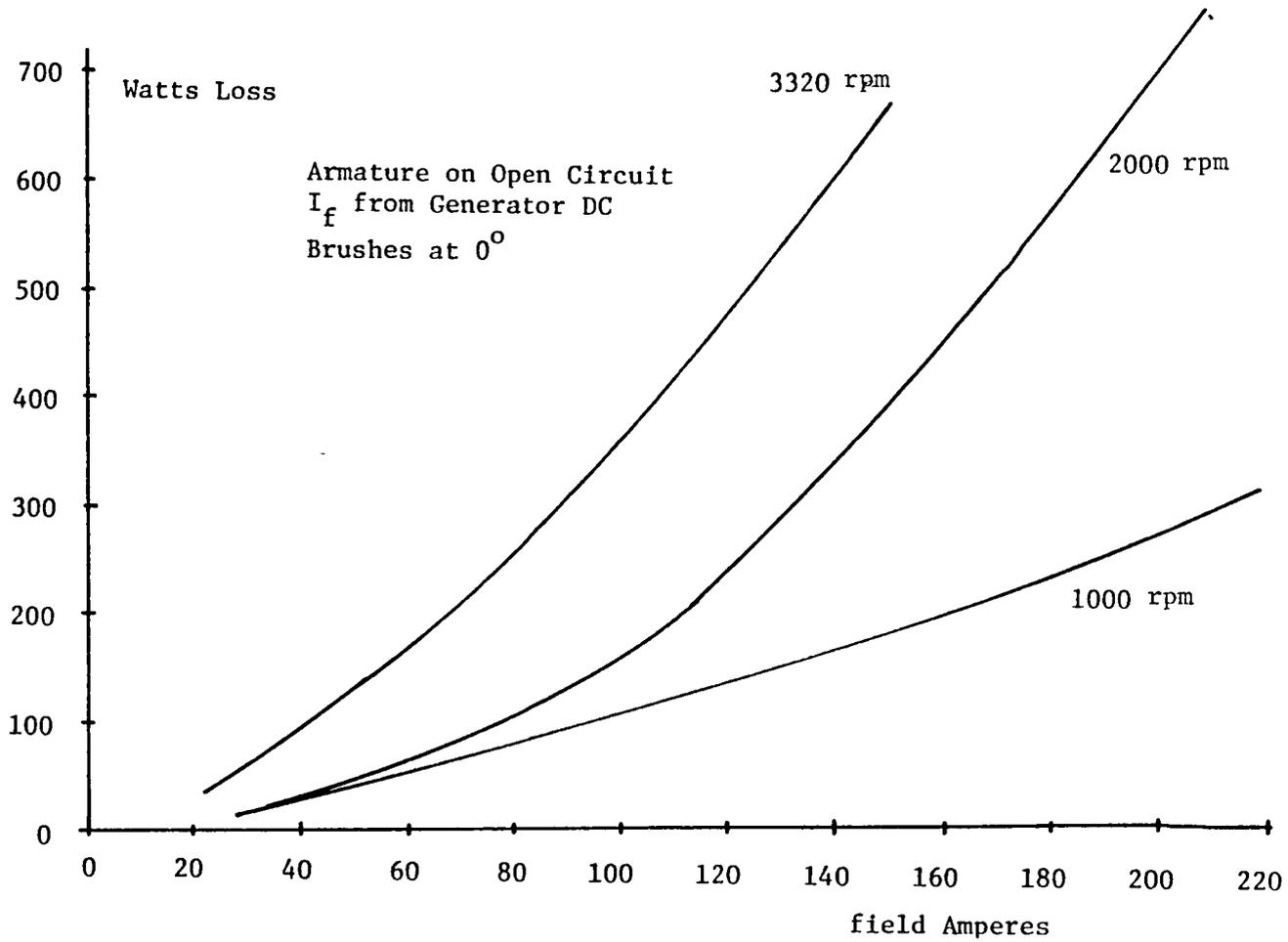
Figure 44 BLUE Motor Losses in Commutated Coils
As a Function of Speed and Brush Position
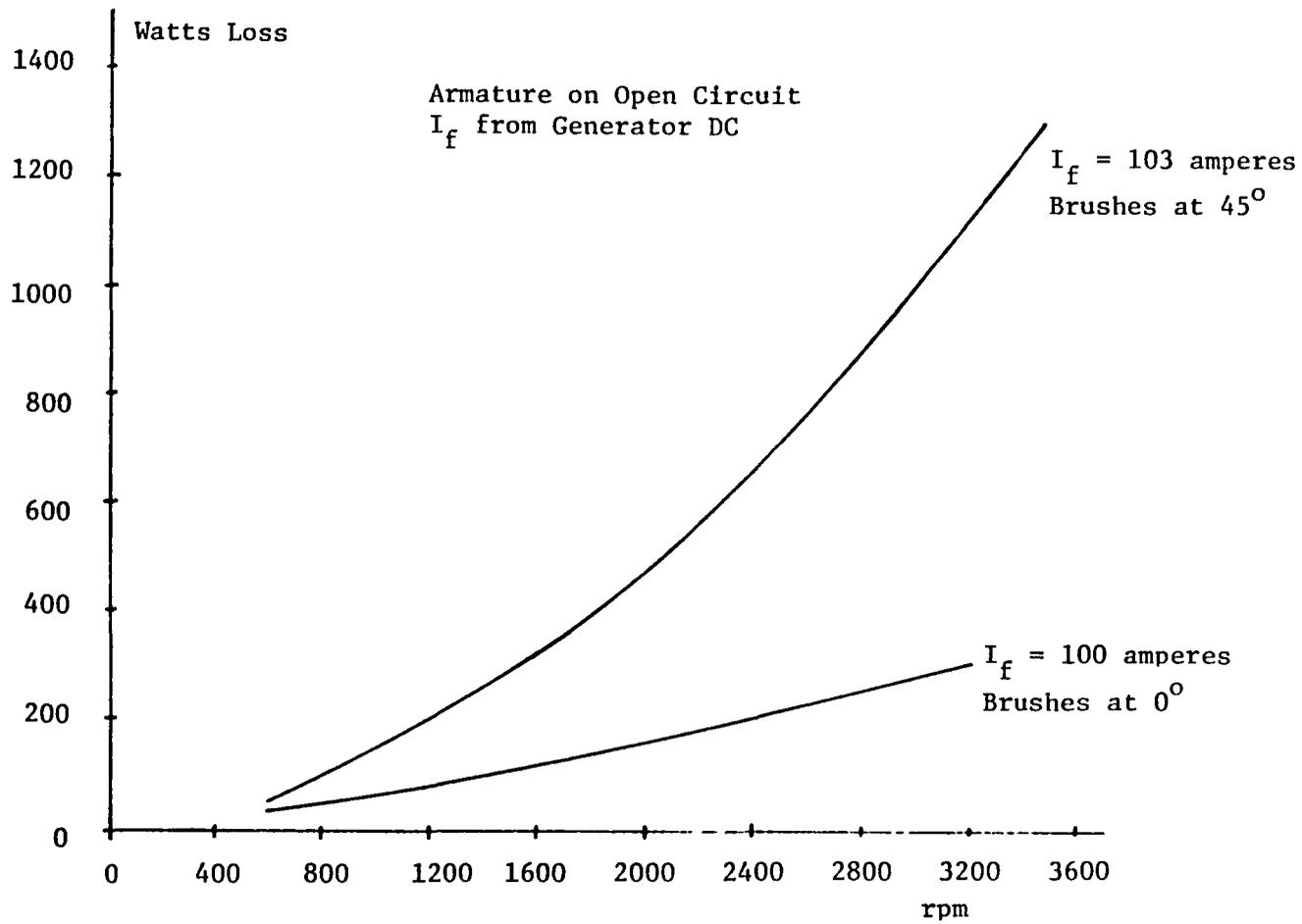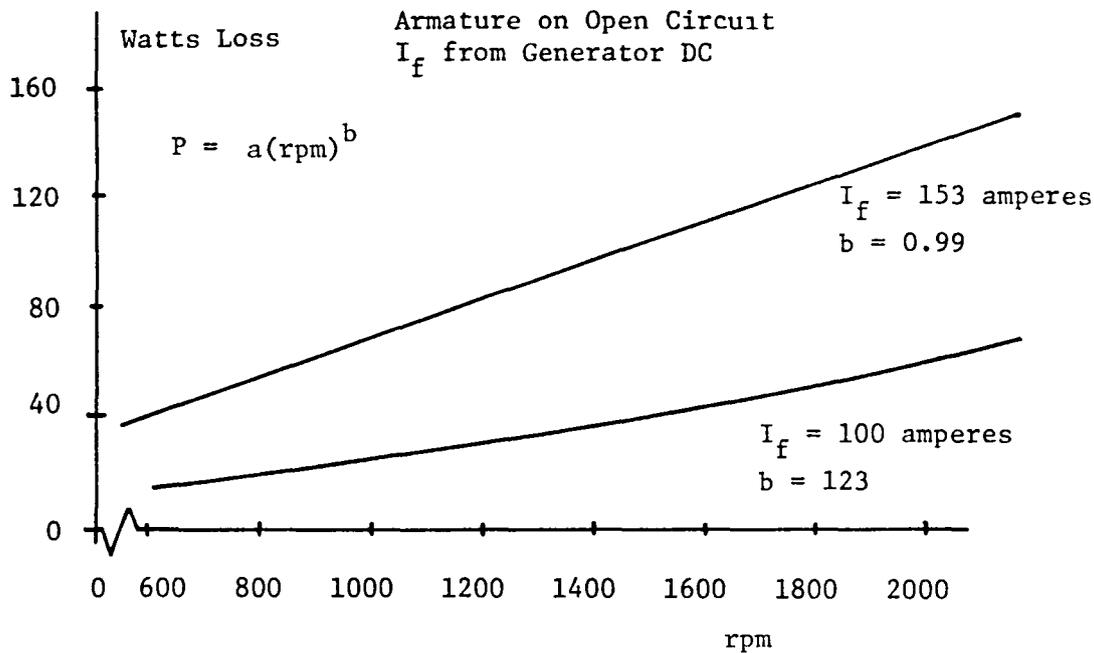
Figure 45   RED Motor Losses in Commutated Coils
As a Function of Speed and Excitation

The variation, at constant speed, with field current is less than the theoretical squared value because of saturation of the magnetic circuit.

Figure 44 and 46 show the effects of improper brush location. For the RED motor, at 155 amperes, 1400 rpm, a 10° electrical shift increased the losses by 17% over the 0° loss, whereas a 20° shift increased the losses by 113%. For the BLUE motor, a 45° electrical shift increased the loss at 2400 rpm, 100 amperes, by 225%. Figure 47 is similar to Figure 46, except it is for the brush shift effect when the motor is chopper controlled at a frequency of 77 Hz. Comparison of these two figures indicated about a 75% increase in P_c due to the 77 Hz harmonic currents. Figure 48 demonstrates a direct comparison between P_c from dc and from 77 Hz operation, with the brushes on magnetic neutral.

For the RED motor, on dc, at 155 amperes, 42 volts, 1250 rpm, the total losses were observed to be 1318 watts. From Figure 46, at 1225 rpm, P_c = 90 watts. This is 7% of the total loss. Under chopper control, at 77 Hz, under the same current/speed condition, total losses are 3207 watts, with P_c - 156, which is about 5% of the total loss.

Figure 49 depicts the variation of P_c as a function of speed and chopper frequency for two levels of field current for the BLUE motor. As can be seen, P_c increases, for the same field current, with an increase in chopper frequency. It appears that, for a given speed and current (average), P_c increases proportional to approximately the 0.5 power of frequency, rather than linearly as it theoretically should if the harmonic current magnitudes were equal. However as shown previously, the relative harmonic magnitudes decrease with increasing frequency; thus P_c does not increase directly with frequency.
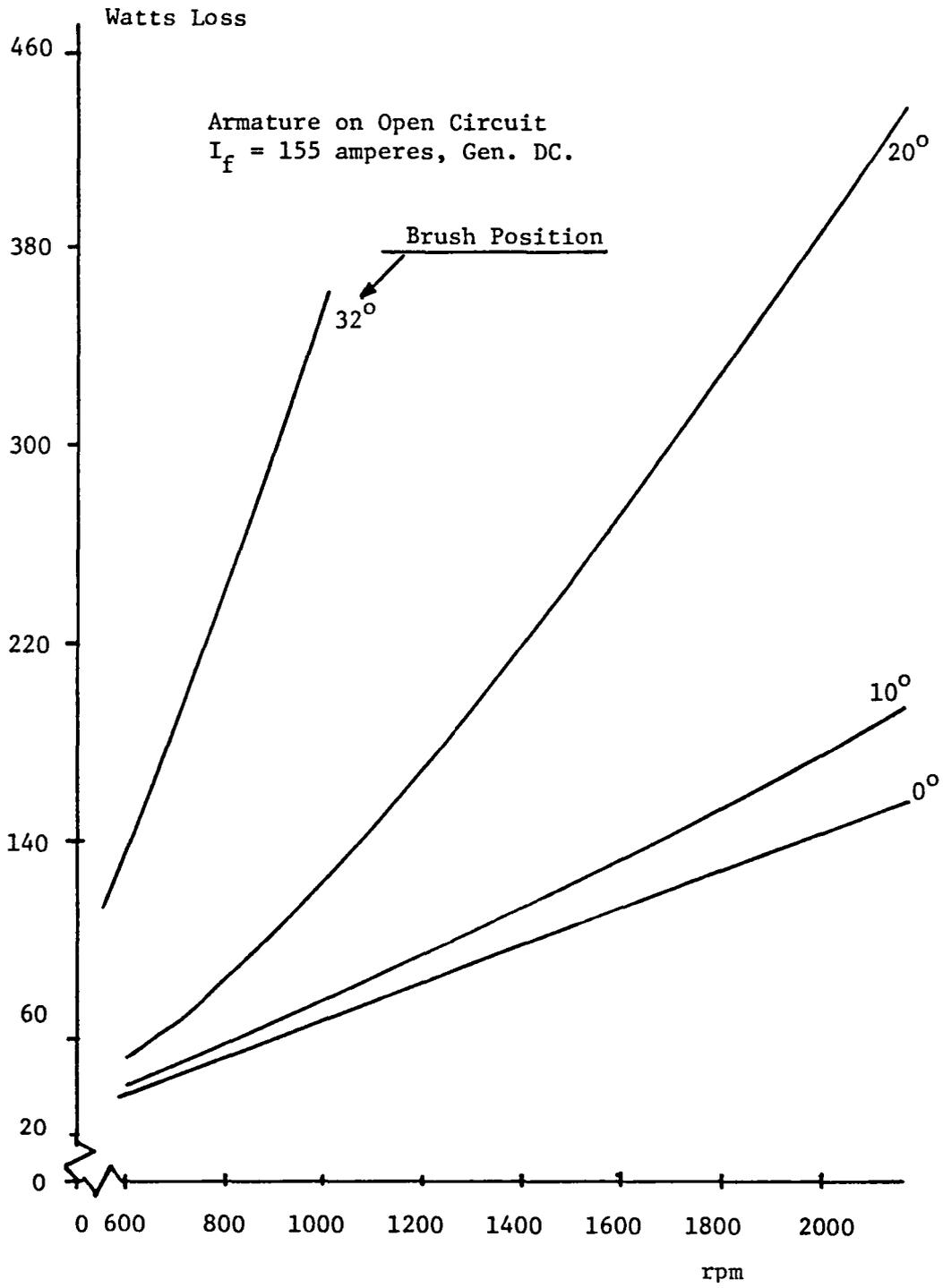
Figure 46 RED Motor Losses in Commutated Coils
As a Function of Speed and Brush Position
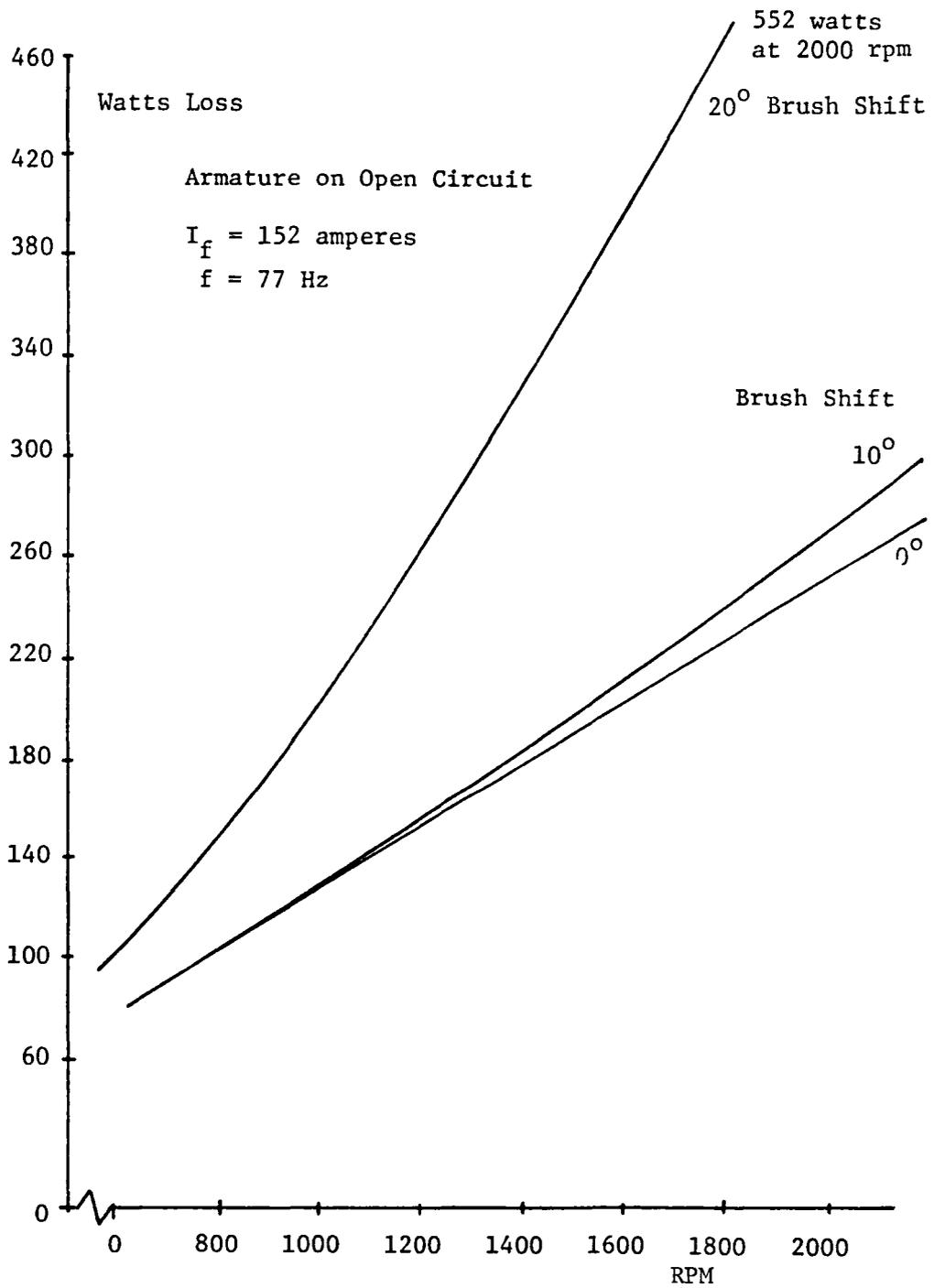
Figure 47 RED Motor. Losses in Commutated Coils
As a Function of Speed and Brush Position
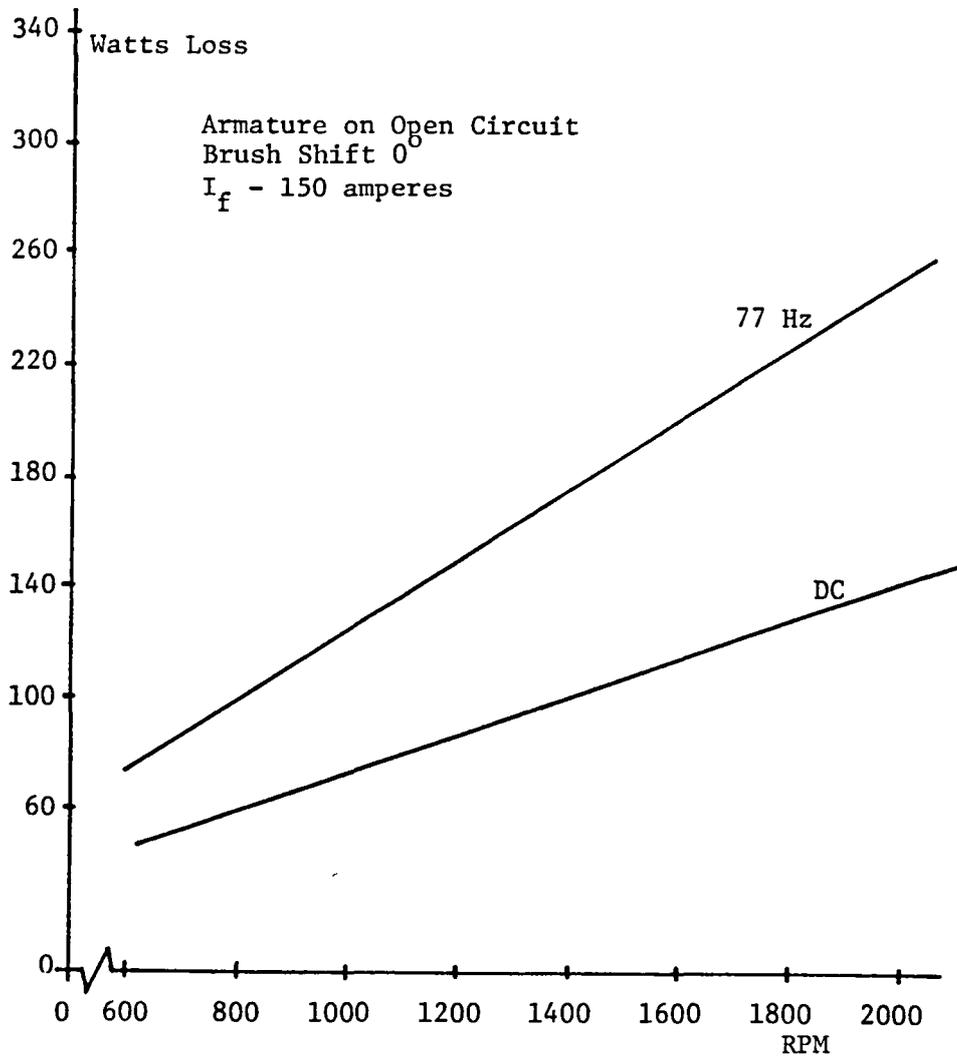
Figure 48 RED Motor. Losses in Commutated Coils
As a Function of Speed. DC v. 77 Hz
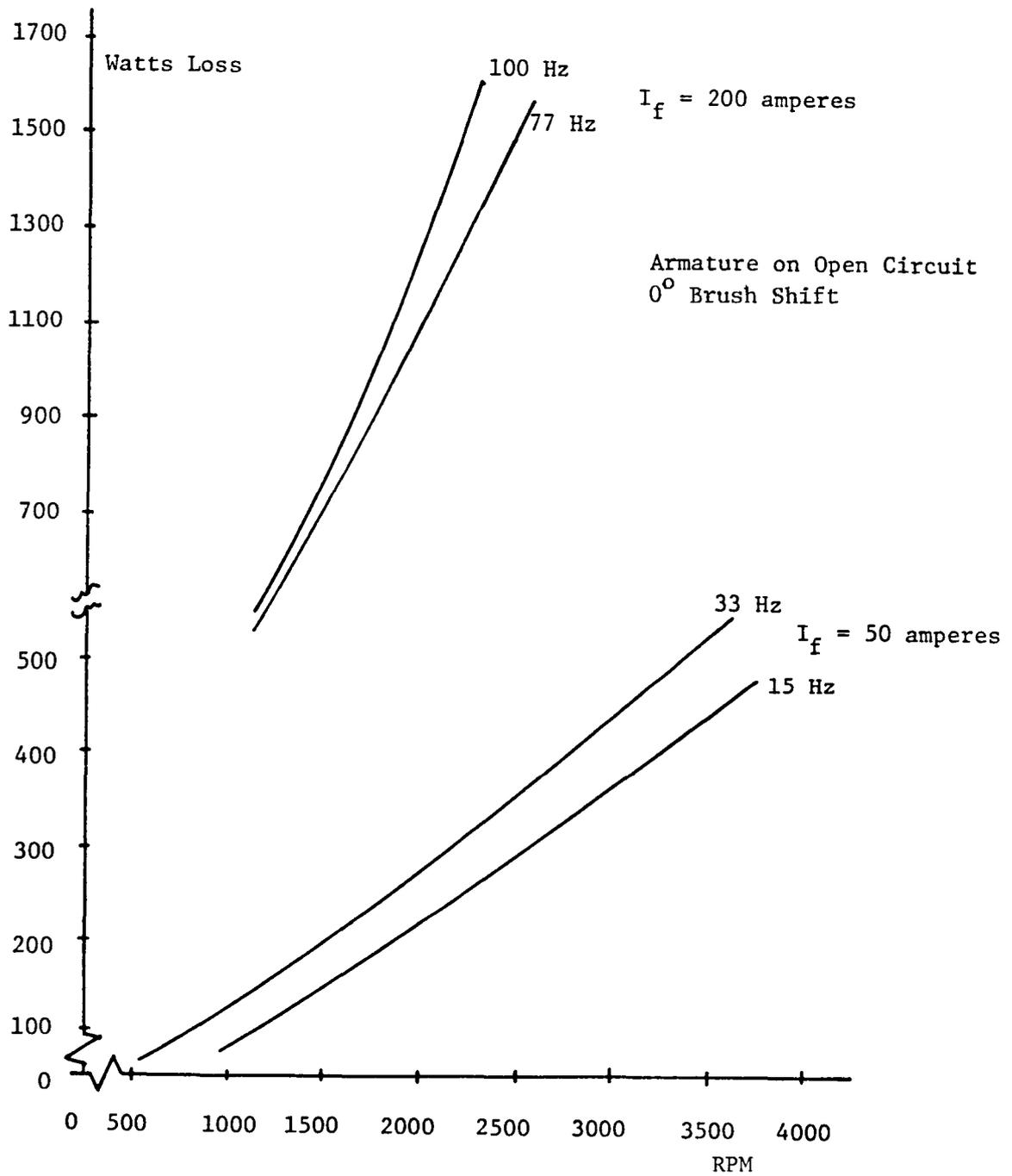
Figure 49 BLUE Motor   Losses in Commutated Coils
As a Function of Chopper Frequency

The following observations can be made, based on the test results:

(a) The loss in the commutated coil can be a substantial portion of the total losses in the motor, if the brushes are improperly located and if the chopper repetition frequency is relatively high. The loss magnitude is very sensitive to brush position--if such position is off by more than 10 - 15 electrical degrees. In an electric vehicle, without interpoles, operation in reverse will result in brushes off magnetic zero by an angle of $60 - 90^{\circ}$ and may cause overheating due to excessive losses.

(b) This loss can be reduced by decreasing the number of turns shorted during the commutating process. This is accomplished by using a wave winding and/or increasing the length of the commutator which permits narrower brushes while retaining the same brush cross sectional area.

5. Loss Due to Brush Resistance

Some brush resistance is essential for the commutating process. The basic equation of commutation is:

$$\frac{I_a}{a} \geq \frac{\text{Reactance Voltage} - \text{Commutating emf}}{R} \tag{69}$$

where: Reactance voltage is the rotational emf in the coil due to armature cross magnetizing flux plus the induced emf due to self and mutual inductance and changing current. The commutating emf is the rotational emf due to interpole flux or flux resulting from brush shift and R is the contact resistance between commutator segment and brush plus internal brush resistance.

By establishing the commutating emf to the proper value, minimum R can be utilized, i.e. brush material yielding minimum contact drop and internal brush resistance (low resistivity).

One of the motors tested was known to have electrographitic brushes. The motors had measured voltage drops of 0.5 and 0.53 volts, indicating that they were both probably equipped with electrographitic brushes. Electrographitic brushes are composed of amorphous carbon material subjected to high temperature to obtain a more graphic structure. Also available are metal-graphite brushes, made from natural graphite and finely divided metal powders (copper, silver, etc.) Both materials yield low (below 0.22) coefficients of friction. However the metal graphite brush with silver can yield an internal resistivity two orders of magnitude lower than that of the electrographitic brush and is recommended for applications such as these motors, i.e. relatively high current, low voltage, with minimum losses.

For the motors at rated ouput (200 amperes) the brush loss amounts to 106 watts. This cannot be reduced below some minimum value, but any reduction does improve efficiency and reduces heating at the commutator surface.

6. Losses Due to the Free Wheeling Diodes (FWD)

The controller used in this investigation had two FWDs, one paralleling the armature only and the other paralleling the armature and the series field. In tests made in the running mode, the former diode carried no measurable current. The tests were made on the RED motor, with brushes at -28° at frequencies of 100, 200 and 400 Hz. Observed results for the armature and field diode are tabulated in Table 8.

TABLE 8 FWD (Diode) Currents

$\dfrac{T_o}{T}$	freq-uency	I_{motor} Ave	I_{diode} Ave	I_{diode} peak	I_{diode} min	Δi $I_p - I_{min}$	$\dfrac{I_d}{I_m}$	RPM
0.43	100	193	86.5	265	91	173.5	0.449	800
0.48	200	189	85.5	259	118	141	0.452	800
0.48	400	199	93.1	221	129.5	91.5	0.467	800
0.43	400	109	55.8	123.5	70.6	53	0.514	1500

Power dissipated in the FWD was measured as 74 watts, at 86.5 amperes, average, yielding an average voltage drop, across the diode, of 0.86 volts. In each of the above runs, a pronounced 1100 Hz oscillation was evident. Figure 50 is typical of the diode currents observed.
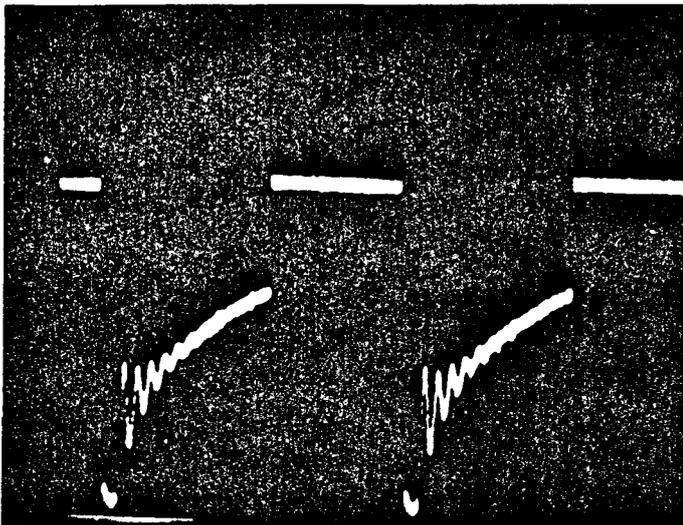
Diode Current

2 ms/cm.

50 amperes/cm

Condition:

100 Hz

$\dfrac{T_o}{T} = 0.43$

Figure 50 FWD Current

The only use of the armature-only FWD is in the event power plugging is to be Used for braking or in the event the car started rolling backward when connected for forward operation.

7. Losses Due to Shaft, Bearing, Housing Current From Shaft Induced Emf.

An emf can be induced in the motor shaft because of an unsymmetrical distribution of flux between the poles, which results in a net flux encircling the shaft and/or capacitive coupling between windings and the magnetic core in conjunction with current harmonics. Large machines with pedestal type bearings usually have one pedestal insulated from the machine base to preclude the damaging effects to the bearing surface that result if such currents exist. Small machines generally do not experience this problem. However, in the course of this investigation it was felt that it would be desirable to quantitatively examine the magnitude of the parameters to determine if a significant loss was present due to the phenomena.

The BLUE motor, with non-symmetrical pole geometry, was the motor tested. This motor has a laminated magnetic frame clamped between aluminum end bells. The bearing at the end opposite the commutator was replaced by a thinner, smaller diameter bearing surrounded by an insulating material, thereby "opening" the closed conducting path formed by armature, shaft, bearings and frame (housing). An electrical connection was then made between the frame and shaft (via a slip ring) across the insulated spaces between bearing and housing. A Kelvin Bridge measurement indicated 0.760 ohms resistance existing between the two points. (The contact resistance between laminations probably accounts for this relatively high value of ohmic resistance).

The motor, with armature circuit open and no excitation, was then driven over the speed range from 500 to 1650 rpm with no field excitation. The dc voltage measured (with a high input impedance electronic digital voltmeter) ranged from 1.0 mv to 2.3 mv. A true rms voltmeter indicated from 215 mv at 500 rpm up to 650 mv at 1650 rpm. Background noise, i.e., at zero speed, was measured at 0.05 and 7.5 mv, respectively.

At 1650 rpm, with ripple free dc current applied to the series field (over the range 52 amperes up to 187 amperes), the dc volts fluctuated from 1-5 mv, the true rms voltage from 700 to 820 mv. The test was then repeated using a 100 Hz repetition rate chopper current for field excitation. No apparent difference in induced voltage magnitude between chopper current and ripple free dc voltage was noted. It was concluded that even in a motor with unsymmetric pole structure this type of loss is negligible and should not be of concern from an efficiency standpoint.

Iron Hysteresis Losses

8. In the Magnetic Structure Due to Chopper Harmonics

The series field current contains harmonics due to chopper control. The harmonics do provide excitation resulting in harmonic flux which does result in core loss (hysteresis and eddy current). This loss cannot be calculated with any degree of accuracy but overall magnitude can be estimated.

The 1st harmonic is the predominant harmonic and was used for estimating the harmonic current core loss.

The iron in the magnetic path of the BLUE motor is estimated to weigh 115 lbs. Flux density is estimated (average) at 1.0 Weber/meter^2 at 100 amperes average current. From Figure 10, at 100 Hz chopper repetition rate, the fundamental harmonic is approximately 40 amperes rms, yielding a resulting flux density of 0.4 Weber/meter^2. Using Core Loss curves for 29 gauge, M-22 non-oriented steel, the loss at 100 Hz is less than 0.01 watts per pound.

Again, referring to Figure 10, the 400 Hz fundamental harmonic is only about 1/3 that of the 100 Hz current. Hysteresis loss is proportional to the frequency and to a power of the flux density (between 1.5 and 2 is an accepted range). For the 400 Hz current, a loss of less than 0.025 watts per pound is projected.

It is concluded that this is an insignificant loss for the BLUE motor which has a laminated frame. If the machine has a solid frame, not recommended for use with a chopper, as does the RED motor, the hysteresis (and eddy current) losses could be substantial, however.

9. In the Pole Face Due to Variation of Flux Due to Slot Openings

Based on the estimates made in 8, above, it can be concluded that this loss is negligible also, if laminated poles are used.

Mechanical Losses

10, 11. Bearing and Brush Friction and Windage

These losses include brush friction, bearing friction and windage. Total mechanical losses can be obtained by measuring the power necessary to drive the armature with zero excitation on the machine, then raising the brushes and again measuring the power as speed is varied. The latter yields the bearing friction and windage; the difference between the two power requirements yields brush friction.

Bearing friction and windage cannot realistically be separated by measurement, although empirical equations for these quantities are available. For example, the power required for bearing friction, P_Γ, is empirically given as:

$$P_\Gamma = K(rpm)^{5/3} \tag{70}$$

where K is a constant dependent of bearing dimension and loading.

Windage power, P_ω, is theoretically:

$$P_\omega = \pi \, C_d \, \rho \, R^4 \, \omega^3 \, \ell \tag{71}$$

where   R = radius
           ℓ = length
           ρ = air density
           ω = speed
           C_d = skin coefficient

and:

$$\frac{1}{C_d} = 2.04 + 1.768 \, \ell n \, (R_e \sqrt{C_d}) \tag{72}$$

where: R_e = Reynolds number.

This equation represents turbulent flow conditions. The difficulty in applying this is determination of R_e for the complex geometry of the armature, with slots, poles and gaps. The only usefulness of the equation is in noting the variation of P_w with R, ω. It should be recalled that for a given speed, power rating of a motor is proportional to $R^2\omega\ell$. Thus to attempt to decrease P_w by decreasing R or ω, would be counterproductive. The only reasonable design steps to be taken are to reduce surface irregularities on the armature (slots, end connections) as much as possible and to use highest quality bearings.

Calculation of power loss to overcome brush friction, P_b, is suggested in IEEE #113 (43f. 1) as:

$$P_b = KvA \tag{73}$$

where   K = 0.004 for carbon, graphite and electrographitic brushes
        = 0.0025 for metal graphite brushes
        v = surface velocity, meters/min.
        A = brush area, square centimerers

Calculated values are:

BLUE MOTOR:	A = (8)(5.04) = 40.32 cm^2
(2000 rpm)	v = (0.327)(2000) = 654 meter/min.
	P_b = (0.004)(40.32)(654) = 105 watts
RED MOTOR:	A = (8)(4.16) = 32.28 cm^2
(2000 rpm)	v = (0.400)(2000) = 800 meter/min
	P_b = (0.004)(32.28)(800) = 103.3 watts

Figures 51 and 52 depict the results of measurements taken on the RED and BLUE motors. The bearing friction loss, P_r, and the windage loss, P_w, are plotted as $(P_r + P_w)$ and also total rotating losses, P_r, are shown as functions of speed. The difference between these two is the brush friction loss, P_b. As can be seen, the brush friction power loss is linear with speed. However, at 2000 rpm, measured values are:

BLUE motor, P_b = 180 watts

RED motor, P_b = 440 watts

It can be concluded that the IEEE formula does not give accurate results, at least for these motors.

The measured brush pressure on the RED motor brushes was found to be 7 psi, vs. 3.8 psi on the BLUE motor (usually brush pressure is approximately 4 psi). This may have been an attempt to secure low contact voltage drop across the brush-
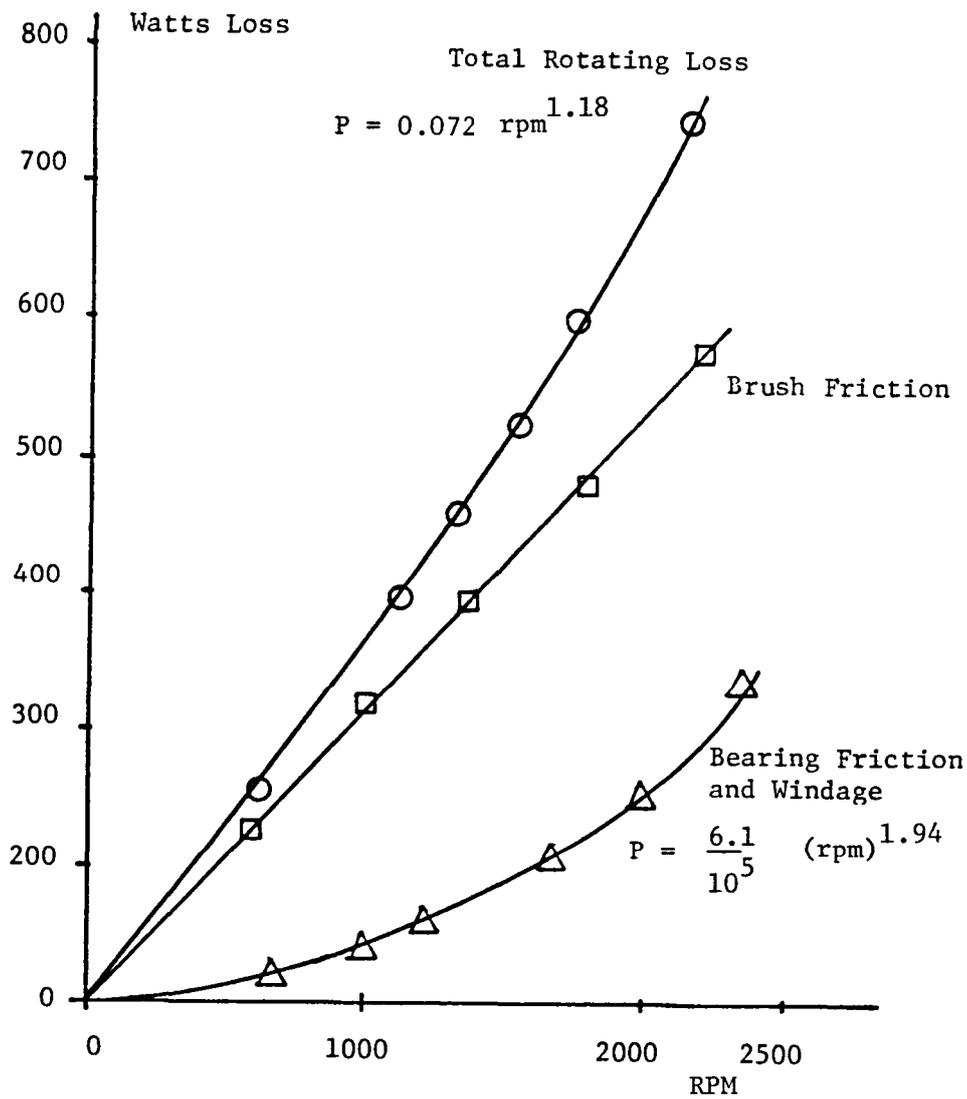
Figure 51 RED Motor. Rotating Losses as a Function of Speed

Figure 52 BLUE Motor. Rotating Losses as a Function of Speed
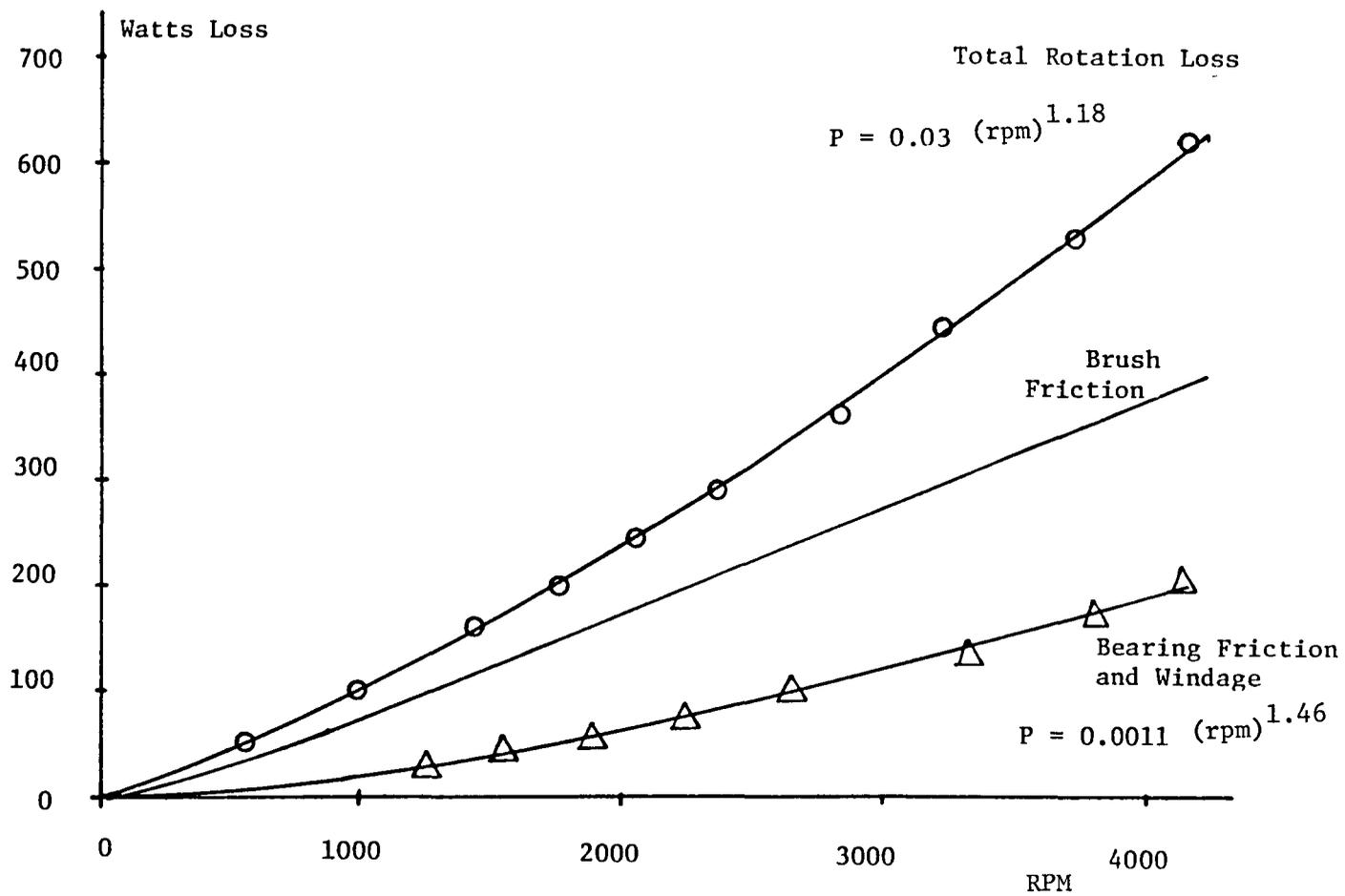
commutator surface for the RED motor. However, it appears unproductive in that the voltage drop across the brushes was 0.050 volts for the RED motor vs. 0.053 volts for the BLUE motor. At 200 amperes, this is a reduction of only 0.6 watts.

In order to verify the effect of brush pressure contibuting to the higher rotating losses of the RED motor, calculations were made to determine the coefficient of friction of each, using brush area, commutator radius and brush pressure.

The coefficients obtained were

$$\text{BLUE Motor} \qquad \mu = 0.19$$

$$\text{RED Motor} \qquad \mu = 0.22$$

Low friction electrographitic brushes are so classified, generally, if $\mu < 0.22$; thus it appears that the added rotational losses of the RED motor are due to high brush pressure.

Using a curve fit routine the following empirical relationships were obtained:

<u>BLUE Motor</u>

$$(P_r + P_\omega) = (0.0011)(rpm)^{1.46}$$

$$P_{rot} = (P_r + P_\omega) + P_b = (0.03)(rpm)^{1.18}$$

<u>RED Motor</u>

$$(P_r + P_\omega) = \left(\frac{6.2}{10^5}\right)(rpm)^{1.935}$$

$$P_{rot} = (P_r + P_\omega) + P_b = 0.074\ (rpm)^{1.18}$$

It is interesting to note that total mechanical rotating losses vary to the same power for both motors.

To evaluate the per unit loss that mechanical losses comprise, at maximum load, i.e. 200 amperes on ripple free dc:

<u>BLUE Motor</u>   (1635 rpm, $P_r = 202$)

$$\frac{P_r}{I^2 R} = 0.167; \qquad \frac{P_r}{P_{out}} = 0.03$$

RED Motor   (965 rpm, P_r = 280)

$$\frac{P_r}{I^2 R} = 0.198 \qquad \frac{P_r}{P_{out}} = 0.042$$

At lighter loads, i.e. 100 amperes

BLUE Motor   (2260 rpm, P_r = 290)

$$\frac{P_r}{I^2 R} = 9.6 \qquad \frac{P_r}{P_{out}} = 0.094$$

RED Motor   (1940 rpm, P_r = 570)

$$\frac{P_r}{I^2 R} = 1.6 \qquad \frac{P_r}{P_o} = 0.17$$

This indicates that total rotating losses play a very important role in motor efficiency at lighter loads, where EVs cruise! Attempts to secure low brush voltage drop by large brush pressure should be carefully evaluated against the increased friction losses that result.

12. Ventilation Losses

The BLUE motor requires external ventilation ("of not less than 250 cfm air flow"). It has two 3-inch ports for entrance and egress of cooling air. These openings are in the end opposite the commutator end and are spaced 90° apart, as shown in figure 53. At the commutator end, the four brush rigging access openings are provided with a metal cover which prevents air from being discharged through the openings. Therefore it appears the manufacturer intended air to enter one port; discharge out the other. However, examination of the two ports and their location with respect to the non-symmetrical pole spacing indicates that one port is directly over an opening of only 0.75 in.^{2}, the other over an opening of 8.6 in.^{2} (the word opening referring to interpolar area, and providing a passage down to the opposite end, where the commutator is located.) In addition, the two ports are connected by, in effect, paralleled 3-inch dia- meter flow areas (area between the end of the armature and the end bell of the housing). This does not appear to be a desirable ventilation arrangement in that if the commutator access panels are in place and one port is for entrance air, the other for egress air, little or no ventilating air will flow over the armature, across the commutator and return. Instead, it will divide through the paralleled 3-inch diameter flow areas. Thus it seems only proper to duct exter- nal air into the two 3-inch diameter ports and let it flow to the opposite end,

across the armature, thru the interpole area and egress through the brush/commutator access openings, with cover removed.

IEEE 113 (ref. 1) provides the following formula for calculation of power necessary to provide ventilation as follows:

$$P = \frac{0.117 \; Qp}{\eta} \; watts \qquad (74)$$

where: Q = volumetric flow, cubic feet/min.

p = pressure, in inches of water

η = blower efficiency.

In order to determine p and η as a function of Q, an air blower, driven by a shunt wound dc motor, was ducted into the air entrance ports on the motor and exhausted to the atmosphere through the brush access openings. The power to drive the air blower and the flow were measured as the blower speed was varied.

The ratio of p/η was found to be approximately $(0.04)Q^{1/2}$. From this the power requirement for ventilation, for the BLUE motor, is calculated as

$$P = (0.117)(0.04)Q^{1.5} \; watts \qquad (75)$$

yielding 18.5 watts at 250 cfm flow, for the BLUE motor and the blower used. (Estimated blower efficiency, 80%). For an 80% efficient blower, the pressure drop across the BLUE motor is 0.506 inches of water at 250 cfm.

Based on the 20 hp size motors, the expected approximately 20 watts loss is not significant. However, if an external source for blower air is required, extreme care must be exercised in manifold and duct design. Consideration of use of ram air ducted to the motor should be made.
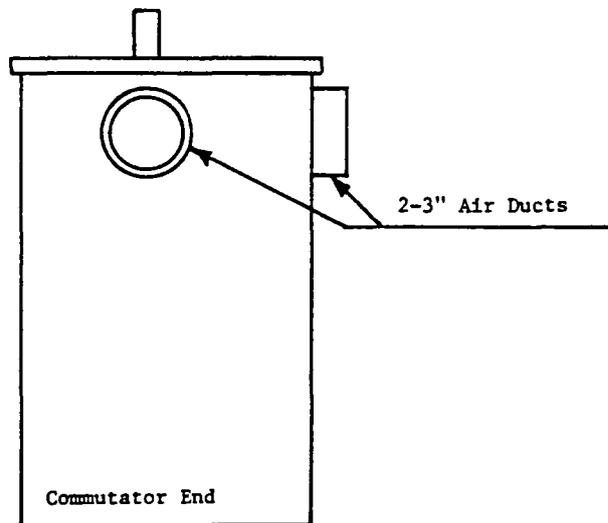

Figure 53 BLUE Motor Ventilation Ducts

CHAPTER 4

CONCLUSIONS

General

1. IEEE #113, "Standard Test Code for Direct Current Machines" is not adequate
    as a test code for chopper controlled motors in that it does not address test
    procedures, necessary instrumentation, losses and frequency effects associated
    with the chopper/motor combination. The apparent resistance and inductance
    of the motor vary widely with frequency and degree of magnetic saturation
    (average chopper current). A procedure for determining these values was
    developed.
2. Motor nonlinearities and "skin effect" phenomena preclude accurate analytical
    predictions of harmonic current magnitude. Actual values can be obtained
    only by measurements and tests.
3. Measurements must be made using wide band width instruments and noninductive
    shunts.
4. The conventional motor model does not yield accurate performance and behavior
    to be expected of the motor when chopper controlled. Calculated values of
    efficiency and speed are the parameters with the largest error. The effi-
    ciency of the motor decreases with decreasing load and chopper repetition
    (frequency) rate.
5. Improperly located brushes have a very detrimental effect on motor perfor-
    mance and losses. Motors for chopper control in EV applications should have
    interpoles so that brush rigging can be fixed in position and the brushes
    do not have to be shifted. Mislocation of the brushes can easily occur dur-
    ing maintenance and also during reverse operation.

Summary on Loss Mechanisms

1. Efficiency of a motor is sharply reduced when it is chopper controlled. The
    higher the chopper frequency, the less the reduction in efficiency.
2. The decrease in efficiency is more pronounced at lower values of average
    current.
3. Chopper control introduces additional losses not accounted for from consider-
    ation of harmonic currents and apparent resistance, as measured.
4. Eddy current losses in the armature due to tooth saturation and the main flux
    can be significant. For example, for the RED motor, at 2000 rpm this loss
    was calculated as 52% of the rated I^2R values.

    This loss can be mitigated by:
    (a) reducing conductor height
    (b) using deeper slots
    (c) using more iron (less flux density) in the motor.

5. Eddy current losses in the armature due to cross slot leakage flux may be
    significant. This loss is one of the major components of "stray load" loss.
    Current harmonics due to chopper control increased this loss about 25% over
    the loss that exists without the harmonic currents. This loss can be greatly
    reduced if fine stranded conductors are used, since the loss is proportional
    to the square of the height of the conductor. Also, increasing the chopper
    frequency decreases this loss, since harmonic current magnitudes decrease
    with increasing frequency.

6. Losses in the pole face iron due to slot effect are negligible if the poles are laminated, but a major loss if the poles are solid iron.
7. Nonconducting banding (such as Kevlar) should be used to secure the armature winding end turns, to eliminate banding losses due to harmonic fluxes in the area.
8. Equalizer connection losses are nonexistent in a wave wound machine and are minimized in a lap winding if the ratios

$$\frac{\#\ of\ commutator\ bars}{parallel\ paths/2} \quad and \quad \frac{\#\ of\ slots}{parallel\ paths/2} \quad are\ integers.$$

9. Losses in the coils undergoing commutation can be substantial if the brushes are located very far (10-15 degrees) off magnetic neutral and they increase with chopper frequency. The loss can be reduced by decreasing the number of turns shorted during the commutating process - using a wave winding or by using longer, less wide brushes (increasing commutator length). Interpoles will eliminate the need for brush shift and are strongly recommended.
10. Brush loss can be minimized by utilizing metal graphite brushes with silver if good commutation exists. Again, interpoles are strongly recommended.
11. With a FWD diode having 0.86 volt drop, 75 watts diode loss was measured at full load current. It is important to select a low voltage drop diode for this application.
12. Losses due to shaft to bearing to housing currents due to shaft induced emf are negligible.
13. Hysteresis losses in the magnetic structure due to chopper harmonics are negligible with laminated magnetic circuit. It is recommended that a laminated frame also be utilized.
14. Attempts to secure low brush voltage drop by large brush pressure should be evaluated against increasing brush friction loss.
15. For an internally fan ventilated motor of the size for EV, the fan loss is on the order of 0.33% of the output power rating. This type of ventilation is recommended to avoid duct losses. For an externally ventilated motor, the ducting and manifold should be carefully designed to minimize losses. Consideration of the usage of ram air for cooling should also be given in lieu of blower produced ventilation.

Motor Design Considerations

The ratio of peak power to average power required by an EV varies from about 5/1 in heavy city traffic to 3/1 in suburban/rural driving situations. Thus, the motor design must be based on commutation limit as opposed to the traditional thermal considerations. In order to achieve ability to commutate relatively high short time overloads, the use of a laminated (thin) steel frame and interpoles are a must. In addition, the added cost of utilizing compensating (pole face) windings should be evaluated based on the reduction in motor size, possible if high overloads can be accommodated. It should be recognized that if compensating windings are used they must be stranded to keep eddy current losses to a minimum.

Because a motor for EV application must also carry its power supply, high efficiency over the entire operating range is a major design objective. Typically 1 kW-hr of lost energy requires carrying an additional battery weight on the order of 30 kg (66 lb).

Another objective not normally considered in design of motors for conventional industrial applications is that of achieving relatively high circuit inductance.

Increasing inductance tends to suppress harmonic current magnitudes, thus increasing the efficiency. In addition, it tends to minimize chopper-motor interface problems in that it decreases the rate of rise of chopper current each cycle. The high inductance should be concentrated in the field circuit to minimize reactance voltage during commutation.

Because of the unavoidable electrical leakage paths that will develop in an EV environment, the electrical system voltage levels will probably be established at between 96 and 120 volts, which means a rather heavy current requirement for motors in the 15-30 kw power range. In general, system voltage level does not appreciably affect the weight of the motor. However, this voltage range does not indicate a clear choice of the use of a lap or wave winding. Yet a wave winding appears to offer advantages in that it does not need an equalizer winding.

DESIGN DETAILS OF MOTORS TESTED (From Manufacturer or Physically Measured)

RED MOTOR

Open ventilation with internal fan (fan removed for tests)

(150 CFM @ 2000 rpm)

Speed 1800-2500 rpm

Rated Current: Armature 175 amperes

Voltage: 144 Maximum

Wave Wound (2 parallel paths), No interpoles

4 pole, 27 slots, 6 conductors/slot, 81 commutator bars, Z = 54 conductors

Field Winding: 20 turns/pole, Series (No shunt)

Frame Material: Wrought iron

Pole and Armature: Laminated, M-27 electric sheet steel

                    0.46 mm (0.018 inches, 26 gauge)

Armature Radius: 92.075 mm (3.625 in.)

Air Gap: 3.23 mm (0.127 in.)

Stack Length: 96 mm (3.78 in.)

                    Pole face arc span: 63.59 mechanical degrees, 1.109 rad

Pole face area: 0.0101 m^2 (15.726 $in.^2$)

Brushes: 8 electrographic (#417 stackpole or #201c Kirkwood)

                    Force: 1800-2200 grams (3.96 – 4.84 lb)

                    Area: (each 13x32 mm) 416 mm^2 (0.645 in^2) each

Commutator: 400 mm (15.748 in) circumference.

                    Each segment 3.9 mm (0.15 in) width

                    0.8 mm (0.03 in.) separation.

Each brush spans 3 commutator segments (3 coils). Total of 6 coils shorted

during commutation. See Figure 54

Figures 55 and 56 depict frame, field winding and slot dimensions.

Armature Resistance (dc)   0.0189 ohms

Field Resistance (dc)   0.0165 ohms

(All Fields in Series)
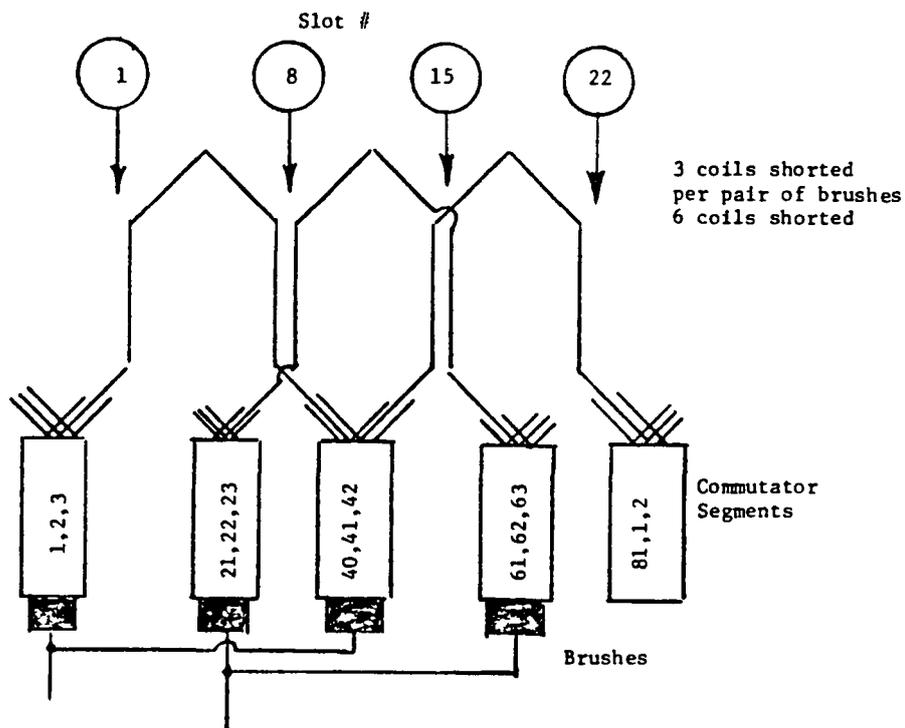
Figure 54   RED Motor (Wave) Coils Shorted During Commutations
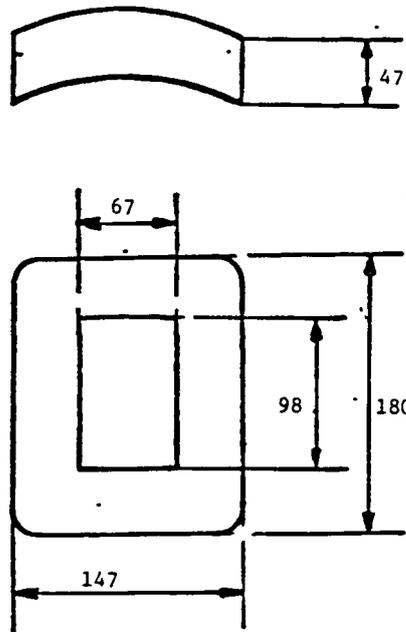
Dimensions of the field winding (in millimeters)
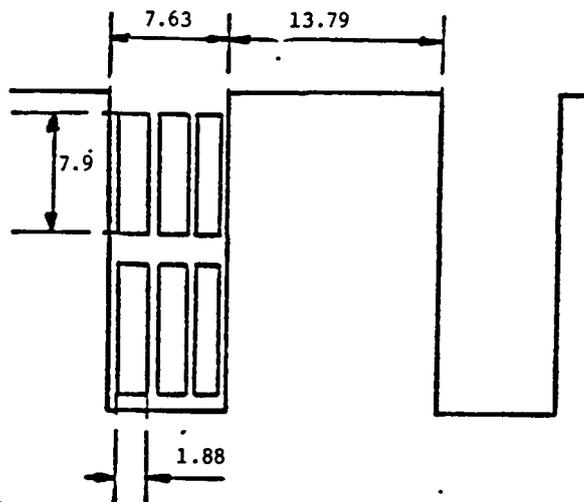
Dimensions of slot and armature conductors (in millimeters)

Figure 55   RED Motor, Field and Slot Detail
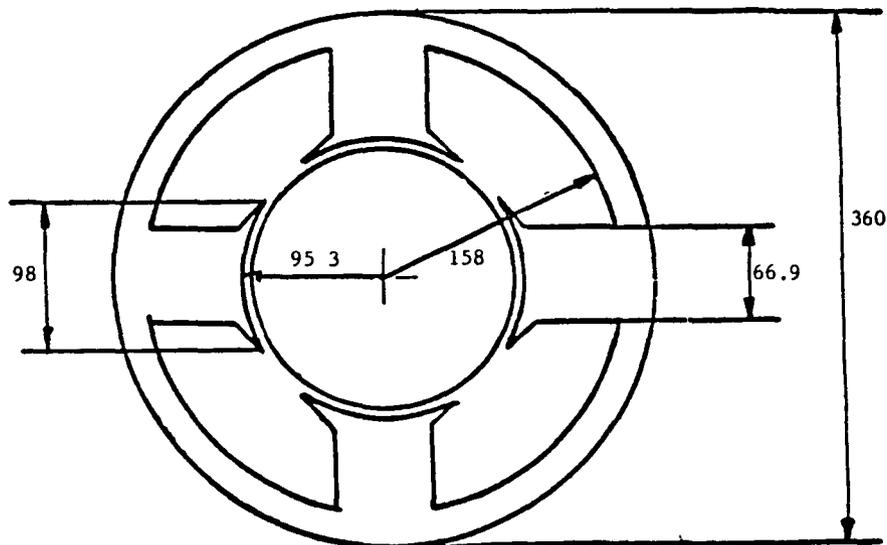
Dimensions of rotor and stator (in millimeters)

Figure 56   RED Motor, Rotor and Stator Dimensions

BLUE   MOTOR

External Ventilation, 250 CFM external blower required.

Speed: 4000 rpm, 20 hp (maximum)

Rated Current: 208 amperes

Voltage: 84 volts

Lap Wound (4 parallel paths). No interpoles. Equalizer Winding Present.

4 pole, 32 slots, 4 conductors/slot, 2 turns/coil (4 - #15)

      64 Commutator Bars, Z = 256

Field Winding:	24 turns/pole, Series (No Shunt). (1 = #4, square)
Frame Material:	Integral with poles
Pole and Armature:	Laminated, 24 gauge Electrical Sheet
	0.635 mm (0.025 in.)
Armature radius:	75.8 mm (2.984 in.)
Air gap:	1.59 mm (0.0625 in.)
Stack Length:	92.1 mm (3.625 in.)

Pole face arc span: 53 mechanical degrees, 0.925 rad

Pole face area: 0.0066 m^2 (10.22 in.^{2})

Brushes: 8

     Force: 1365 grams, (3 lb)

     Area: (each 15.9 x 31.75 mm) 504 mm^2 (0.7813 in.^{2})

Commutator: 326.67 mm (12.86 in.) circumference. Each segment

     3.97 mm (0.156 in) width, 1.016 mm (0.04 in) separation.

Commutator is skewed 2.17 degrees, hence, each brush bridges 4 commutator

segments (3 coils). Total of 12 coils shorted during commutation. See

Figure 57.

Figures 58 and 59 depict frame and slot dimensions.

Armature Resistance: (dc); 0.011 ohms

Field Resistance: (dc); 0.008 ohms

Armature Inductance 0.16 mH (Saturated)

Armature Inertia 1.4 lb-ft^2
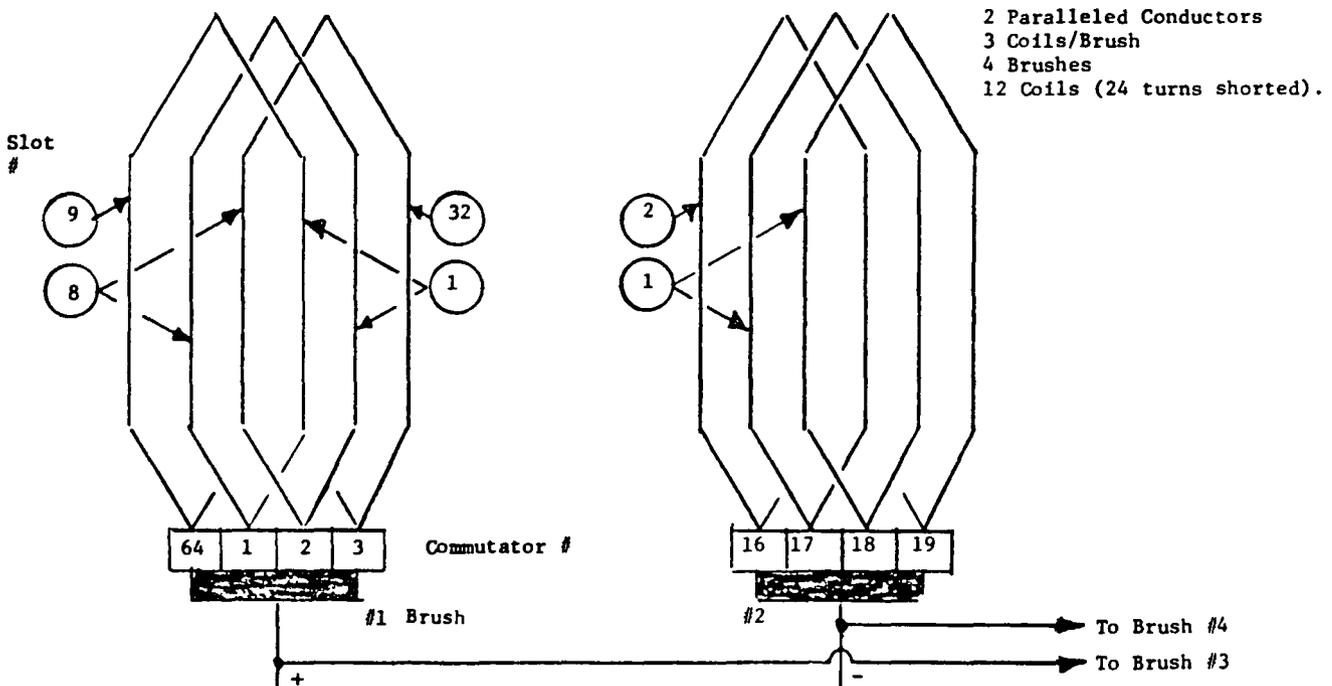
Figure 57 BLUE Motor (Lap) Coils Shorted During Commutation
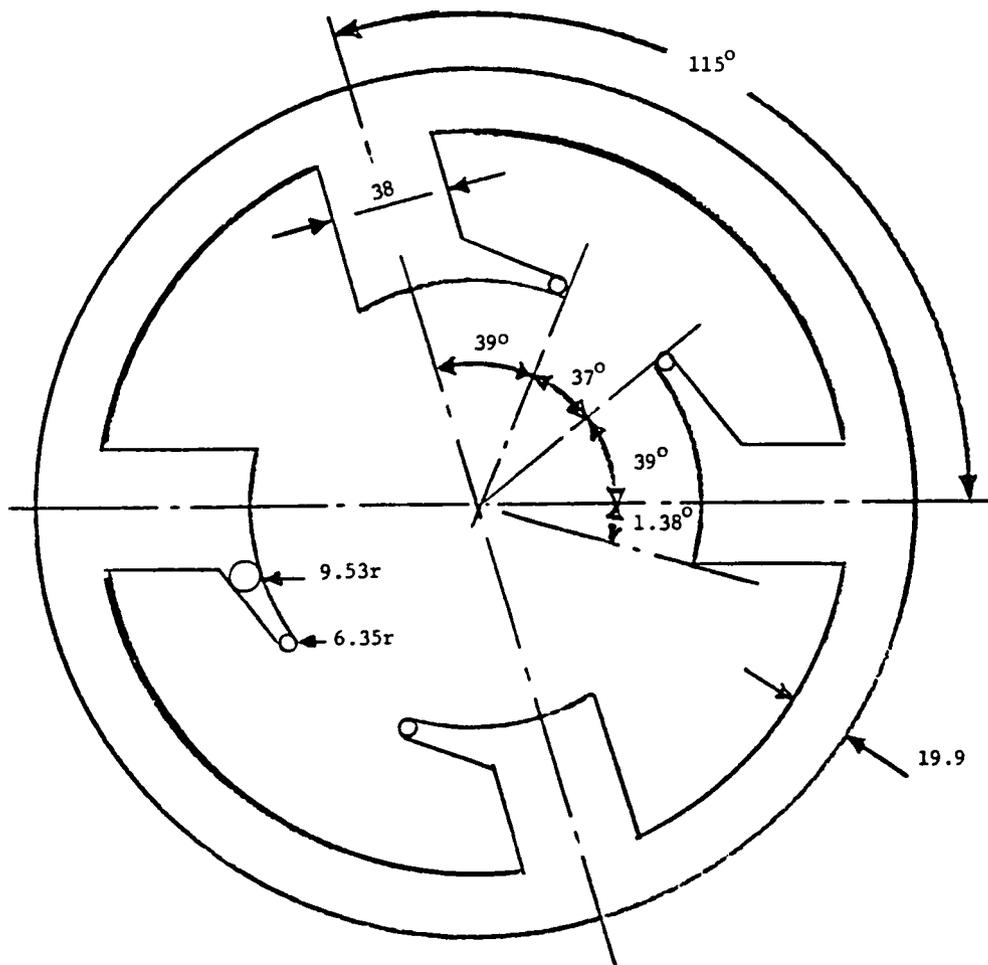
Figure 58   BLUE Motor, Frame Dimensions (in millimeters)
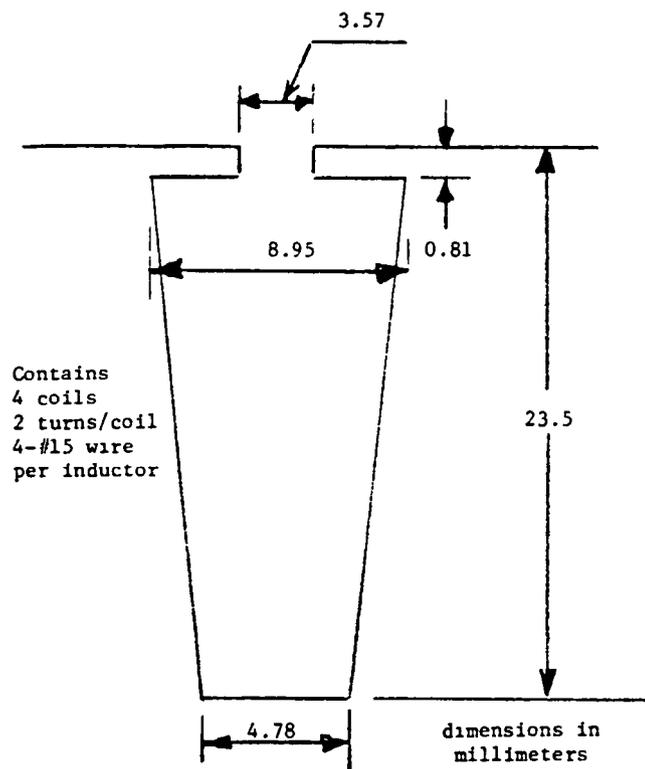
Figure 59 BLUE Motor, Slot Detail

APPENDIX B

EV MOTOR APPLICATION

An excellent exposition on aspects of EV design and performance, including infor-
mation on laboratory and field test, EV components, motors, etc. is contained in
"STATE-OF-THE-ART ASSESSMENT OF ELECTRIC AND HYBRID VEHICLES" prepared by NASA-
Lewis Research Center CONS/1011-1, UC-96)(Ref. 11).   In this appendix a brief
discussion will be presented in order to acquaint motor designers with the appli-
cation aspects of motors for EV applications.

A number of factors enter into the determination of the motor and control scheme
for the drive train in electric vehicles. Basic decisions to be made are:
(not necessarily in order):

1) Type of motor, i.e. series or shunt?

2) If shunt wound,

    a) constant field excitation or controlled variable excitation?

    b) How will armature voltage be controlled - by chopper or switched
        in finite, discrete steps?

    c) transmission gear ratios?

    d) is regeneration to be utilized?

3) tire size

4) system voltage

5) vehicle performance, based on frontal area and weight, to include the
    following:

    a) maximum acceleration

    b) maximum speed on a specified maximum grade for a minimum time
        period

    c) cruise speed

    d) top speed

    e) regeneration, if utilized

Since these require varying speed/torque and speed/power combinations and result
in an intermittent load on the motor, a standardized duty cycle must be resorted
to in order to establish a rating, based on thermal and commutation considera-
tions, for the motor. The speed requirements will fix the drive train gear
ratio/motor speed-torque relationships.

The Society of Automotive Engineers has established various driving cycle sche-
dules which can be used as standardized requirements for evaluation purposes.
Figure 60 depicts the driving cycle for SAE J 227 B, C and D schedules.

-109-
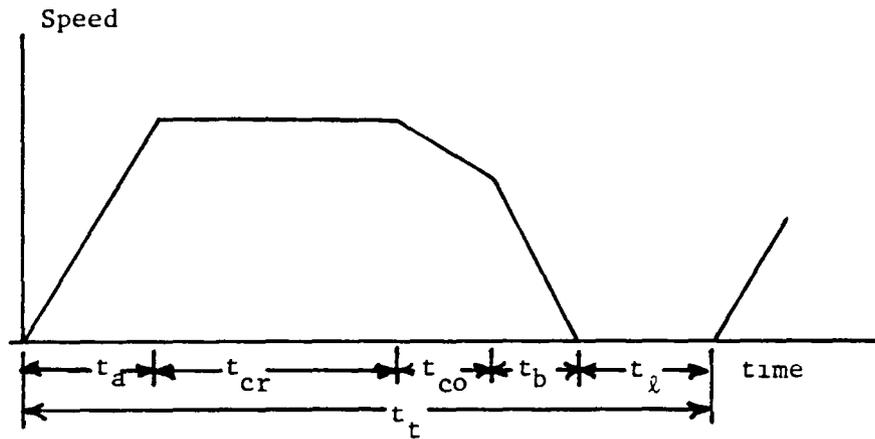
Speed

	B	C	D
Maximum Speed Km/hr, (mph)	32 (20)	48 (30)	72 (45)
Accelerating Time, T_a, seconds	19	18	28
Cruise Time, t_{cr}	19	20	50
Coast Time, t_{co}	4	8	10
Brake Time, T_b	5	9	9
Idle Time T_i	25	25	25
Total Time, t_t	72	80	122
Approx Number of cycles/mile	4-5	3	1

Note B - fixed route urban driving, $a = 1.54$ ft/sec^2
      C - variable route urban driving, $a = 2.44$ ft/sec^2
      D - variable route, suburban driving, $a = 2.34$ ft/sec^2

Figure 60   SAE J 227 Road Cycles

The motor must be capable of supplying sufficient power to overcome the following load conditions.

1. Aerodynamic drag

2. Rolling resistance

3. Changing grade

4. Acceleration requirements

5. Provide for losses in the mechanical gearing and bearing friction in the mechanical drive train

Aerodynamic Drag

The power to overcome aerodynamic drag is calculated from:

$$P_d = \frac{6.762}{10^6} \ (C_d A)(mph)^3 \quad hp \tag{76}$$

where: A = frontal area in ft^2

C_d = drag coefficient

mph = miles per hour velocity

A typical EV will have a frontal area of 20 ft^2 and a C_d of 0.3.

Rolling Resistance and Changing Grade

The power consumed in overcoming rolling resistance (tire friction) and changing grade can be calculated from

$$P = \frac{2.7}{10^5} \ (W)(mph)(\%) \quad hp \tag{77}$$

where: W = (or is) vehicle weight

% is percent grade (increase in elevation in feet per hundred feet of travel)

or is the coefficient of friction, μ, (tires to road) multiplied by 100,

typically, $0.012 < \mu < 0.017$

with conventional bias tires at the upper value and steel belted radial tires at the low end. It is a function of speed, also (ref. 11).

Acceleration Requirements

Power requirements to accelerate are based on acceleration rates expressed in $feet/sec^2$. Rates are listed under the SAE Schedule for each cycle.)

TABLE 9 Conversion Factors

Multiply the first column of the tables below
by the appropriate number to obtain the units
in the horizontal row.

	$\dfrac{\text{Meter}}{\text{sec}}$	$\dfrac{\text{Km}}{\text{hr}}$	$\dfrac{\text{Miles}}{\text{hr}}$	$\dfrac{\text{Feet}}{\text{min}}$	$\dfrac{\text{Feet}}{\text{sec}}$
$\dfrac{\text{Meter}}{\text{sec}}$	1.0	3 6	2.24	197	3 28
$\dfrac{\text{Km}}{\text{hr}}$	0 277	1 0	0 621	54 7	0 912
$\dfrac{\text{Miles}}{\text{hr}}$	0 477	1.61	1 0	88	1.46
$\dfrac{\text{Feet}}{\text{min}}$	0.0051	0.013	0 011	1 0	0 0167
$\dfrac{\text{Feet}}{\text{sec}}$	0.305	1.097	0 682	60	1 0

	Horsepower	Killowatts
Horsepower	1 0	0 746
Kilowatts	1 341	1

	lb	Kg
lb	1	0 454
Kg	2 20	1

$$P_a = \frac{8.28}{10^5} (W)(a)(mph) \quad hp \tag{78}$$

where a is the acceleration rate, feet/sec^2.

A table of conversion factors is presented in Table 9.

EXAMPLE: For a 3000 lb. EV, with $C_d A = 6.0$ and $\mu = 0.012$.

Determine the maximum power and the series wound motor size required for this vehicle to meet the SAE 226C Schedule. It will be driven on 5 mile trips, 6 times/day, and must climb a grade for 5 seconds at 30 mph during each cruise cycle. It should be capable of a top speed of 55 mph.

Using the relationships above, the specified performance requirements, and assuming a drive train efficiency of 95%, the power requirements are calculated as follows:

accelerating	0-30 mph, 18 seconds	25.58 hp
cruising	30 mph	6.51 hp
grade climbing	10% at 30 mph	31.77 hp
top speed	55 mph	27.67 hp

Figure 61 is a plot of the motor power required during a Schedule C driving cycle. As can be seen, grade climbing is the most demanding of the various operations and the motor selected must be capable of delivering 31.77 hp on a short time overload basis.

To determine the continuous power rating of the motor, the root mean square power (heating effect) must be determined. Under Schedule C, there are 3 cycles/ mile, and 15 cycles/hr for 5 mile trips. With the specification of 6 trips/day, analysis over a 1 hour time frame should be adequate, for a preliminary analysis. Note that the scedule does not include specifications with respect to length of time at maximum speed.

$$P_{rms} = \left(\frac{1}{T} \int P(t)^2 dt \right)^{\frac{1}{2}} \tag{79}$$

$$P_{rms} = \left(\frac{15}{3600} \left(\int_0^{18} \left(\frac{25.58\ t}{18} \right)^2 dt + \int_{18}^{33} (6151)^2 dt + \int_{33}^{28} (47)^2 dt \right)^{\frac{1}{2}} \right) = 6.31\ hp$$

It should be noted that the motor is not delivering power during coast or braking periods (42 seconds out of each 80 second cycle), which accounts for the low ratio (1/5) of rms power to peak power.

To determine a motor rating and visualize the effect of ability to commutate over- loads consider the following:

If the tire diameter is D feet, maximum velocity is v ft/sec, and a motor speed step down gear of ratio, G/1, is between motor and axle, the motor speed, in radians/sec. is:

$$\omega_m = \frac{2G}{D} v \tag{80}$$

or, in terms of speed in rpm, v in mph,

$$N = (27.884)(\frac{G}{D})(mph) \tag{81}$$

A typical series motor characteristic is shown in Figure 62. This is the open circuit saturation characteristic reduced to per unit and is thus a plot of torque/armature ampere and emf/angular velocity in per unit as a function of per unit field current. Applying a curve fit routine to the data yields:

$$(\frac{T}{Ia})_{pu} = (\frac{E}{\omega})_{pu} = 0.95 \, I_f^{0.454} \tag{82}$$

The equations describing the series motor can then be formulated as (assuming $I_a = I_f$):

$$T_{pu} = 0.95 \, I^{1.454} \tag{83}$$

$$\omega_{pu} = \frac{V - IR}{0.95 \, I^{0.454}} \tag{84}$$

$$P_{pu} = (T_{pu})(\omega_{pu}) \tag{85}$$

where: V = per unit applied voltage = $\frac{T_o}{T}$ (Source voltage)

R = per unit armature and field resistance.

Values of I from 0.2 to 3.0 per unit chosen and T, ω and P were calculated for V = 1.0, 0.8, 0.6, etc. For the values calculated at a specific current value, the T vs ω curves and the P vs. ω curves, shown in Figures 63 and 64 were constructed (based on an assumed value of R = 0.045 per unit). Figure 64 also has the per unit current loci drawn in.

The EV power requirements in the previous example can be used with these "universal" motor characteristics to demonstrate how a motor rating can be determined and to illustrate the influence of a motor's ability to commutate overloads on the motor size required.

Using the power requirements from the example:

Accelerating	25.58 hp at 30 mph	(2180 rpm)
Cruise	6.51 hp at 30 mph	(" ")
Grade Climbing	31.77 hp at 30 mph	(" ")
Top speed	27.67 hp at 55 mph	(3995 rpm)
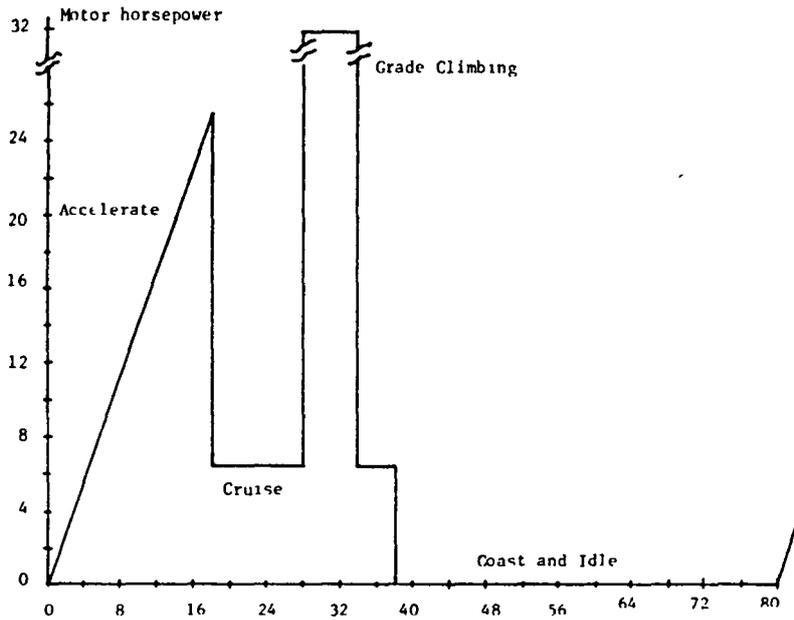
Figure 61   Schedule C Power Requirement (Example)
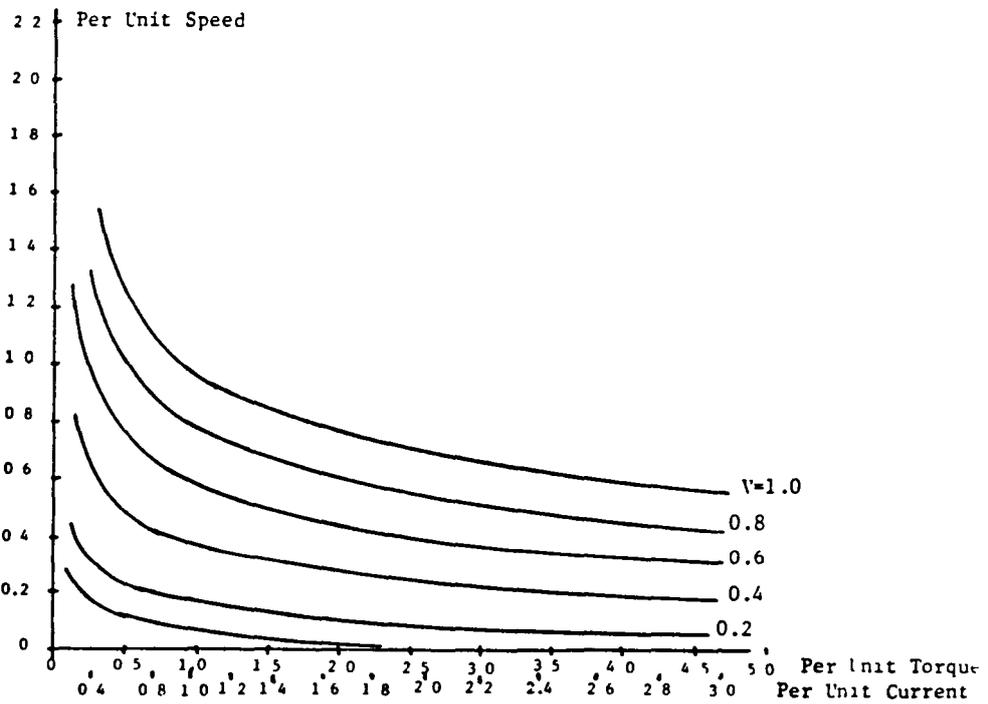
Figure 63   Torque/Current v. Speed, Universal Series Motor

$\frac{I}{I_f}$ or $\frac{E}{\omega}$, K

per unit

$K = 0.951 \, I_f^{0.454}$ p.u.

Field Current

Figure 62 Universal Series Motor OCS Curve
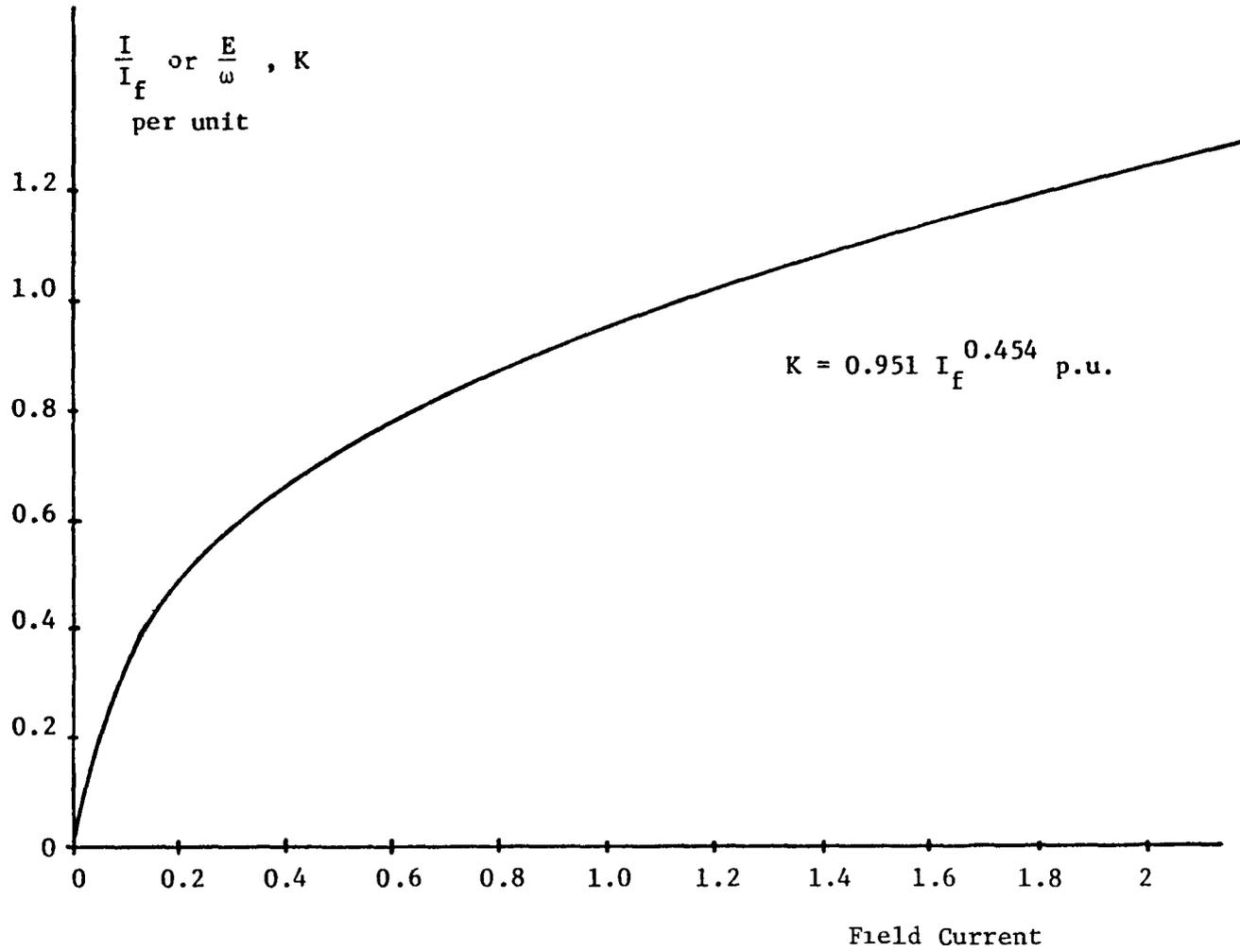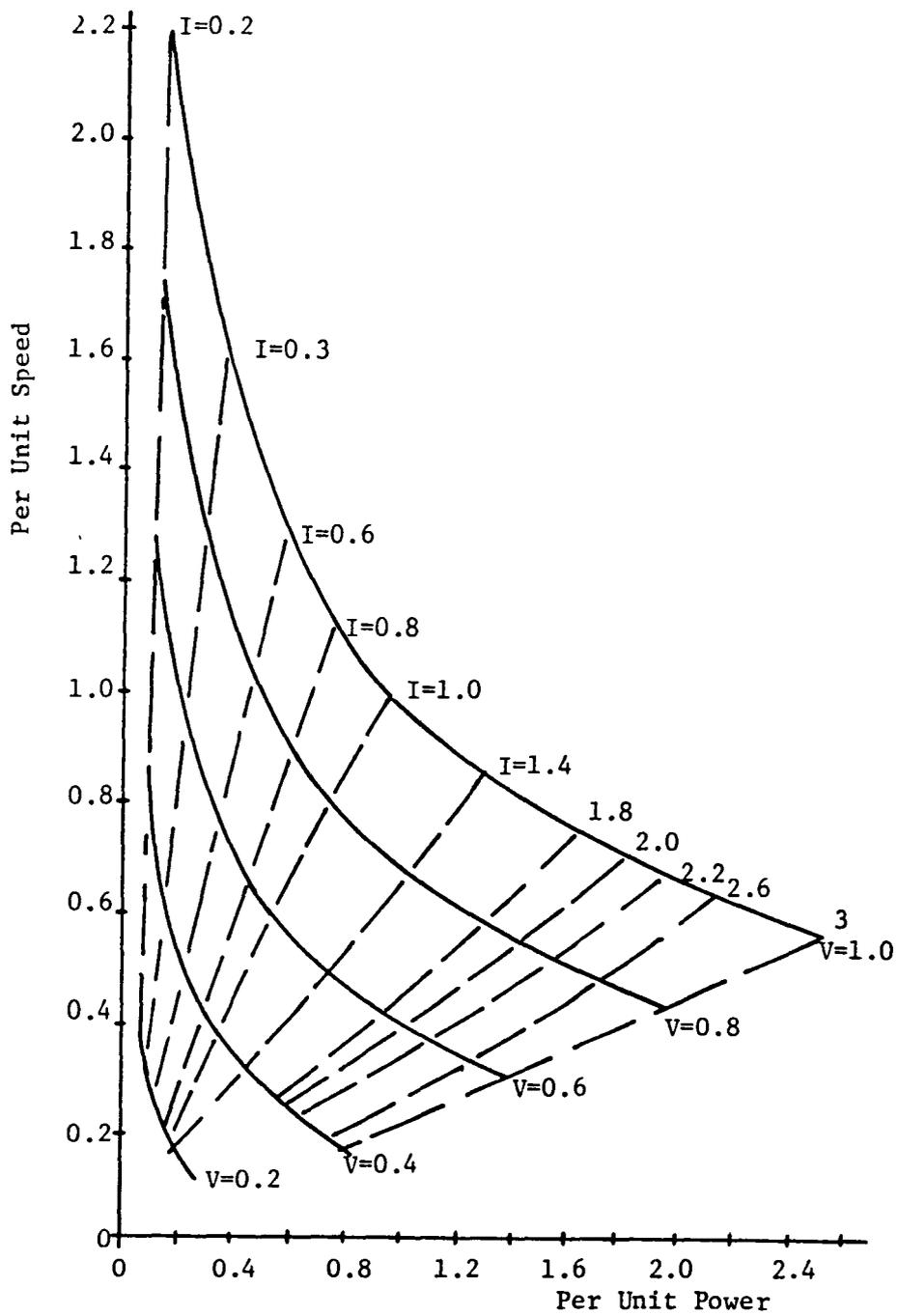
Figure 64   Universal Series Motor Curves

Axis labels: Per Unit Speed (vertical), Per Unit Power (horizontal)

Curve labels: I=0.2, I=0.3, I=0.6, I=0.8, I=1.0, I=1.4, 1.8, 2.0, 2.2, 2.6, 3, V=1.0, V=0.8, V=0.6, V=0.4, V=0.2

Assume that top speed is chosen as 0.8 per unit. With V = 1.0 the per unit power is 1.45. If the efficiency is assumed to be 74.6%, the motor rating for the top speed requirement is:

$$P = \frac{27.67}{1.45} = 19.08 \sim 20 \text{ kw}$$

From Figure 64:

$$I = 1.5 \text{ pu} \qquad N = 0.8 \text{ pu}$$

Grade climbing will require a per unit power of:

$$P = \frac{31.77}{20} = 1.59$$

at a speed of $(\frac{30}{55})(0.8) = 0.44$

From Figure 64, for this power and speed,

$$I = 2.5, \ V \sim 0.75$$

For cruise: N = 0.44, and

$$P = \frac{6.51}{20} = 0.325$$

$$I = 0.8, \ V = 0.4$$

For the maximum power during acceleration,

$$P = \frac{25.58}{20} = 1.28 \text{ at } N = 0.44$$

$$I = 2.1, \ V = 0.7$$

If top speed had been chosen as 1.0 per unit the operating conditions would be as follows: V = 1.0 and the per unit power is 0.96. The motor rating is:

$$P = \frac{27.67}{.96} = 28.8 \sim 30 \text{ kw}$$

Grade climbing requires a per unit power of: $P = \frac{31.77}{30} = 1.06$

at a speed of (30/55)(1.0) = 0.55 yielding I = 1.6 and V = 0.73

For cruise: N = 0.55

$$P = \frac{6.51}{30} = 0.22$$

$$I = 0.5 \qquad V = 0.4$$

For acceleration: $P = \frac{25.58}{30} = 0.85 \text{ at } N = 0.55$

$$I = 1.4 \qquad V = 0.68$$

If the EV is to use a 5.21/1 differential and 2 foot diameter tires, top speed of 55 mph results in a motor speed of:

$$N = (27.884) \ (\frac{G}{D}) \ (\text{mph}) = 4000 \ \text{rpm.}$$

For the 20 kw motor, this is a per unit speed of 0.8. Therefore, the motor would be rated 20 kw, 4000/0.8 = 5000 rpm and must be capable of commutating 2.5 per unit current on grade climbing.

For the 30 kw motor, its rated speed would be 4000 rpm, but it need only have the capability of commutating 1.6 per unit current maximum.

In general, armature physical size is inversely proportional to speed. In the example above, the ability to commutate 3.5 per unit current permits selection of a 20 kw motor, 5000 rpm which would be a smaller, lighter motor than would be required if commutation ability were limited to 1.6 per unit current requiring a 30 kw, 4000 rpm selection. Another advantage in using the smaller motor is that at cruise the motor power output is a higher percentage of its rated power than is the situation for the larger motor. Since the efficiency decreases at light loads on a motor, the use of the smaller motor results in increased efficiency during the cruise condition.

Motor example used for preliminary selection of an EV motor power and speed rating dramatically points up the need for the EV motor to have the ability to commutate high, short time overloads. The ratio of peak power to average power required by an EV varies from about 5/1 in heavy city traffic to 3/1 in suburban/rural driving situations. Thus, the motor design must be based on commutation limit as opposed to the traditional thermal constraint approach.

Because a motor for EV application must also carry its power supply, high efficiency over the entire operating range is a major design objective. Typically 1 kW-hr of lost energy requires carrying an additional battery weight on the order of 30 kg (66 lb).

Another objective not normally considered in design of motors for conventional, industrial applications is that of achieving relatvely high circuit inductance. Increasing inductance tends to suppress harmonic current magnitudes, thus increasing the efficiency. In addition, it tends to minimize chopper-motor interface problems in that it decreases the rate of rise of chopper current each cycle.

Because of the unavoidable electrical leakage paths that will develop in an EV environment, the electrical system voltage levels will probably be established at between 96 and 120 volts, which means a rather heavy current requirement for motors in the 15-30 kW power range. In general, system voltage level does not appreciably affect the weight of the motor. However, this voltage range for the power rating range does not indicate a clear choice of the use of a lap or wave winding. Yet a wave winding appears to offer advantages in that it does not need an equalizer winding.

In order to achieve ability to commutate relatively high short time overloads, the use of a laminated (thin) steel frame and interpoles are a must. In addition, the added cost of utilizing compensating (pole face) windings should be evaluated based on the reduction in motor size possible if high overloads can be accommodated.

It should be recognized that if compensating windings are used, they must be stranded to keep eddy current losses to a minimum.

The electromagnetic power developed in a dc motor armature is given by:

$$P = EI = \left(\frac{Z\phi pN}{60a}\right) I \qquad (86)$$

where: Z = number of armature inductors
ϕ = flux/pole, webers
P = number of poles
N = rpm
I = armature current, amperes
a = parallel paths in the armature

Defining the specific electrical loading, q, and the specific magnetic loading, B, as:

$$q = \frac{IZ}{a\pi d} \quad \text{ampere inductors/meter} \qquad (87)$$

$$B = \frac{p\phi}{\pi D \ell} \qquad (88)$$

where: ℓ = armature core length, D = armature diameter

$$\text{Then:} \quad P = \frac{\pi^2 D^2 \ell NqB}{60} \qquad (89)$$

It is important to note that, in EV applications, where the ratio of average to peak power is low, specific electrical loading can be quite high, relative to industrial type motor design and is realistically limited only by commutation capability and not thermal considerations.

High q permits a lower specific magnetic loading which in turn results in lower losses and higher efficiency. However, lower specific flux density should be obtained by larger diameter, rather than larger core length. Longer core length increases the cooling problem as well as introducing mechanical problems such as shaft deflection and increases the overturning moment, for horizontal mounting.

Studies (ref 12) have shown that high specific electrical loading, obtained with a wave winding, can result in substantial weight reductions for the motor. Figure 65, reproduced from that reference, shows the influence of specific loading and armature diameter on the weight of a 40 kw shunt motor.

The main considerations in ability to commutate are the reactance emf in the coils being commutated and the presence of armature reaction. Interpoles can nullify the reactance emf. The actual reactance voltage is dependent upon slot permeance, conductor current, speed, and armature length. On the basis that the EV application stresses high speed and high specific electrical loading, this armature reactance voltage can be decreased by a larger air gap and larger diameter (shorter length) armature. The larger air gap means more turns/pole for the field, which increases the total circuit inductance, which is desirable. Only a compensating winding can eliminate armature reaction.

In order to increase the ability to commutate, one tends to design the motor using the greatest number of commutator bars; yet using the lowest number of turns per coil (which yields the maximum slot space factor) which tends to

increase the armature diameter. For a fixed brush width, this means more coils shorted during commutation which increases the losses.
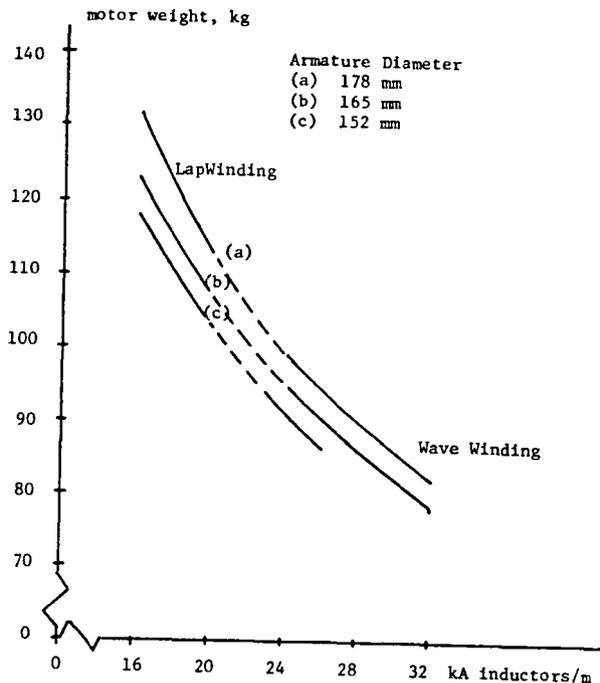

Figure 65 Weight/Winding Relationships

Steps taken to increase the ability to commutate (including the use of compensating windings) all tend to decrease armature inductance. However, as noted above, a larger diameter armature results in more turns on the field which increases the circuit inductance. The field inductance (and number of turns) can also be increased by connecting all field windings in parallel, which requires p times as many turns than if the field windings were all in series.

Motor inductance can be controlled in the design of the motor (ref 13). The important parameters which affect the inductance are as follows:

__Armature:__

$$L = K_1 \frac{Z^2 \ell}{Qa^2 w} \frac{(d_2 + d_1)}{3}$$

(90)

where:
- Z = armature inductors
- ℓ = stack length
- Q = number of slots
- a = number of parallel paths
- w = slot width
- d_1 = depth of copper in the slot
- d_2 = depth from top of the tooth to the top of the conductor

<u>Poles</u>

$$L = K_2 \frac{hn^2 \ell p}{ga^2}$$

(91)

where: h = pole height
          n = number of turns
          p = number of poles
          g = air gap
          ℓ = length of pole
          a = number of parallel paths in pole windings

CHOPPER CONSIDERATIONS

The chopper thyristors must, of course, have a voltage and current capability exceeding the system voltage and maximum current which will be required.

In the above example, note that grade climbing (31.77 hp) occurs at V = 0.7 p.u. If a 15 hp motor was chosen, I_{pu}, for grade climbing would be:

$$I_{pu} = \frac{P}{V} = \frac{31.77}{(15)(0.7)} = 3.0 \text{ p.u.}$$

(92)

If a 120 volt system were used, and a 15 hp motor with, say, 75% efficiency was chosen, per unit current would be 125 amperes and the chopper thyristor current rating must be 375 amperes or greater. The chopper should have a current limit control feature, also.

For "soft" starts, it is desirable to start with a very low voltage, i.e. 0.03 - 0.05 per unit, requiring a ratio T_o/T of the same magnitude. In choppers which utilize the on time, T_o, for charging the commutating capacitor, minimum T_o is fixed. If, for example, minimum on time is 0.001 seconds, and minimum desired voltage is 0.03 per unit, the maximum starting chopper frequency is $f = \frac{1}{T} = \frac{0.030}{0.001} = 30$ Hz. As shown in CHAPTER 2, the efficiency is quite dependent upon chopper frequency, increasing with frequency. Thus, the chopper control should have the ability to increase the frequency at which the chopper is operating to an upper limit as quickly as possible, subject of course to the minimum "on time" constraint imposed by the commutating capacitor charging scheme.

Motor circuit inductance is an important factor in the selection and application of a chopper controller because the thyristors have a maximum dI/dt rating. Since maximum rate of rise of current is determined by system voltage and circuit inductance, these parameters must be controlled to yield a specified maximum value. Chopper designs tend to be conservative with respect to operating conditions relative to thyristor allowable maximum ratings. Informal discussions with chopper designers indicate they prefer dI/dt to be less than 500 or 600 amperes per millisecond.

As shown in CHAPTER 2, inductance decreases with frequency and care should be taken to evaluate dI/dt at the highest frequency the chopper will operate at.

Reference 14 provides background information on motors and choppers. Reference 15 presents an excellent discussion of the various chopper types and their advantages and disadvantages.

REFERENCES

1) IEEE Standard #113 "IEEE Standard Test Code for Direct Current Machines," 1973 IEEE, Inc., 345 E. 47th Street, New York, NY 10017

2) Saunders, R.M., "Measurement of DC Machine Parameters," American Institute of Electrical Engineers, Vol. 70, 1951.

3) Hamilton, H.B., "An Investigation of Possible DC Power Sources for Testing Electric Vehicle Motors," submitted to NASA-Lewis/DOE under Grant #NSG 3136, 1978. (Report)

4) Hamilton, H.B., McBrien, E.F., Strangas, E., "A DC Power Source for Testing Battery Powered Electric Vehicle Motors," presented at the 1979 IEEE, IAS Society Meeting, Cleveland, OH, Oct. 1979, and in the Conference Proceedings, pp. 989-994.

5) Franklin, P.W., "Theory of the DC Motor Controlled by Power Pulses," Parts I and II. Presented at the 5th Annual Meeting of IEEE, IAS Gp. Chicago, Ill., Oct. 1970.

6) DeWolf, F.T., "Measurement of Inductance of DC Machines," IEEE Trans. PAS, Sept./Oct. 1979, Volume PAS-98, No. 5, pp. 1636-1644.

7) Hamilton, H.B. and Strangas, E., "Series Motor Parameter Variations as a Function of Frequency and Saturation," IEEE Trans. PAS, July/Aug. 1980, Vol. PAS-99, pp. 1567-1574.

8) "Direct Current Machines," BOOK, Liwschit-Garik and Whipple. Van Nostrand Co., Princeton, NJ, 1961, pp. 176, 179.

9) "Direct Current Machinery," BOOK, Kloeffler, Brenneman, Kerchner. The MacMillan Co., New York, 1934, p. 79.

10) "Transient Performance of Electrical Power Systems," BOOK, R. Rudenberg, McGraw-Hill, 1950, MIT Press, 1970, p. 117.

11) NASA-Lewis Research Center, "STATE-OF-THE-ART ASSESSMENT OF ELECTRIC AND HYBRID VEHICLES" MCP/M1011-01, UC-96 available from NTIS, U.S. Dept. of Commerce, 5285 Port Royal Road, Springfield, VA 22161.

12) Thompson, M.A. and Waters, L.A., "The Design of DC Commutator Motors for High Performance Electric Vehicles," SAE Paper #740169.

13) Snively, H.D. and Robinson, P.B., "Measurement and Calculation of DC Machine Armature Inductances" AIEE Transactions, 1950, Vol. 69, pp. 1228-1237.

14) Kusko, A., "Solid State Motor Drives," BOOK, MIT Press, Cambridge, MA, 1969.

15) Maxda, F.F., "Thyristor Control," BOOK, Chapter 5 and Appendix to Chap. 5, Newner-Butterworth, London, 1973.

NON CITED REFERENCES

Hamilton, H.B., McBrien, E.F., Strangas, E., "Chopper Controlled DC Traction Motor Testing: Some Methods and Results," presented at the Monterrey, Mexico IEEE Meeting, September 1979 in Monterrey, Mexico.

Knowlton, A.R., "Standard Handbook for Electrical Engineers," 8th Edition, BOOK McGraw-Hill Book Co., NY (7-120).

Ewing, J.S., "Lumped Circuit Impedance Representation for DC Machines," IEEE PAS Transactions, Vol. PAS-80, No. 4, April, 1968.

Dubey, G.K. and Shepherd, " Analysis of DC Series Motor Controlled by Power Pulses," Proc. IEEE, Vol. 122, 1975.

Yanase, A., "Starting Characteristics of Chopper Controlled DC Series Motor with Non-linear Magnetization Curve," EE in Japan, Vol. 97, No. 1, 1977.

Strangas, E., "The Time Dependent Finite Element Modeling of the Electro-magnetic Field in Electrical Machines - Methods and Applications," Ph.D. Dissertation. University Microfilms, Ann Arbor, Michigan, 1980.

Strangas, E., Hamilton, H.B., "Computer Modeling of Chopper Controlled DC Machines," presented at the International Conference on Electric Machines, Sept. 1980, Athens, Greece.

Strangas, E., Hamilton, H.B., "A Model for the Chopper Controlled DC Series Motor," to be presented at the IEEE Summer Power Meeting, 1982.

Hamilton, H.B., "Why a Standard for Chopper Controlled DC Motors for Electric Vehicles?" SAE Technical Paper Series #820400 and in SAE P-105, "Developments in Electric and Hybrid Vehicles."

1 Report No	2 Government Accession No	3 Recipient s Catalog No
NASA CR-167845		

4 Title and Subtitle	5 Report Date
LOSSES IN CHOPPER-CONTROLLED DC SERIES MOTORS	April 1982
	6 Performing Organization Code
	778-36-06

7 Author(s)	8 Performing Organization Report No
Howard B. Hamilton	
	10 Work Unit No

9 Performing Organization Name and Address	11 Contract or Grant No
University of Pittsburgh Pittsburgh, PA 15261 .	NSG-3163
	13 Type of Report and Period Covered

12 Sponsoring Agency Name and Address	Contractor Report
U.S. Department of Energy Office of Vehicle and Engine R & D Washington, D.C. 20585	14 Sponsoring Agency Code Report No.
	DOE/NASA/3163-1

16 Abstract

Motors for electric vehicle (EV) applications must have different features than dc motors designed for industrial applications. The EV motor application is characterized by the following requirements.

(1) The need for highest possible efficiency from light load to overload, for maximum EV range.
(2) Large short time overload capability. The ratio of peak to average power varies from 5/1 in heave city traffic to 3/1 in suburban driving situations.
(3) Operation from power supply voltage levels of 84-144 volts (probably 120 volts maximum).

The objectives of the research program were the design and fabrication of a test facility suitable for conducting tests of EV motors, to develop test procedures, to obtain data which can be used to isolate losses, to visualize where motor design changes can and should be made, to indicate problem areas arising from chopper control, and to make recommendations with respect to test procedures, instrumentation and chopper operating modes.

A test facility utilizing a dc generator as a substitute for a battery pack was designed and utilized. Criteria for the design of such a facility are presented. Two motors, differing in design detail, commerically available for EV use were tested.

Losses measured are discussed, as are wave forms and their harmonic content, the measurements of resistance and inductance, EV motor/chopper application criteria, and motor design considerations.

17 Key Words (Suggested by Author(s))	18 Distribution Statement
Electric vehicles dc Motors Chopper controller Motor losses	Unclassified - unlimited STAR Category 33 DOE Category UC-96

19 Security Classif (of this report)	20 Security Classif (of this page)	21 No of Pages	22 Price*
Unclassified	Unclassified	124	A06

End of Document